UNIVERSITY OF WARWICK

SOME STUDIES OF MOLECULAR STRUCTURE BY DEUTERIUM MAGNETIC RESONANCE

by

JEREMY ROYSTON

A thesis submitted in partial fulfilment of the requirements of the degree of Doctor of Philosophy.

School of Molecular Sciences

May, 1969.

... the affair was arranged in the Scientific Manner which suited better to this Age of Wonders.

Viscount Kirkwall,
'Four Years in the Ionian'.
1864.

ACKNOWLEDGEMENTS

I would like to thank Professor Irving (University of Leeds) and Professor T.C. Waddington for providing the facilities for this research, and my supervisor, Dr. J.A.S. Smith, for his constant advice and encouragement.

I am grateful to the members of the mechanical and glassblowing workshops in the School of Chemistry, University of Leeds, and in this department, for their help in building apparatus, and to all the members of the NMR group for their helpful discussions.

Finally, I would like to thank the Science Research Council and my father for their financial support during this project.

SUMMARY.

Single crystals of cupric acetate monohydrate dimer-d_{16} and potassium sulphamate-d_2 were studied by deuterium magnetic resonance. The theory of magnetic resonance in quadrupolar nuclei is briefly described, followed by a description of the apparatus used and the experimental technique. Several computer programs were written in Elliott ALGOL 60 for the calculation and interpretation of the results.

The quadrupolar coupling constant and asymmetry parameter for the methyl group deuterons in cupric acetate were found to be :-

$$e^2qQ/h = 55.6 \pm .4 \text{ kHz}, \eta = .13 \pm .02 \text{ at } 0^\circ\text{C}.$$

At 77°K the results were unchanged. The departure of η from the expected value of zero was explained on the basis of the indirect electric field effect. After a critical review of other work on coupling constants in C-D compounds, a value of 168 ± 5 kHz was deduced for e^2qQ/h in the static $-CD_3$ group in cupric acetate.

Potassium Sulphamate-d_2 was studied at -78°C. The results were :-

$$e^2qQ/h = 206.9 \pm 1.4 \text{ kHz}, \eta = .14 \pm .01.$$

A comparison with the results for urea showed that the magnitude and directions of the principal components of the efg tensor appeared to be controlled by hydrogen bonding.

CONTENTS.

CHAPTER IV - CALCULATIONS

CHAPTER V - CUPRIC ACETATE MONOHYDRATE DIMER.

RESULTS AND DISCUSSION.

CHAPTER I.

INTRODUCTION.

The purpose of this chapter is to give a very short review of the information obtainable from deuterium magnetic resonance studies of single crystals.

The electric field gradient (efg) tensor for each crystallographically different deuteron can be obtained from a study of at least two rotation patterns about different axes (5/4). Its eigenvalues and eigenvectors can yield structural information. Most work has been done on molecules containing water of crystallisation, where it was found (1/1) that the largest principle component of the efg tensor (ϕ_{zz}) was very sensitive to the distance between the two oxygen atoms in the hydrogen bonding system. Blinc and Hadzi (2/1) showed that there was a smooth variation of ϕ_{zz} as the O-O distance was varied from compound to compound. The ϕ_{zz} eigenvector was always along the O-D direction, and ϕ_{yy} was close to the normal to the O-D...O plane. In other, non-hydrogen-bonded compounds ϕ_{zz} was found to be always along the X-D direction.

It is possible to calculate the efg tensor components from the electronic wave function, for example

$$\phi_{zz} = \langle\psi|(3\cos^2\theta-1)/r^3|\psi\rangle$$

The operator for ϕ_{zz} does not commute with the energy operator, so the value of ϕ_{zz} is very sensitive to the wave function used. Thus

a comparison of the calculated value of ϕ_{zz} with the experimental value is a sensitive test of a wave function. In the case of deuterium it is especially sensitive because the nuclear contribution is always close in magnitude, but opposite in sign to the electronic contribution. Another advantage in using the efg at the deuteron as a test of a wave function is that the efg calculation does not have to take into account the Sternheimer anti-shielding effect (3/1).

Deuterium magnetic resonance has been used to investigate crystal ferroelectric and anti-ferroelectric properties, since these are often dependent on the ordering of the protons (4/1). An example is KD_2PO_4, where the quadrupolar splitting changes at about -50° when the deuterons start to tunnel between the two sides of the double potential minimum. Spin-lattice relaxation time measurements (5/1) give information on the tunnelling rate.

CHAPTER II.

THEORY.

II. 1 Introduction.

The splitting of nuclear magnetic resonance lines in single crystals by the interaction of the nuclear electric quadrupole moment with the electric field gradient at the nuclear site was first reported by Pound (1/2). In the following theory it is assumed that the interaction energy of the magnetic dipole of the nucleus with the external magnetic field is very large compared with the quadrupolar interaction energy. The quadrupole effects can then be treated as a perturbation of the magnetic interactions. The resonance line due to a single type of nucleus can be split into 2I components, whose splittings are dependent on the crystal orientation in the magnetic field. It can be shown (5/4) that at least two rotation patterns are necessary to give the eigenvalues and eigenvectors of the electric field gradient tensor.

The purpose of the following part of this chapter is to present the results of the theory of electric quadrupole effects in magnetic resonance, without detailed derivations, which may be found in references 1/2 and 2/2.

II. 2 Energy levels of a magnetic dipole in a magnetic field.

A nucleus contains charged particles of angular momentum so that it may possess a total magnetic moment $\underline{\mu}$ and total angular momentum $\underline{J}$. The two vectors can be taken to be parallel or anti-parallel, so we

can write

$$\underline{\mu} = \gamma \underline{J} \tag{1.1}$$

γ is a scalar known as the gyromagnetic ratio of the nucleus. We can define an angular momentum operator I by the equation (reference 2/2, p.17)

$$\underline{J} = \hbar \underline{I} \tag{1.2}$$

The application of a magnetic field $\underline{H}$ produces an interaction energy of the nucleus of $-\underline{\mu}.\underline{H}$. The Hamiltonian is therefore simply :-

$$\mathcal{H} = -\underline{\mu} \cdot \underline{H} \tag{1.3}$$

If the field is of strength H_o along the z-axis, then

$$\mathcal{H} = -\underline{\mu}\, \hbar H_0 I_z \tag{1.4}$$

The eigenvalues of this Hamiltonian are multiples of the eigenvalues of I_z, so the allowed energy levels are

$$E_m = -\gamma \hbar H_o m \qquad m = I, I-1, \ldots, -I \tag{1.5}$$

It can be shown that an alternating magnetic field applied perpendicularly to the static field, of angular frequency ω such that

$$\hbar\omega = \Delta E \tag{1.6}$$

will induce transitions between adjacent m-levels, which are separated by ΔE. Thus

$$\hbar\omega = \Delta E = \gamma \hbar H_o$$

or

$$\omega = \gamma H_o \tag{1.7}$$

II. 3 The nuclear electric quadrupole Hamiltonian.

The charge distribution in a nucleus of spin greater than $\frac{1}{2}$ is non-spherical. If we consider Figure 1, then in (a) the electrostatic energy

of the nucleus is higher than in (b).

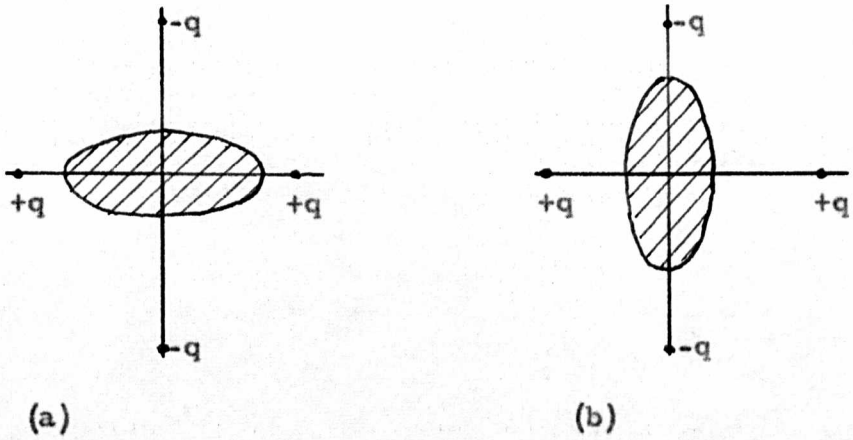

Figure 1.

To put this quantitatively, the interaction energy E of a charge distribution ρ with a potential V due to external charges is

$$E = \int \rho(r) V(r) d\tau \tag{1.8}$$

If we expand V(r) in a Taylor series about the origin, then

$$V(r) = V(0) + \sum_i x_i \left.\frac{\partial V}{\partial x_i}\right)_{r=o} + \frac{1}{2!}\sum_{i,j} x_i x_j \left.\frac{\partial^2 V}{\partial x_i \partial x_j}\right)_{r=o} \cdots \tag{1.9}$$

where x_i (i=1,2,3) stands for x,y,z respectively.

Defining

$$V_i = \left.\frac{\partial V}{\partial x_i}\right)_{r=o}$$

$$V_{ij} = \left.\frac{\partial^2 V}{\partial x_i \partial x_j}\right)_{r=o} \tag{1.10}$$

we have, to second order

$$E = V(0)\int \rho\, d\tau + \sum_i V_i \int x_i \rho\, d\tau + \frac{1}{2!}\sum_{i,j} V_{ij} \int x_i x_j \rho\, d\tau \tag{1.11}$$

If the origin is at the mass centre of the nucleus, the first term is the electrostatic energy of the nucleus considered as a point charge. The

second term contains the electric dipole moment of the nucleus, but it can be shown that it is zero, since the mass centre and charge centre coincide. The third term is the electrical quadrupole term. We can find principal axes of the potential V such that

$$V_{ij} = 0 \text{ if } i \neq j \tag{1.12}$$

V must satisfy Laplace's equation :-

$$\nabla^2 V = 0 \tag{1.13}$$

so at the origin

$$\sum_i V_{ii} = 0 \tag{1.14}$$

V is known as the electric field gradient (e.f.g.) tensor. It can be shown by a rather long derivation, that the quadrupolar Hamiltonian, in terms of the principle components of V, is

$$\mathcal{H}_Q = \frac{eQ}{4I\,(2I-1)} \left[V_{zz}(3I_z^{\,2}-I^2) + (V_{xx}-V_{yy})(I_x^{\,2}-I_y^{\,2})\right] \tag{1.15}$$

where I is the total angular momentum of the system, and I_x, I_y, I_z are the angular momentum operators.

It is usual to define two quantities η and q by the equations

$$eq = V_{zz}$$

$$\eta = (V_{xx} - V_{yy})/V_{zz} \tag{1.16}$$

The principle axes are defined such that

$$|V_{zz}| \geqslant |V_{yy}| \geqslant |V_{zz}| \tag{1.17}$$

By Laplace's equation

$$|V_{zz}| = |V_{yy}| + |V_{xx}| \tag{1.18}$$

So V_{yy} and V_{xx} must have the same sign, and η lies between 0 and 1.

The quantities V_o, $V_{\pm 1}$, $V_{\pm 2}$ will be used later; they are defined by

$$V_o = V_{zz}$$

$$V_{\pm 1} = V_{zx} \pm i\, V_{zy}$$

$$V_{\pm 2} = \tfrac{1}{2}\,(V_{xx} - V_{yy}) \pm i\, V_{xy} \qquad (1.19)$$

The V_{ij}'s are in an arbitrary, non-principal set of axes.

II. 4 Energy levels in a strong magnetic field.

The effect on the energy levels and frequencies of q, η and the orientation of the applied magnetic field relative to the principal axes is now described. Ω and q appear in the Hamiltonian only as a product, so neither can be determined directly. The sign of $q\Omega$ and the senses of the principal axes cannot be determined. In section II 2 the eigenvalues of the Hamiltonian $\mathcal{H}_M = -\gamma \hbar H_o I_z$ were shown to be

$$E_m = -h\nu_L m, \quad m = -I, -I+1, \ldots, I \qquad (1.20)$$

where ν_L is the Larmor frequency.

When a single crystal is placed in a strong magnetic field, the Hamiltonian, assuming no direct interactions of the spins with each other, can be expressed by

$$\mathcal{H} = \mathcal{H}_M + \mathcal{H}_Q \qquad (1.21)$$

If the crystal is in a strong magnetic field so that $\gamma \hbar H_o \gg e^2 q\Omega$, then the energy levels corresponding to the Hamiltonian above can be obtained by using perturbation theory. The energy of the perturbed Zeeman level, which in the limit of zero perturbation is characterised by the magnetic quantum number m, is given by

$$E_m = - m\gamma\hbar H_o + eQ\,(3m^2-2)V_o/2$$

$$- \frac{m}{12\gamma\hbar H_o}\left(\frac{eQ}{4}\right)^2 ((7-8m^2)V_{+1}\,V_{-1} + (3-2m^2)V_{+2}V_{-2}) \qquad (1.22)$$

This is for a nucleus with I=1. The energy levels are dependent on the irreducible tensor components V_o, $V_{\pm 1}$, $V_{\pm 2}$; hence they depend on the crystal orientation with respect to the magnetic field. These efg tensor components were defined in the coordinate system in which the spin angular momentum is quantised. Since $\gamma\hbar H_o \gg e^2qQ$, the magnetic field direction is the axis of quantisation. A transformation of the tensor in the magnetic field axis system into a system based on the crystal gives the dependence of the energy levels on the crystal orientation. The transformation properties of tensors are described by Nye (3/2).

In the experiment transitions between adjacent m- levels are observed. The two allowed frequencies are :-

$$\nu_{01} = \nu_{10} = (E_0 - E_1)/h$$
$$= \gamma H_0/2\Pi - 3eQV_0/4h + \frac{1}{2\gamma\hbar H_0 h}\left(\frac{eQ}{2}\right)^2 (-V_{+1}\,V_{-1} + V_{+2}\,V_{-2}) \qquad (1.23a)$$

$$\nu_{-10} = \nu_{0-1} = (E_{-1} - E_0)/h$$
$$= \gamma H_0/2\pi + 3eQV_0/4h + \frac{1}{2\gamma\hbar H_0 h}\left(\frac{eQ}{2}\right)^2 (-V_{+1}\,V_{-1} + V_{+2}\,V_{-2}) \qquad (1.23b)$$

We can see from these equations that the three equally spaced Zeeman levels all shift so that the centre of gravity of the allowed frequencies remains at the Larmor frequency, if only the first order effects are

taken into account. Second order effects only shift the centre of gravity. If we measure the frequency difference, $\Delta\nu$, of the two transitions, then the second order terms disappear. From equations 1.23

$$\Delta\nu = \nu_{-10} - \nu_{01} = 3eQV_0/2h \tag{1.24}$$

II. 5 Prediction of the rotation pattern.

Equation 1.24 can be used to predict and interpret the rotation patterns. From equation 1.19, V_0 is the magnitude of the electric field gradient in the direction of the magnetic field. It should be noted that in the following part the transformations are made from the fixed laboratory set of axes into the direction of the magnetic field, rather than in the direction suggested in the previous section. This gives exactly the same expressions. The various axial systems are defined in section 6 of chapter IV.

We start with the electric field gradient tensor, ϕ, for the deuteron, in the orthogonal crystallographic system

$$\phi = \begin{vmatrix} \phi_{11} & \phi_{12} & \phi_{13} \\ \phi_{12} & \phi_{22} & \phi_{23} \\ \phi_{13} & \phi_{32} & \phi_{33} \end{vmatrix} \tag{1.25}$$

The transformation matrix, A, for the transformation of the orthogonal crystallographic axes to the fixed laboratory axes has the elements

$$A = \begin{vmatrix} a_{11} & a_{12} & a_{13} \\ a_{21} & a_{22} & a_{23} \\ a_{31} & a_{32} & a_{33} \end{vmatrix} \tag{1.26}$$

We then transform the tensor in the fixed laboratory system into the rotated set based on the magnet, using the transformation matrix R, given by

$$R = \begin{vmatrix} \cos\theta & 0 & -\sin\theta \\ 0 & 1 & 0 \\ \sin\theta & 0 & \cos\theta \end{vmatrix} \tag{1.27}$$

where θ is the magnet rotation angle. Thus the tensor ϕ, when transformed into the magnet based system gives ϕ':-

$$\phi' = RA\,\phi\,A_t R_t, \tag{1.28}$$

where A_t indicates the transpose of A.

Put $\quad RA = T.$ (1.29)

We are only interested in ϕ'_{33}, which is equal to V_0 in equation 1.19. Since T is a unitary matrix

$$\phi'_{33} = \sum_{k=1}^{3} \sum_{l=1}^{3} T_{3k}\, T_{3l}\, \phi_{kl} \tag{1.30}$$

Only T_{31}, T_{32}, and T_{33} are required.

$$T_{31} = a_{11} \sin\theta + a_{31} \cos\theta$$

$$T_{32} = a_{12} \sin\theta + a_{32} \cos\theta$$

$$T_{33} = a_{13} \sin\theta + a_{33} \cos\theta \tag{1.31}$$

By substituting (1.31) in (1.30) and collecting terms, ϕ'_{33} becomes

$$\phi'_{33} = A + B \sin 2\theta + C \cos 2\theta \tag{1.32}$$

where

$$\begin{vmatrix} A \\ B \\ C \end{vmatrix} = \begin{vmatrix} \frac{1}{2}(1-a_{21}^2) & \frac{1}{2}(1-a_{22}^2) & \frac{1}{2}(1-a_{23}^2) & -a_{21}a_{22} & -a_{21}a_{23} & -a_{22}a_{23} \\ a_{11}a_{31} & a_{12}a_{32} & a_{13}a_{33} & a_{11}a_{32}+a_{31}a_{12} & a_{11}a_{33}+a_{31}a_{13} & a_{12}a_{33}+a_{32}a_{13} \\ \frac{1}{2}(a_{31}^2-a_{11}^2) & \frac{1}{2}(a_{32}^2-a_{12}^2) & \frac{1}{2}(a_{33}^2-a_{13}^2) & a_{31}a_{32}-a_{11}a_{12} & a_{31}a_{33}-a_{11}a_{13} & a_{32}a_{33}-a_{12}a_{13} \end{vmatrix} \begin{vmatrix} \phi_{11} \\ \phi_{22} \\ \phi_{33} \\ \phi_{12} \\ \phi_{13} \\ \phi_{23} \end{vmatrix} \qquad (1.33)$$

The rows of the 3 x 6 matrix and the 6 x 1 matrix composed of elements of ϕ can be regarded as vectors in a 6 space. If they are called M_A, M_B, M_C, ϕ_m respectively, then (1.33) can be rewritten in the form of scalar products of vectors,

$$A = M_A \cdot \phi_m$$

$$B = M_B \cdot \phi_m$$

$$C = M_C \cdot \phi_m \qquad (1.34)$$

The program SPECTRUM (Chapter IV, section 7) calculates the values of A, B and C. The reverse process, of calculating the elements of ϕ (equation 1.25) from experimental data, is accomplished in the program TENSOR (Chapter IV, section 8), but it is first necessary to describe the solution of linear equations where there are more equations than variables. This theory is also used in the least squares analysis of the rotation patterns (Chapter IV section 4).

II. 6 Least squares analysis.

We have n observed values of a variable Y, which is related to the m $(m < n)$ quantities x by the set of linear equations

$$y_n = \sum_{i=1}^{m} f_{ni} \; x_i \tag{1.35}$$

where the f's are functions of n, i and any other variable, the x_i's are to be determined, and y_n is defined by :-

$$Y_n^{obs} = y_n + E \tag{1.36}$$

where Y_n^{obs} is the observed value of y_n

E is the error in the determination.

Equation (1.36) is exact, so the problem is to find the most probable values of the x_i's. If the errors are normally independently distributed, then the most probable solution is the one which minimises the sum of the squares of the errors. In matrix notation, equations (1.35) and (1.36) can be written as

$$Y = Fx \tag{1.37}$$

so the least squares solution for x is (3/2 p 158 - 169)

$$x = (F_t \, F)^{-1} \, F_t \, Y. \tag{1.38}$$

where F_t is the transpose of F.

The variance of x_i is given by (reference 4/2)

$$\sigma^2(x_i) = C_{ii} \, S^2/(n-m) \tag{1.39}$$

where $C = (F_t F)^{-1}$,

S^2 is the sum of the squares of the errors.

II. 7 Calculation of the components of the efg tensor from experimental results.

The constants A, B, C (equation 1.32) are obtained for each of the deuterons in the three experimental rotation patterns. For one deuteron there are three sets of A, B, C, so we have nine simultaneous equations in the six unknown components of the efg tensor in the crystallographic system. They are :-

$$\begin{vmatrix} A_a \\ B_a \\ C_a \\ A_b \\ B_b \\ C_b \\ A_c \\ B_c \\ C_c \end{vmatrix} = \begin{vmatrix} M_{Aa} \\ M_{Ba} \\ M_{Ca} \\ M_{Ab} \\ M_{Bb} \\ M_{Cb} \\ M_{Ac} \\ M_{Bc} \\ M_{Cc} \end{vmatrix} \begin{vmatrix} \phi_{11} \\ \phi_{22} \\ \phi_{33} \\ \phi_{12} \\ \phi_{13} \\ \phi_{23} \end{vmatrix} \qquad (1.40)$$

where A_a is the value of A in the a'-axis rotation pattern, and

M_{Aa} is the value of M_A (eg. 1.34) for the a'-axis rotation pattern, its value is calculated from the transformation matrix.

It should be remembered that the M's are vectors in a 6-space. Equation (1.40) can be solved for ϕ by the method described in the previous section. A rough idea of the accuracy of the results can be obtained from the variances of each, and from the sum $\phi_{11}+\phi_{22}+\phi_{33}$, which should be zero.

The eigenvectors and eigenvalues of the tensor are calculated by the computer procedure SYMMETRIC QR 2 (6/4).

CHAPTER III

Section 1. Apparatus.

A block diagram of the apparatus used to obtain deuterium magnetic resonance spectra is shown in Figure 1.

Spectrometer.

The spectrometer was built by John Clifford (1/3), to a design by Robinson (2/3). The theory of its operation is given by Robinson in the same paper.

The detector current is measured by a 25 μA meter, its magnitude is dependent on the r.f. voltage at the sample coil. The r.f. level was calibrated by connecting a low impedance output signal generator (Marconi TF 2002 with 50Ω pad and known output voltage), to the spectrometer instead of the sample coil. The generator frequency was adjusted to 18.3 MHz, the usual operating frequency, then it was possible to draw a graph of detector current against r.f. level.

Originally, a spectrometer designed by Blume (3/3) was built. This was a crystal-controlled Pound-Knight-Watkins oscillator. It was chosen because of the high frequency stability (better than 10 ppm per hour) and very low oscillation level (down to 700 μV) obtainable. The compounds which were to have been studied would have been easily saturated, and it was felt that a lower radio-frequency level than that obtainable with a conventional PKW oscillator was necessary.

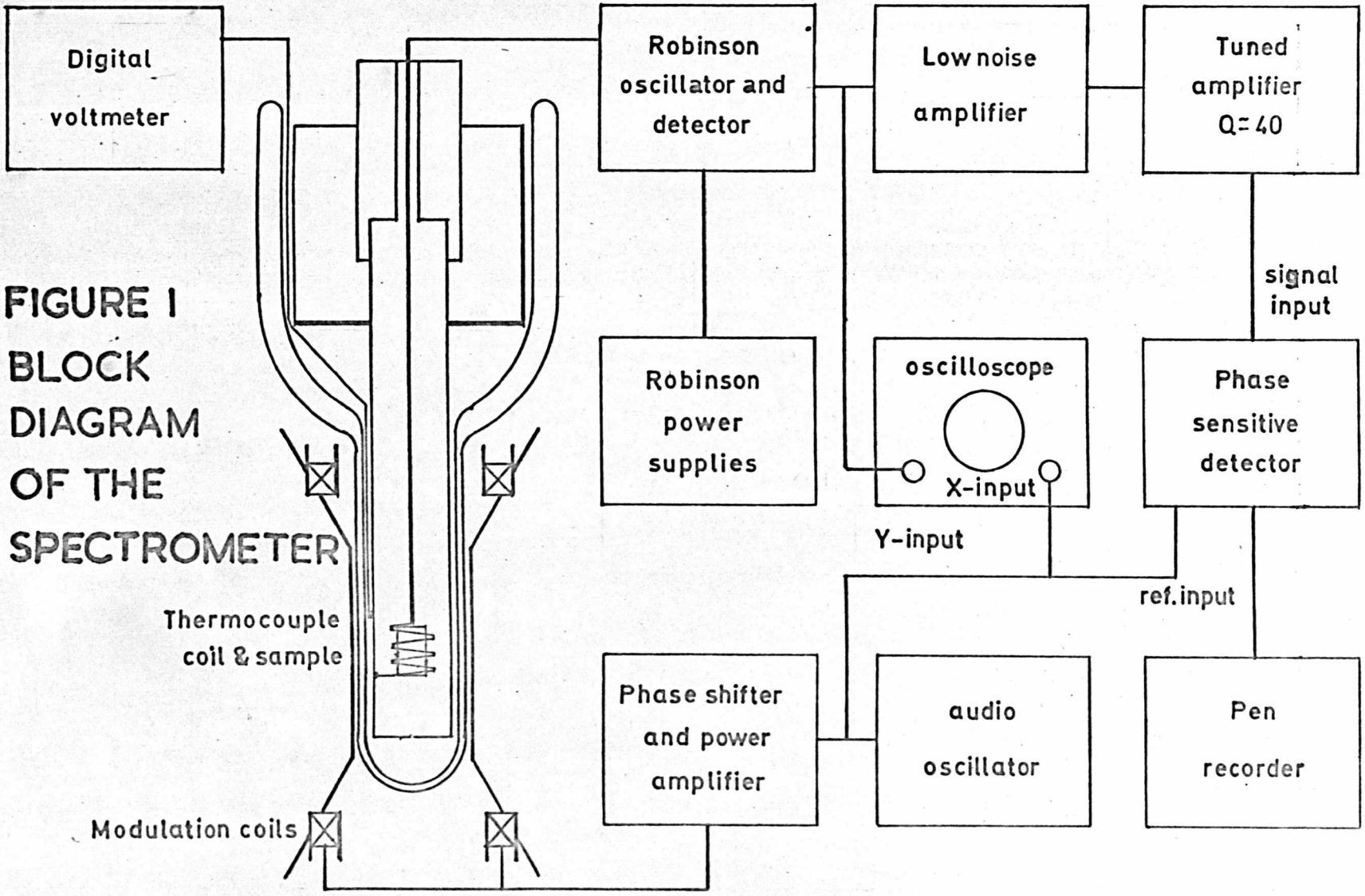

FIGURE 1
BLOCK DIAGRAM OF THE SPECTROMETER

However, it was found to be much less sensitive than ideal. Deuterium magnetic resonance spectra of a sample of heavy water in a 1 mm diameter glass tube were recorded. Under identical conditions of magnetic field r.f. level and modulation depth it gave a signal noise ratio at least four times worse than that given by the Robinson oscillator. Robinson (2/3) shows that in a typical case a marginal oscillator can be about 3.5 times less sensitive than ideal. A discussion of noise in the PKW oscillator may be found in references 2/3, 4/3, 14/3.

Magnet System.

The magnet was a 15" Varian V3800 on a rotating base, with a VFR 2703 solid state power supply and control unit. The maximum field obtainable is about 2.9T in a $1\frac{1}{4}$" (31.8 mm) gap at 142 amps.

The magnetic field strength is regulated by a negative feedback control loop. A 1290 Hz signal drives a Hall effect sensor in the magnet gap, and is also applied across the end terminals of the field selector potentiometer. The difference between the Hall sensor output and the voltage at the potentiometer slider is amplified, then rectified in a phase-sensitive detector, whose output controls the magnet current. The field strength is therefore controlled by the potentiometer setting. Two small potentiometers are connected in series with the field selector. The first is an incremental control, which gives a manual adjustment range of 100G, the second is a motor driven sweep potentiometer. The sweep ranges are

250 mG to 40 kG in periods of 0.5 to 100 minutes, and the sweep dial is graduated from -50% to +50% .

The long-term field stability is governed mainly by the temperature variations of the Hall coefficient of the field sensor, and of the resistances in the field selector. In practice, it was found that the field at fixed selector setting increased about 100 G at 28 kG in the first three hours after switching on. This initial drift is probably caused by variation in temperature of the pole-piece to which the Hall sensor is attached. The field strength also increased with increasing room temperature. The ultimate stability under ideal conditions was about 2 ppm per minute after 6 hours. The drift might be reduced by thermostatting the Hall probe and control panel.

The magnet and power supply cold plate are cooled by distilled water which circulates through one side of a heat exchanger. The water on the cold side of the heat exchanger is sprayed down a cooling tower against a current of air from a fan. 10 ppm of 'Panacide' (BDH Ltd.) were added to the water in the magnet circuit to prevent algal and bacterial growth. In spite of this, slow growth of algae occurred, so the system was carefully cleaned out with 'Oakite' (Oakite Products Inc., New York) solution every 2 to 3 months.

The magnetic field homogeneity was studied, using a 1 cc. sample of heavy water in the Robinson spectrometer. At the best position the line width was about 260 mG at 28 kG. In this position

the field homogeneity decreased considerably within 400 g of 28 kG. At all field strengths the line width increased even if the sample was moved 1 mm from the best place. Rough measurements showed that there was a difference of about 8 G between the field strength at the position of maximum homogeneity and at a point 15 mm away.

Signal detection

In order to detect the nuclear resonance signal in the presence of noise, the magnetic field was modulated sinusoidally, with an amplitude dependent on the strength of the absorption. For strong signals the modulation depth was 0.5 to 1 gauss, increasing to about 2 g for the weakest signals. The modulation coils consisted of 200 turns of 22 swg enamelled copper wire wound on each of two 6" internal diameter by ½" wide perspex formers. They were connected in parallel and mounted on a step on the pole-pieces, as in Fig. 3. The modulation power source was a Henry's Radio 10 watt audio amplifier.

A Marconi TF 2000 audio frequency oscillator provided the reference signal for the phase sensitive detector and the modulation power amplifier. A phase shifter (AIM Electronics PSA 128) was placed between the audio generator and power amplifier input so that the signal and reference phasing could be adjusted for maximum signal/noise ratio.

The audio frequency output of the Robinson oscillator was first fed into a low noise preamplifier (AIM Electronics LNA 133), then

into a tuned amplifier (AIM Electronics TFO 129), and finally into the signal input of a phase sensitive detector (AIM Electronics PSD 122).

Some early spectra were run using a tuned amplifier which was built to the design of a unit in the Princeton Applied Research 'JB-4' phase sensitive detector. It was used in conjunction with a Brookdeal Electronics LA 655 low frequency amplifier and a PD629 phase sensitive detector. At times a Princeton Applied Research JB-4 phase detector unit was used instead of the AIM Electronics instrument.

Spectra were recorded on a Servoscribe RE 511.20 chart recorder.

A few spectra were run using an Advance HR-96 X-Y recorder. The X signal was taken from a linear potentiometer coupled to the field sweep unit on the magnet control panel. It was found that the recorder sweep was up to ½% non-linear with respect to the magnet sweep dial. With strong signals a higher line position reproducibility was possible, so the X-Y recorder was discarded. The Servoscribe and field sweep motors are both mainsfrequency synchronous types, so there is no possibility of non-linearity.

Probe unit

The objectives for the performance of the probe were:-

a) to give spectra at any temperature from about 40°C down to 77°K, the temperature of liquid nitrogen at atmospheric

pressure. The upper temperature is limited by perspex components in the probe.

b) Both the orientation of a sample with respect to the probe and the orientation of the probe in fixed laboratory coordinates should be able to be measured easily and accurately.

c) It should be possible to load a sample whose melting point is well below 0°C.

The design (Figures 2,3,4) is based on one by Ketudat (5/3). The lowest temperature obtainable with Ketudat's probe was about 93°K, so gas cooling was added.

The probe consists of a copper can 12.7 cm. diameter by 17.5 cm. with a concentric $\frac{3}{4}$" (1.93 cm) o.d. copper tube extending downwards. This tube acts as a heat leak for the sample and as the earth conductor from the sample coil. The other conductor runs coaxially inside the heat leak. In order to minimise heat conduction to the coaxial connector at the top of the probe, the top section of the coaxial line to the coil is made from 1 cm. and 1.5 mm. thin walled german silver tube. The outer tube is supported by a $1\frac{1}{2}$" diameter perspex tube, which carries the coaxial socket.

Inside the copper can is a coil wound from about 3.5m of $\frac{1}{4}$" (6.35 mm) o.d. copper tube. Dry nitrogen, made by boiling liquid nitrogen, passes through this coil, down the inside of the heat leak, and past the sample holder. It comes out of six small holes just

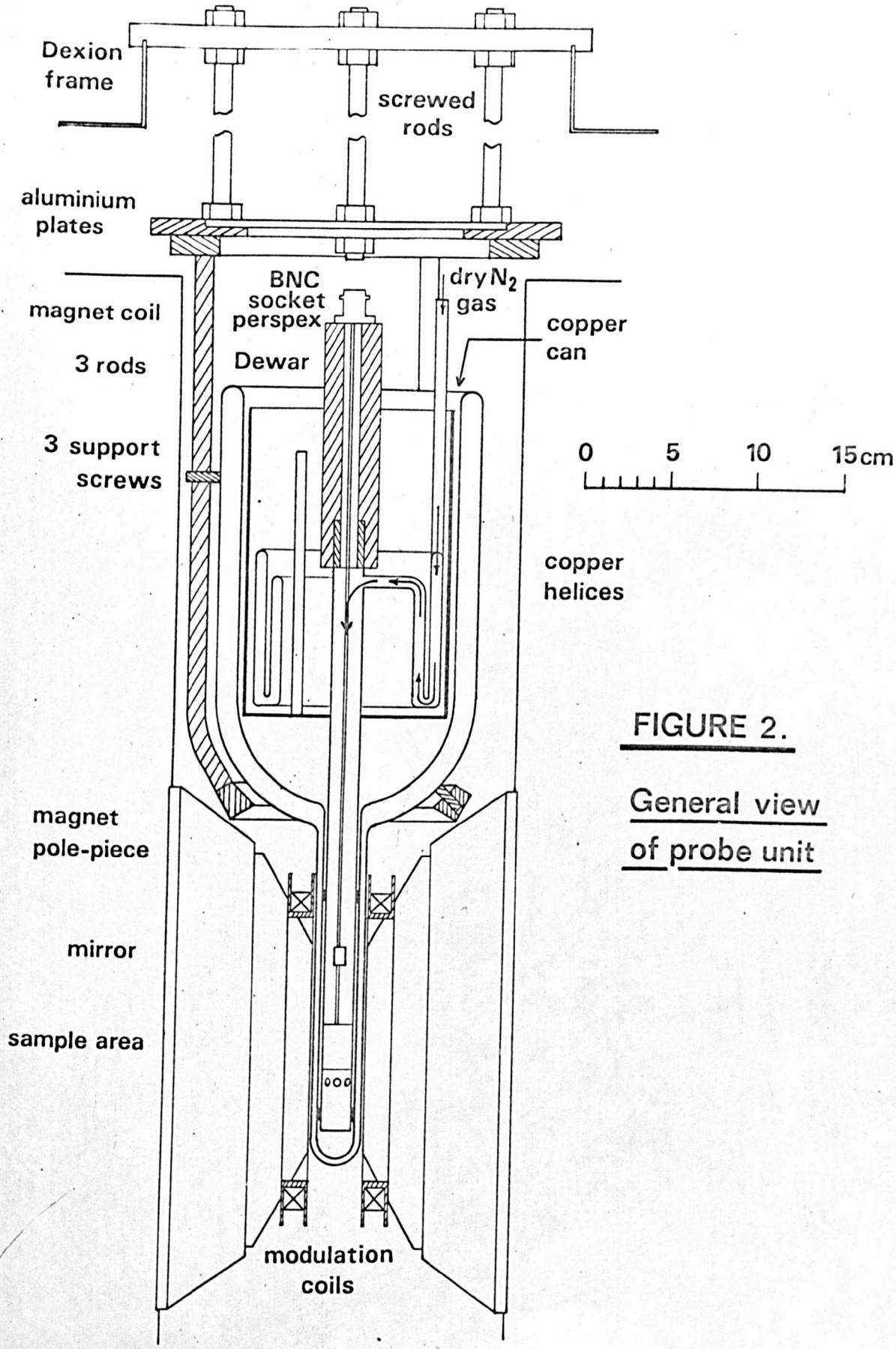

FIGURE 2.

General view of probe unit

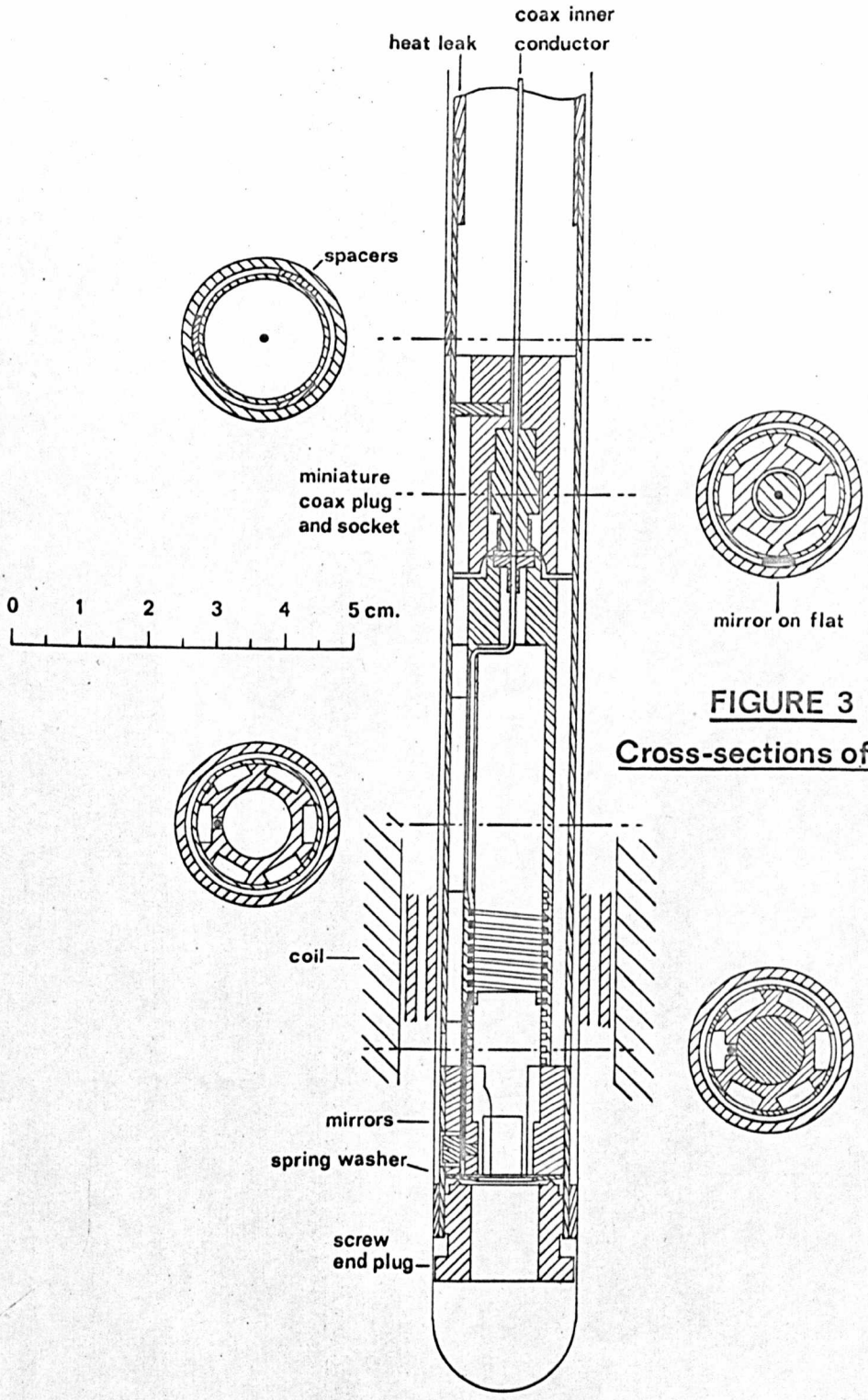

FIGURE 3

Cross-sections of the probe unit

FIGURE 4

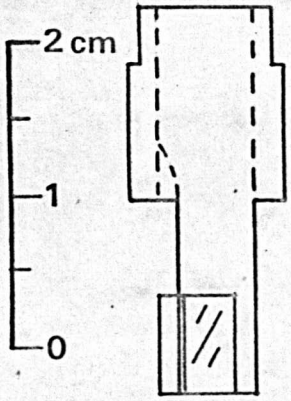

Sample holder

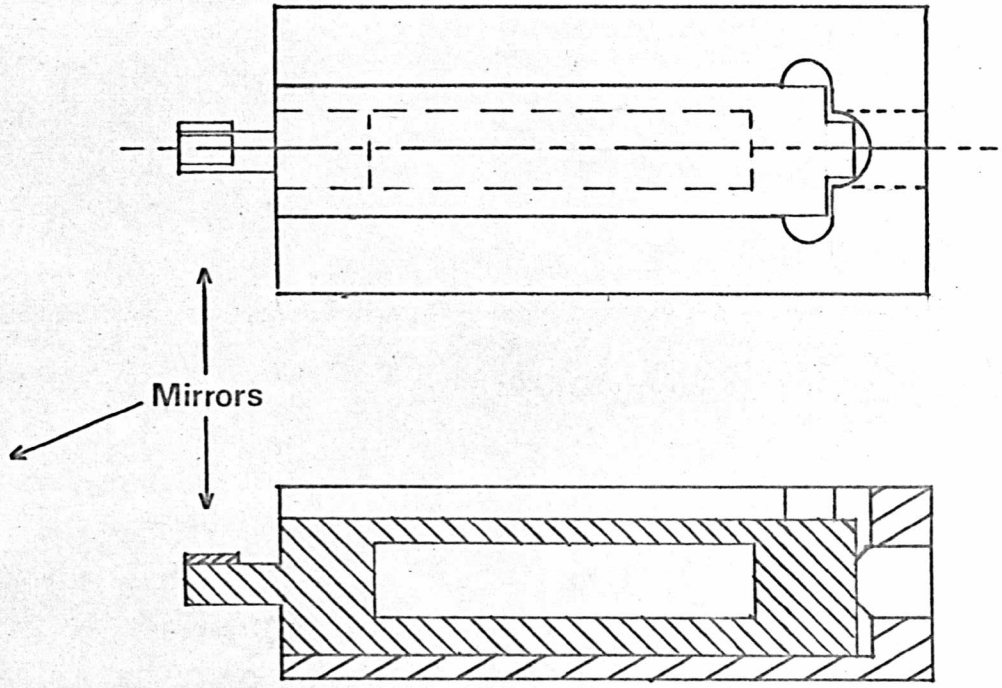

Simplified drawing of the coil assembly in the alignment jig

below the sample and goes up between the Dewar and the outside of the heat leak. A flow rate of about 0.7 litres/minute of gas at -196° reduces the probe temperature from about -180° to -196°.

The probe temperature was measured with two copper-constantan thermocouples whose emf's were determined by a Solartron "LM 1420" digital voltmeter. The reference junctions were maintained at 0° C in distilled water ice. Each thermocouple was stuck with "Araldite" to the outside of the heat leak, one just above the sample, the other about 2 cm below the first. They were connected so that either temperature of each junction, or their difference, could be measured.

A heater coil, wound non-inductively from about 4 m of 38 s.w.g. silk covered constantan wire, was placed on the outside of the heat leak, about 2 cm above the sample. Tests with a Bell 120 Hall effect gaussmeter showed that a direct current of 0.5 amps produced a field of less than 50 mG at the sample. Since the current generally used was less than 0.5 amps, and the magnetic field inhomogeneity was at least 300 mG, it was possible to use a Variac transformer as the power supply for the heater. The probe assembly is enclosed in a silvered glass tail Dewar supported by six screws in a cage surrounding it. These allow precise adjustment of the Dewar orientation in the magnet gap.

Sample holder/coil assembly (Figure 3).

This was originally designed to hold glass sample tubes up to

6 cm long, containing single crystals of low melting point deuterated compounds. The assembly could be made much shorter for single crystals of high melting point compounds.

The coil round the sample is on an external former, in order to attain a high filling factor. A 0.8 mm square thread with a 1.6 mm pitch and 1 cm internal diameter was cut inside the bore of the coil former. $7\frac{3}{4}$ turns of 24 swg enamelled copper wire were wound on the shank of a size W drill (9.75 mm). The former was carefully screwed onto the coil, then the top end of the coil was soldered to the centre conductor of a 4 mm Belling-Lee subminiature coaxial plug screwed to the top of the sample holder. The earth end of the coil passes downwards in a 1 mm slot at the side of the former.

At the top of the coil former is a rectangular piece which engages in a semicircular slot in a polystyrene plug. This design ensures that the sample holder always goes in with the same azimuth, independent of the accuracy of construction. The semicircular slot was cut in the polystyrene plug after it had been fixed in the heat leak, using a 3/8" (.954 cm) end mill. A 3/8" by $\frac{1}{4}$" (.954 x .635 cm) flat was milled on the side of the heat leak at the same time. The normal to the flat is thus accurately parallel to the axis of the semicircular slot. The 3/8" holes in the heat leak were blocked with 20 swg brass discs stuck in place with "Araldite". Later, a small piece of 1.2 mm thick surface aluminised mirror was glued to the flat with "Araldite".

The use of this mirror in the probe orientation procedure will be described in the section on experimental methods.

Sample holder for cupric acetate and potassium sulphamate crystals.

The sample holder is a push fit in the coil former (Fig.3,4). Two flats at right angles to each other were milled on the bottom of the holder. Surface-aluminised mirrors, 5 x 8 x 1.2 mm thick, were stuck with Araldite to the flats. They would only stick well if the backs were lightly ground with 320 grade silicon carbide.

Probe support (Fig.2)

A frame of 1.6" aluminium Dexion was built around the magnet. A bridge of the same material crosses the top of the frame above the magnet gap. The cage around the dewar is suspended by three screwed rods from two perspex bars, which slide on the two lower parts of the bridge. These screws were adjusted to make the top ring of the cage horizontal, using a spirit level. The adjustments of the probe orientation were thus :-

1) backwards and forwards, by sliding the whole probe. The perspex bars have $^3/_{32}$" (2.4 mm) slots which engage on the lower part of the bridge, so the probe cannot rotate;

2) sideways, by fixing the bridge to the frame by screws in slots, so that it can be moved sideways;

3) up and down, by using the screwed rods.

Finally, the Dewar tail is made parallel to the magnet pole

faces by adjustment of the three top screws in the cage. The probe orientation was very stable and only needed occasional checks, even after it had been removed and replaced several times.

Field measuring probe (Figure 5).

A 120 MHz transistorised proton magnetic resonance probe designed by Robinson (6/3) was built. Two modifications were made. The first was to use ME 3002 (Micro Electronics) npn silicon transistors and the second to use varactor tuning instead of a conventional variable capacitor. This allowed remote tuning by a potentiometer with none of the vibration which would result from manual tuning. An STC BA 110 varactor diode was tried first, but a Siemens BA 139 gave a much greater tuning range, about 3 MHz compared with 0.7 MHz. The sample was a short section of 4.5 mm nmr tube filled with about .05M acidified ferric chloride solution in water.

The oscillator was built on double sided printed circuit board enclosed in a small Eddystone diecast box. The sample coil was at the end of a 15 cm coaxial line made from ¼" o.d. copper tube and 12 swg copper wire with PTFE spacers. In use the box rested on a perspex strip wedged between the magnet coils, and the sample rested against the Dewar, in the centre of the gap. By suitable adjustment, the field measuring probe sample could be set in the position of maximum field homogeneity when the main probe was slid

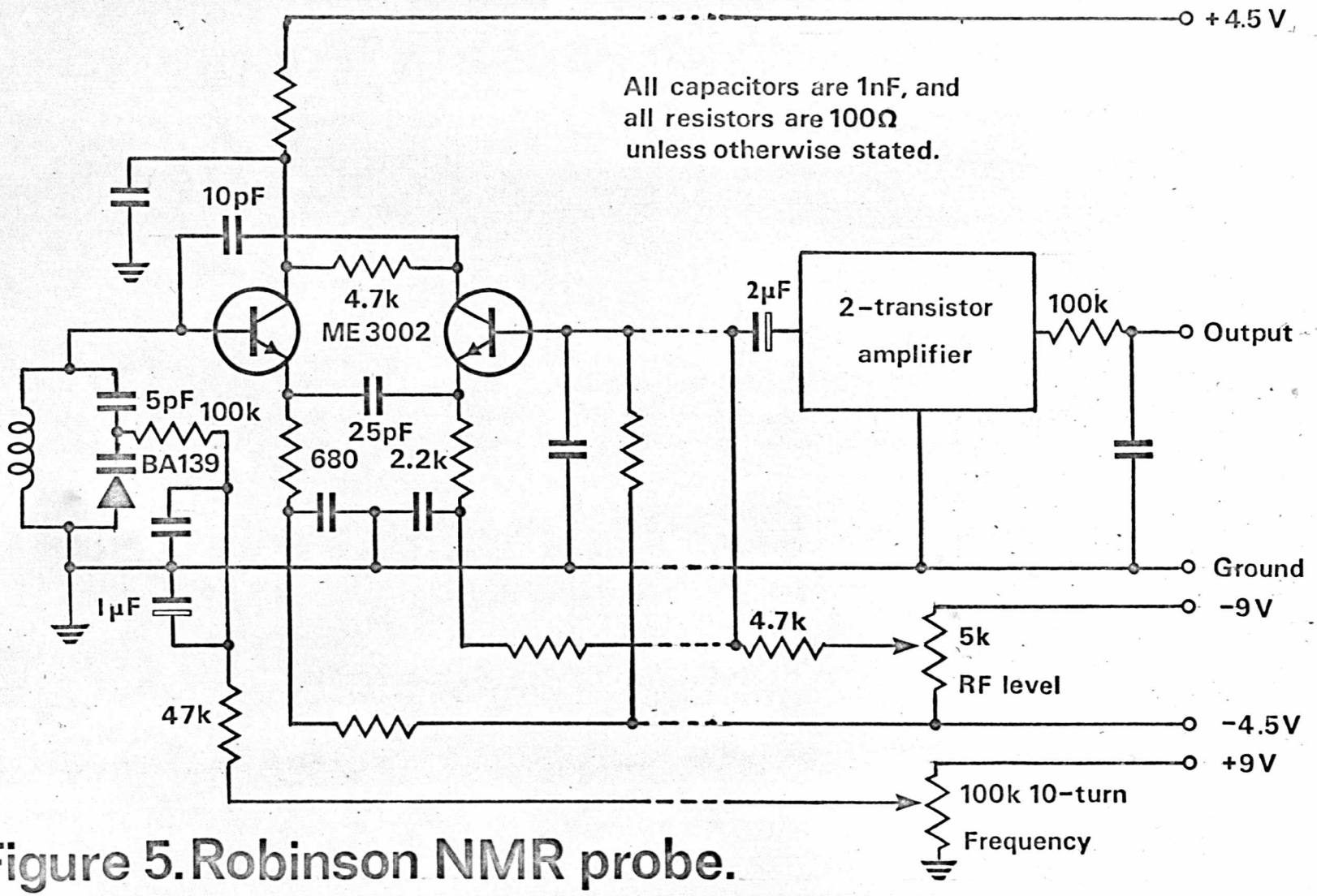

Figure 5. Robinson NMR probe.

Figure 6. Crystal growing apparatus.

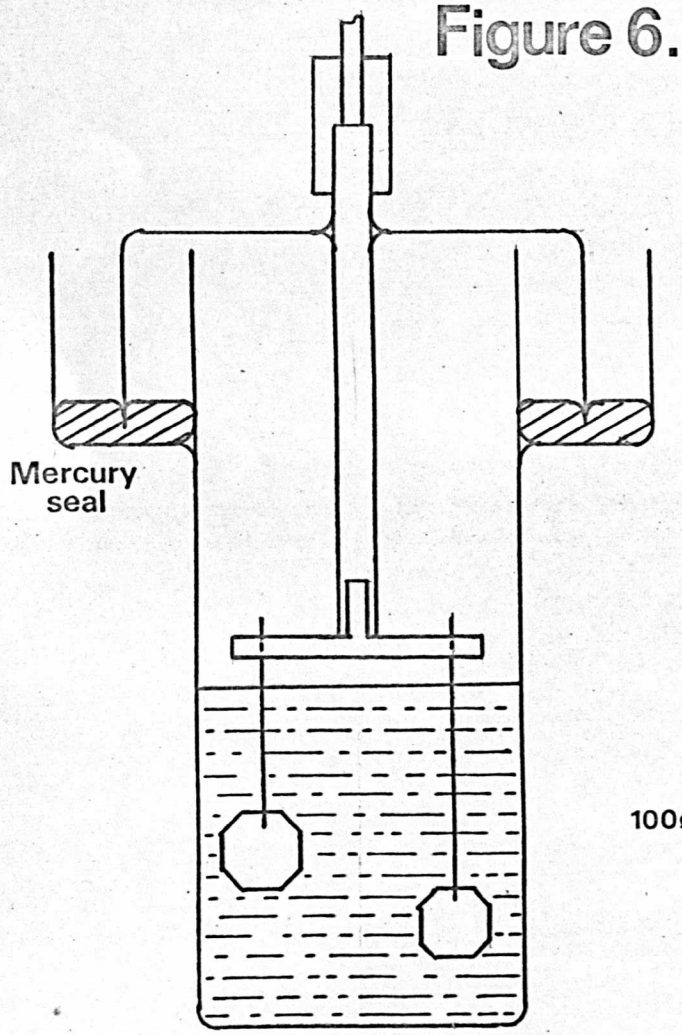

Crystal growing container. Scale ~ ⅔ full size

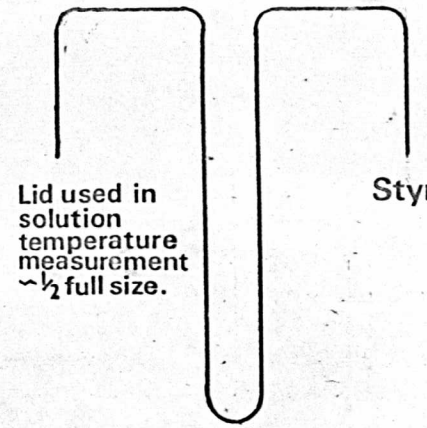

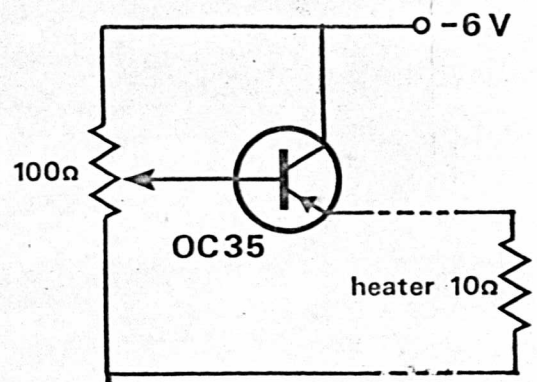

Heater power supply

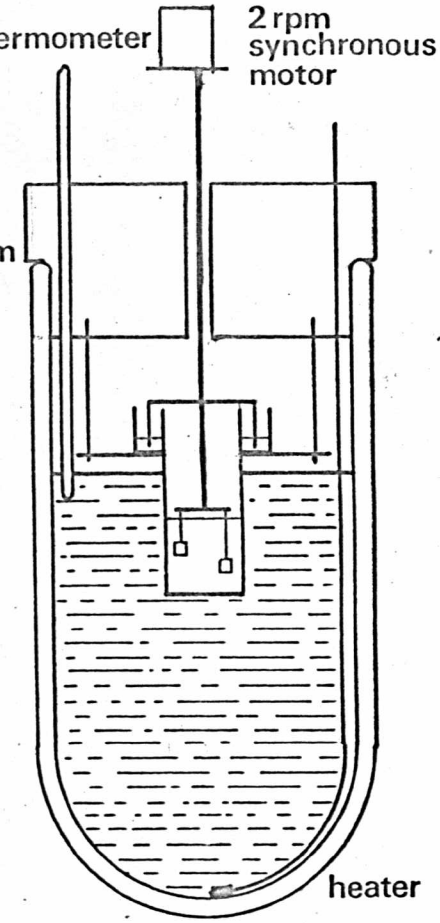

Apparatus for growing KND_2SO_3 crystals

1.5 cm backwards. The signal to noise ratio was at least 80:1 with a 0.1 mS. time constant before the oscilloscope input.

Crystal growing apparatus (Fig.6)

The crystals which were grown were deuterated, so it was necessary to protect the crystal growing solution from atmospheric moisture. A mercury seal was used so that the seed crystal could be rotated at 2 revolutions per minute by an electric motor. The methods by which single crystals were grown are described in the section on experimental methods.

PART 2. EXPERIMENTAL METHODS.

Dewar silvering.

The Dewar round the probe unit required a clear band on the tail so that the mirror on the heat leak would be visible. The filling tube was placed at the bottom of the tail. The whole Dewar was first silvered, using the technique described in reference 7/3, with the exception that the solutions were cooled to about 2° so that the silver only started to deposit on the glass after the Dewar had been filled. The Dewar was carefully washed out, then the silver on the tail was dissolved off up to the correct height with a solution (8/3) consisting of :-

Potassium cyanide	1.5 gm.
100 volume hydrogen peroxide	5 ml.
Distilled water to	100 ml.

The solution had to be freshly prepared.

After careful washing the tail was resilvered to leave a gap of about 1.5 cm.

Cupric acetate -d_{16} preparation and crystal growth.

Cupric hydroxide (10 gm) was prepared as in (9/3). It was dried in a vacuum dessicator at 40°, and iodimetric determination of the copper (10/3) showed that it was 98.5 ± 0.3% pure.

4.9 gms (.05 moles) of the cupric hydroxide and deuterium oxide (15 ml) were placed in a 250 ml flask with a reflux condenser.

Acetic acid - d_4 (.105 moles = 6.3 ml) was added slowly down the condenser, then the suspension of cupric acetate was gently refluxed and heavy water added until all the acetate had dissolved. The solution was cooled in ice, and after decantation the precipitated salt was re-dissolved in heavy water (105 ml). This solution was kept in a closed flask at 35° for one day to make it saturated at that temperature. It was then transferred to the crystal growing apparatus. About 3 gms of undissolved cupric acetate were left.

Most of the operations in growing the crystal were performed inside a polythene glove bag filled with dry nitrogen. At some stages exposure to the atmosphere was inevitable. However, an infra-red spectral analysis by the method of Gordon (11/3), of a little water distilled from the solution in which the crystals were grown showed that it contained 2.2 $\pm$ 0.1% hydrogen. The spectrum was kindly run by Mr. T. Matts on a Cary 14 spectrometer.

Seed crystals of the protonated salt about 1mm across were made by slow cooling of a saturated solution of Analar cupric acetate. Two seeds were stuck with Araldite to the nylon threads in the growing apparatus, then they were placed in the solution, which had been previously warmed to about 1° above the saturation temperature. The container and crystals were placed in foamed polystyrene 'Igloo', containing about 1 litre of water at 36°. To prevent heat loss by evaporation a drop of light oil was put on the water surface, and a polystyrene lid put over the Igloo. After connecting the growing

apparatus to the motor above it, the solution was allowed to cool for 1 - 2 days. The crystals were removed and spurious growths were cleaned off them. The crystals on the bottom of the container were dissolved by heating the solution to about 60°. Occasionally, about 0.3 gm of cupric acetate-d_{16} were added to make up for the amount lost to growth on the crystals. This process was repeated until the crystals had grown to 14 - 15 mm maximum dimension.

Potassium Sulphamate.

Potassium hydroxide (18.7 gm =.33 moles) dissolved in water (30 ml) was added slowly to an ice-cooled s olution of sulphamic acid (32.3 gm =.33 moles) in water (150 ml), so that the temperature did not rise above 40°. The pH of the solution was adjusted to 7, using dilute potassium hydroxide or sulphamic acid and Whatman's narrow range pH paper. The resultant solution was filtered through sintered glass into a round-bottomed flask and evaporated to dryness in a rotary vacuum evaporator. The solid was dissolved in heavy water (40 ml), evaporated to dryness and redissolved in heavy water (50 ml).

It can easily be shown, assuming an equilibrium content for the reaction :-

$$KSO_3NH_2 + D_2O \rightleftharpoons KSO_3ND_2 + H_2O$$

of one, that the product will contain at least 98% deuterium.

The solubility of potassium sulphamate is very high and extremely temperature dependent. It was therefore necessary to cool the solution very slowly, using the apparatus shown in Fig. 6. A little

light oil was spread on the water surface to prevent heat loss by evaporation. At 32° the water cooled about 2.5° per day at 22° ambient. In order to reduce the cooling rate, a heater in the form of a 1.0w resistor coated in Araldite was added. The heat loss was about .17W per degree difference between the water and the room temperature. The power required to increase the temperature at .01°C per hour was .15W. The heater power supply is shown in Fig. 6.

Small seeds were grown by cooling a concentrated solution of potassium sulphamate. They were tabular on (100), forming plates about 1 x 5 x 10 mm with (001) and (010) as easy cleavage planes. Since the crystals grew fastest along the c axis, the seeds were made shortest in this direction. It was found that the crystals would not grow properly if the (100) face (the largest one) was stuck to the nylon thread. The crystal was therefore fixed to the thread by the (110) or $(\bar{1}10)$ face, using the following method. A little "Araldite" was placed on the end of the thread, which was then put in contact with the crystal. The Araldite was melted by bringing a hot soldering iron close to the crystal - it then flowed on to the crystal.

The potassium sulphamate solution was kept in a sealed flask in the Dewar full of water at 32°. The saturated solution was transferred to the growing apparatus. After warming the water to 32.2° the container was removed, and the seeds were placed in it. They were replaced in the Dewar, then the motor was connected.

The solution was kept at 32.2° for about a day to dissolve off the surface of the crystal, then it was cooled at .8 to 1.0 degrees per day by suitable adjustment of the heater. When the temperature had dropped to about 25° the crystals were removed. They were dried carefully and stored in a sealed container.

The crystals were, in general, too large to fit in the probe unit. They were each stuck with paraffin wax to a ground steel flat, the (100) face being in contact with the flat. The flat was held in a machine vice on a horizontal milling machine. The vice was turned round until the c-axis was parallel with the plane of the cutter, a .01 inch (.254 mm) slitting saw. The machine vice had a graduated circle on its base, and all readings were referred to the above orientation. It was found that a cut of 7 - 8 thous. (.2mm) depth and feed rate of 18 thous. (.45 mm) per revolution of the cutter at the lowest speed was the largest possible without chipping the crystal. As soon as the cut had been completed, the exposed surface was painted with a solution of polystyrene in carbon tetrachloride. A suitable shaped crystal was cut and stuck to the sample holder with Araldite. This method gave a very flat and accurate cut.

Crystal alignment technique.

After the crystal had been stuck to the sample holder in the appropriate orientation the two were mounted on a "Techne" two circle optical goniometer.

It was found that due to some inaccuracy of construction of the goniometer, the axis of the vertical circle was not perpendicular to the plane containing the telescope and collimator when the horizontal circle reading was 90°. A .1 inch slip gauge, whose faces were optically plane parallel was fixed with plasticine to the goniometer head. The horizontal circle and the goniometer head were both adjusted until the reflections from the two faces of the gauge were successively on the cross-hairs of the telescope. This occurred at a reading of 89° 12', so 48' was added to all horizontal circle readings. The corrected readings will be quoted in all cases.

The sample holder orientation was adjusted so that the reflections from both small mirrors occurred at 90° on the horizontal circle. The mirror and crystal face normal directions were each measured at least twice. In many cases the reflections were very diffuse. The contrast of the image could often be increased by a variation of the Foucault test (12/3). A straight edged piece of black card was held between the eye and the eyepiece. It was moved across the eyepiece, and the distance was varied until the field of view blanked out uniformly. At other distances one side of the field blanked out before the other. The direction of the card edge was also varied, keeping it perpendicular to the telescope axis. At one position the background brightness decreased considerably, but the reflection intensity was little reduced. It was

therefore possible to attain higher accuracy in the face normal direction measurement. The effect is not easy to explain, but as in the true Foucault test, only light going in exactly the right direction can pass the card, while the diffuse light is intercepted by it.

After the above measurements, the crystal holder was pushed into the coil former. It was necessary to make one of the two mirrors on the sample holder parallel to the mirror on the probe unit. The coil former and sample holder were therefore placed in a jig (Fig.4).

The semicircular slot is accurately perpendicular to the base of the jig. The rectangular slot is parallel to the base and to the sides. The jig and coil former were placed on a plane mirror, then a white straight edge was held parallel to the jig axis about 40 cm above the mirror. On looking vertically downwards from above the straight edge it was possible to see it imaged in the mirror on which the jig was resting. The jig position was adjusted until the image was along the axis of the coil former, then the sample holder was twisted until the straight-edge image in the small mirror was colinear with the other image. The two mirrors were then parallel in a direction perpendicular to the holder axis. To measure the deviation of the small mirror in the direction of the axis, the straight edge was turned through 90° in a plane parallel to the mirror.

An image of the straightedge was visible in each mirror. The separation of the two was determined by comparison with the gap between the jaws of a micrometer. The reproducibility was about .01 inches (.25 mm), equivalent to about 2 minutes of arc.

The misalignment of the other small mirror was similarly measured after turning the jig so that it lay on one side.

This procedure makes one mirror parallel to the mirror on the heat leak and determines the error of the axis defined by the two mirrors relative to the probe axis.

The sample holder was lightly glued to the coil former with "Durofix" or polystyrene cement.

The coil former was pushed into the heat leak until it engaged in the semicircular slot. It was followed by a copper earth block, a spring washer and a screw plug. The earth end of the coil passes through a hole in the earth block and contact is made by a 6 BA screw which holds the wire down. After this the whole probe was put in the Dewar, which was already in its cage. A permanent mark on the Dewar was always placed under the same screw in the cage.

Once the probe was in place it was necessary to compare the azimuth of the normal to the mirror on the heat leak relative to the scale on the base of the magnet.

A 2.5 cm diameter circle of surface aluminised mirror was stuck with Araldite to an aluminium block, all of whose faces were

accurately perpendicular to each other. The block was made from aluminium so that it would not damage the magnet pole pieces when it was wedged just in front of the probe with a piece of thick card. It was also possible to make azimuth measurements while the magnet was on.

A collimator was set about 2m from the two mirrors and threw a parallel beam of light on both mirrors. It was found that the Dewar walls behaved as a weak cylindrical positive lens. Maksutov (13/3) showed that the inverse focal length of a shell of a sphere is approximately

$$\frac{1}{f} = -\frac{d}{R_1^2}\frac{(n-1)^2}{n^2}$$

where d is the thickness of the shell,

R_1 is the radius of the concave surface,

n is the refractive index of the material of the lens.

Substituting appropriate values for the Dewar, the focal length is about -44 cm. A small positive cylindrical lens of 50 cm focal length (2 dioptres) was fixed to the aluminium block to compensate for the Dewar lens. In this way the reflection from the small mirror on the heat leak was reduced in width from about 15 cm to 7 cm.

By suitable adjustment of the height of the collimator, the magnet azimuth, and the aluminium block, it was possible to centre the reflection from the large mirror on the reflection from the probe

mirror, the light from both mirrors falling on a strip of tracing paper fixed about 10 cm above the collimator. The repeatability was much better than 0.1°. It is obvious, if the separation of the mirrors in the direction of the collimator is small, that they are parallel in azimuth.

The probe azimuth was usually checked a few times during a set of spectra, since it could be disturbed when the Dewar was filled with coolant.

Magnetic field measurements.

The apparatus which was used to measure the magnetic field strength is shown in Fig. 7. Many parts of it were common with the main spectrometer, so for each field measurement certain connections in the main spectrometer were altered to form the field measuring equipment. The signal generator was a Marconi type TF 2002, but for later spectra a Schlumberger FSX 3003 frequency synthesiser was used.

Since the signal generator gave a maximum frequency of 70 MHz, and a frequency of 120 MHz was required, its frequency was multiplied by placing a BA 110 varactor diode across the output. The first harmonic frequency was measured with a Hewlett-Packard 5253B heterodyne frequency converter on a model 5245L frequency counter. A flexible wire, about 2m long, was soldered to the live end of the diode, then a few turns of it were wound round the probe

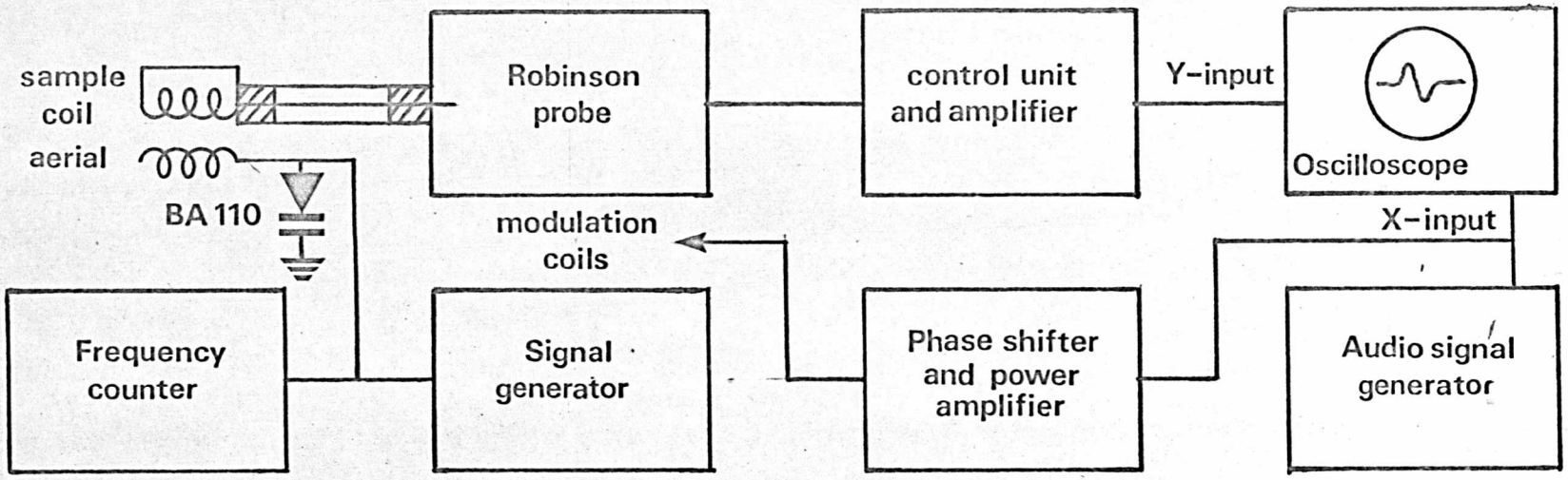

Figure 7 Field measuring apparatus

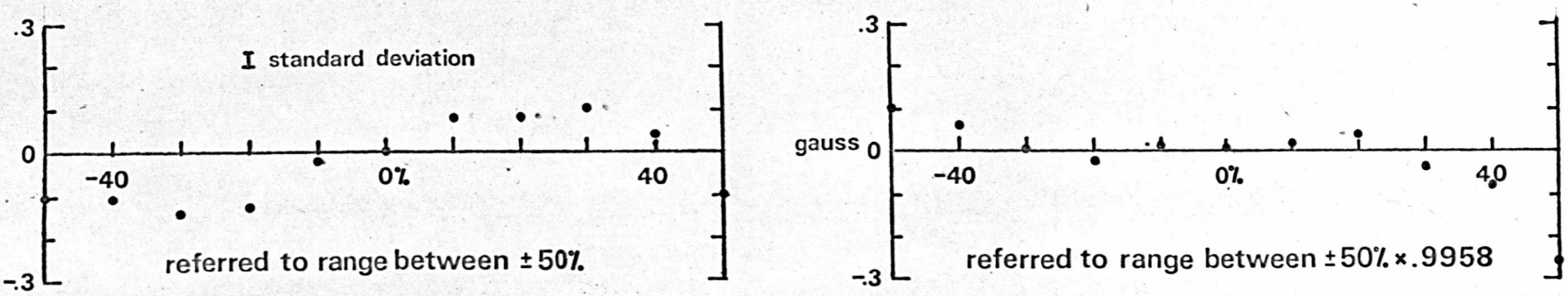

Figure 8 Graphs of Fieldial 100g. sweep range non-linearity.

unit. At the maximum output level of the generator it was found that the oscillator would lock on to the generator frequency over a small range. A nuclear resonance signal could thus be moved on the oscilloscope display by changing the generator frequency.

At very high generator levels a curious effect was noted. If the oscillator was locked onto the generator as above, then detuned, it went out of lock and the difference frequency could be seen on the oscilloscope. On further detuning the difference frequency could no longer be seen. The line shape changed from derivative of absorption to pure absorption, and its strength increased from about .5 volts p/p to nearly 5V. Its position was still controlled by the generator frequency. No explanation can be given for this phenomenon.

Sweep calibration.

The magnet system was allowed to settle down for several hours, then the field measuring spectrometer sample was placed in the position of maximum homogeneity. The modulation frequency was set at 50 Hz, and the depth was about 2 gauss, then the phasing was adjusted until the two proton magnetic resonance signals were coincident on the oscilloscope display (deep sinusoidal modulation gives two signals per cycle). The generator frequency was altered until the spectrometer was in lock. Fine frequency adjustment brought the signal exactly to the centre of the display, at which point the generator frequency was noted. This was repeated until two

readings agreed to within 0.2 kHz. The main source of inaccuracy was jitter in the signal generator output frequency. This was removed in the later measurements by the use of a Schlumberger FSX 3003 frequency synthesiser.

The field sweep was calibrated at 10% intervals on the 100 gauss range. The time of each measurement was noted, then the whole set was repeated. Two field measurements were made with the sweep range off, one at the start and one at the end of the series, so the calibration measurements could be corrected for drift. From these a graph of the deviation from linearity of the sweep was drawn. Two such graphs drawn from measurements made five months apart were compared, the r.m.s. deviation was about .03 gauss. Least squares analysis showed that the field sweep was most linear when referred to a range .42% less than the range between +50% and -50% on the sweep dial. Figure 8 shows the departure from linearity. The corrections for the 250g range were found to be 2.5 times greater than for the 100 g range. This effect must have been due to non-linearity in the field sweep potentiometer. Suitable corrections were included in the computer program DRIFT (Chapter IV).

The sweep range was measured for each rotation pattern. Unless adjustments had been made to the magnet control loop, the sweep range varied no more than 0.1%.

Some measurements were made to check the reproducibility of

a setting on the sweep dial. The sweep range was set to 2.5 kG, then after adjusting the sweep dial to +1 %, the field was measured. The probable error of a single observation was 1.7g, equivalent to about .07g on the 100g range.

Running a single spectrum.

Measurements were made to determine the oscillator frequency and magnetic field drift rates, as well as the absolute positions of resonances. The sequence of operations for a typical spectrum is given below.

The field and frequency were first adjusted to values close to those required.

1) Turn the magnet round to 90° on the rotation scale, then slide the main probe backwards so that the field measuring oscillator can be put in place. Make the appropriate connections for the field measurement, which is made as described above. This is made with the sweep range switch in the off position. The frequency and time of measurement are noted.

2) Slide the main probe back in place and turn the magnet to the required orientation.

3) Measure the Robinson oscillator frequency by observing the zero beat with the signal generator on the oscilloscope. (It was found that the leakage from the frequency counter connected to the signal generator was sufficient to give a strong

beat signal. If the signal generator level was too high, it could pull the oscillator frequency by up to 100 Hz.) The time of measurement is noted.

4) Set the modulation phase to the value which gives maximum signal to noise ratio, and the depth to a suitable value.

5) Set the sweep range and sweep time to the required values, then adjust the sweep dial to a little below the starting percentage of the sweep range. Use the drive motor to drive it to the starting value and stop there. Make sure that the pen recorder chart is moving, then simultaneously start the sweep and move the fine pen position control quickly to make the start reference mark. Note the run start time and percentage.

6) At the end of the run make an end reference mark on the chart as before, when the sweep dial passes some integral percentage. Measure the oscillator frequency, turn the magnet back to 90° and remeasure the magnetic field strength with the sweep range switch in the off position.

Two rubber stamps were used to facilitate making the records for each spectrum.

The use of these readings is described in the next chapter.

CHAPTER IV

Calculations

Since the methods of calculation are so dependent on the experimental technique, a separate chapter is devoted to them.

The programs are so arranged that as much as possible of the calculations were done on the University of Warwick's Elliott 4130C computer, but without losing touch with the intermediate parts. The data reduction was made in several steps so that any errors could be detected before the next stage was begun.

Several programs were written in the algolrithmic language ALGOL (1/4, 2/4). The texts of these are not here, but are available from Dr.J.A.S.Smith (School of Molecular Science, University of Warwick). Figure 1 shows a block diagram of the data reduction, and a short description of each program follows.

In many cases the ALGOL representation of mathematical relationships will be used to facilitate comparison of the following descriptions with the program texts. Identifiers of variables can contain more than one letter, and the symbol * is used for multiplication.

1. DRIFT

This program calculates the position of each spectral line observed, relative to the position at which the absorption of liquid heavy water would occur at the given radio frequency. The positions are corrected for instrumental drift (assumed to be linear with time),

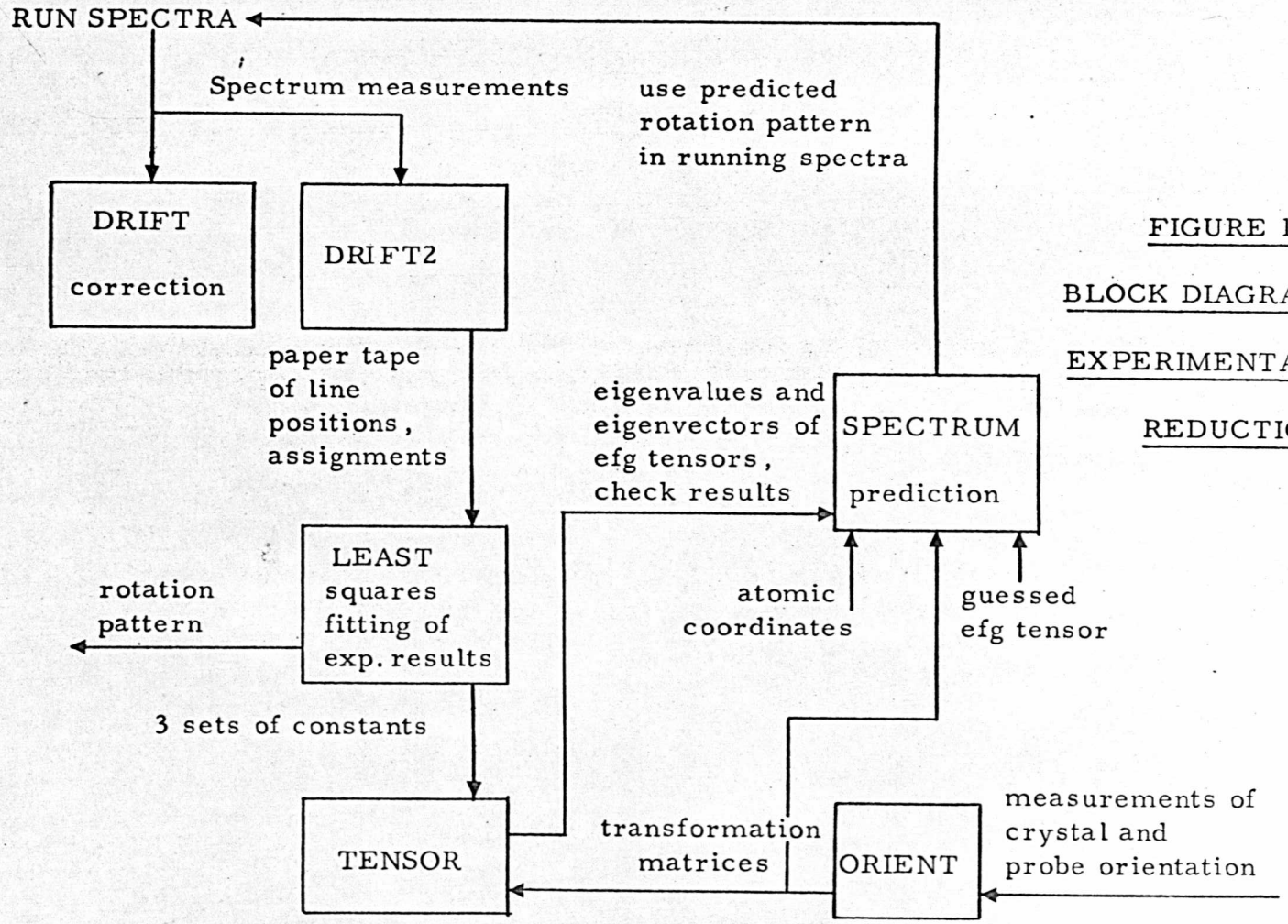

FIGURE 1

BLOCK DIAGRAM OF EXPERIMENTAL DATA REDUCTION

and non-linearity of the Fieldial sweep potentiometer (see chapter III p.36).

The input data for the program is :-

A string, enclosed in string quotes, the reference number of the particular spectrum.

THETA, the reading of the magnet rotation scale in degrees.

TFB the time of measurement of the oscillator frequency at the beginning of the run, in minutes.

FB the oscillator frequency at the beginning of the run, in kHz.

TFE,FB, quantities corresponding to TFB and FB, measured at the end of the run.

TFFB, FFB, TFFE, FFE, correspon d to TFB, FB, TFE, FB, but refer to the measurement of the proton magnetic resonance frequency in the magnetic field used, determined before and after the run. The units of the PMR frequency are kHz. See the note at the end of this list.

T, the time at which the first mark was made on the recorder chart (see chapter III p39).

TR, the sweep time in minutes.

PS, the sweep dial reading at the start of the spectrum.

PE, the sweep dial reading at the end of the spectrum.

I, the number of times which the sweep dial passes from +50% to -50%. The sweep direction is always such that the magnetic field strength increases with increasing time.

SR, the distance between the two marks on the spectrum.

SW, the difference, in gauss, between the field strengths at -50% and +50%, on the sweep range used.

RANGE the nominal sweep range used.

In order to save card punching time, the frequencies and magnetic field strengths noted above are not given as their actual values. The oscillator frequency is set to some nominal value, say 18.235 mHz, at the start of the run, and the magnetic field is set to an appropriate value. The radio-frequency is chosen so that the resonances of interest will fall at a magnetic field corresponding to a PMR frequency of 119.0 to 119.4 mHz, the range where maximum field homogeneity is obtained. FB and FE are the differences of the actual oscillator frequencies from the nominal. FFB and FFE are referred to the nominal oscillator frequency times 6.514196, which is equal to γ_H/γ_D (γ_H from 3/4, γ_D from 4/4).

The following relationships can easily be derived :-

TC = T - PS * TR/100.0

where TC is the time at which the sweep dial passes through 0%

X = (FFE-FFB)/((TFFE-TFFE)*4.2576)

Y = (FE-FB)/((TFE-TFB)* .6536)

The combined drift rate of the oscillator and magnet, in gauss per minute, is :-

B = X - Y

The error in the field strength, in gauss, when the sweep dial passes through 0% is :-

A = (TC-TFFB)*X-(TC-TFB)*Y+FFB/4.2576-FB/ .6536

The drift rates have now been calculated. It is then necessary to find the spectral line positions from measurements on the spectra. The scale of the spectra is :-

S = (102.8*I+PE-PS)/SR percent of sweep dial/cm.

The multiplier 102.8 comes from the fact that there is a gap equivalent to 2.8% between -50% and +50% on the sweep dial. Thus the sweep dial sweeps out (100 + 2.8)% in one revolution. The gap was measured with a steel ruler and compared with the percentage divisions on the sweep dial.

The value of SW is decreased by .42% to give the maximum sweep linearity (see chapter III p39).

The next number on the data card is K, the number of lines in the spectrum, followed by K line-centre distances, DIST [J] , measured from the first mark made on the spectrum. A short note on spectrum measurement is given in the description of the program SIMULATE. The percentage at which the J th line appears is given by

$$P = PS + S^* DIST[J]$$

A small correction, CORN, based on the value of P is calculated - it compensates for the sweep non-linearity. The position, LP [J], of the J th line is

$$LP[J] = (SW+B^*TR)^*P/100.0 + A + CORN$$

The program outputs a table of the line positions, preceded by the spectrum reference number, magnet rotation angles and total drift rate. The sweep dial percentage for each line is printed out for diagnostic purposes.

2. SIMULATE.

A little difficulty was encountered in finding the centre of a line which overlapped with another line. A program was written, which would simulate any nuclear resonance spectrum, using the digital graphplotter as the output device. In this case, a first derivative Gaussian line shape was used, and lines of varying overlap were drawn. In measuring spectra, a base line was first drawn, then any overlapping lines were compared with the simulated ones. A line, perpendicular to the direction of motion of the chart paper, was drawn from the line centre to intersect with the baseline. Finally the line-positions relative to the first mark on the spectrum were measured with a steel ruler.

The rotation pattern was plotted out by hand from the results of DRIFT and compared with the uncorrected pattern which had been

plotted as the spectra were run. Most gross differences arose from errors in the input data for DRIFT. Any residual points were noted and rejected at a later stage.

3. DRIFT 2.

This program only differs from DRIFT in that it produces an 8-hole paper tape containing the coordinates of each point on the rotation pattern. It includes the points which have already been found to be bad ones. The paper tape is used as data for the next program.

4. LEAST.

Each line in the rotation pattern drawn from the results of DRIFT was given an integer number. Each point whose coordinates were given in the paper tape from DRIFT 2 could be assigned to a particular line. These assignments, in the order of the points on the tape, were punched on cards. There were also other data on the cards which controlled the format of the program output.

On reading an integer N, the assignment of a point, from the card, the computer assigns the next number on the paper tape to the next free element of the N th row of an array MTHETA. The following number on the tape goes into the corresponding element of an array MDELTAF. Facilities exist for rejecting points which are obviously a long way from any line, and for assigning one point to more than one line, as happens at a crossing of two or more lines. In general, the assignments and paper tape were checked in a small program,

SORT or SORT2, both of which were almost identical with the section of LEAST described above.

The program continues by fitting each line to the function :-

$$y = a + b \sin 2\theta + c \cos 2\theta$$

where y is in gauss,

θ is the magnet rotation angle

a, b, c are the constants to be determined.

The method used is described in chapter II, page 12. On the first pass it calculates the constants a, b, c, and the distance of each point from the line. Any point which is more than two standard deviations (this distance is called LIMIT in the program) is rejected, and the least squares line is recalculated if one or more points have been removed. With the usual number of points on one line, this procedure would be expected to remove about 5% of the points, and this was found to be true. We could justify the removal of a few points, since it was known that the magnet control system occasionally failed for a short time. The program gives a record of the points removed, the values of a, b, c and their variances, and a table of the line positions and errors on both passes. The variances of a, b and c were usually reduced by 30-50%. Finally, the rotation pattern was drawn by the digital graphplotter. The scale, graduations on the axes, and the title were

FIGURE 2 PART OF THE OUTPUT OF THE PROGRAM LEAST

POTASSIUM SULPHAMATE B-AXIS AT CARDICE TEMP

LINE 1

INPUT DATA AND FIRST ERRORS

THETA	DELTAF	DELF(CALC)	ERROR
0.0	125.1	123.9	1.2
10.0	137.0	136.9	0.1
20.0	131.2	132.8	-1.6
30.0	112.1	112.1	0.0
40.0	78.4	77.3	1.1
60.0	-16.1	-16.8	0.7
70.0	-63.3	-64.6	1.3
80.0	-106.6	-105.3	-1.3
80.0	-103.7	-105.3	1.6
85.0	-121.4	-121.3	-0.1
90.0	-135.7	-133.8	-1.9
100.0	-147.3	-146.8	-0.5
100.0	-147.9	-146.8	-1.1
100.0	-147.6	-146.8	-0.8
110.0	-143.4	-142.8	-0.6
120.0	-120.8	-122.0	1.2
130.0	-83.7	-87.2	3.5
140.0	-43.1	-42.5	-0.6
150.0	6.4	6.8	-0.4
160.0	54.4	54.7	-0.3
170.0	93.7	95.3	-1.6

SIGMA SQUARED = 34.7

A = -4.97 B = 60.78 C = 128.86

VARIANCES ARE 0.29 0.44 0.37

LIMIT= 2.78

POINT AT THETA= 130.0 REMOVED

1 POINT REMOVED

THETA	DELTAF	DELF(CALC)	ERROR
0.0	125.1	123.7	1.4
10.0	137.0	136.9	0.1
20.0	131.2	132.9	-1.7
30.0	112.1	112.3	-0.2
40.0	78.4	77.5	0.9
60.0	-16.1	-16.5	0.4
70.0	-63.3	-64.5	1.2
80.0	-106.6	-105.3	-1.3
80.0	-103.7	-105.3	1.6
85.0	-121.4	-121.4	0.0
90.0	-135.7	-134.0	-1.7
100.0	-147.3	-147.2	-0.1
100.0	-147.9	-147.2	-0.7
100.0	-147.6	-147.2	-0.4
110.0	-143.4	-143.2	-0.2
120.0	-120.8	-122.6	1.8
140.0	-43.1	-43.1	-0.0
150.0	6.4	6.2	0.2
160.0	54.4	54.2	0.2
170.0	93.7	95.0	-1.3

SIGMA SQUARED = 20.2

DELTAF =

-5.145 +61.24*SIN 2THETA +128.9*COS 2THETA GAUSS

VARIANCES ARE

0.23 0.37 0.29

THERE ARE 20 POINTS LEFT

supplied as data on cards. Figure 2 shows part of the lineprinter output of the program.

5. ORDER

The program LEAST fits the experimental data to the function predicted by first order perturbation theory. It was necessary to see if any higher order terms were required. The program ORDER fits the data to the function :-

$$y = a_o^o + \sum_{n=1}^{N} \left(a_n \cos 2n\theta + b_n \sin 2n\theta \right)$$

It uses the same methods as LEAST, but does not output a graph.

6. ORIENT.

This program determines the unitary matrix which transforms the orthogonal crystallographic axes to the fixed laboratory axes.

The right-handed sets of axes used were :-

i) orthogonal crystallographic axes, a', b', c'. In the case of cupric acetate, which is monoclinic, a' and b' were coincident with the crystallographic a and b axes respectively. c' was perpendicular to a' and b'. For orthorhombic potassium sulphamate, the a' b' c' set was coincident with the crystallographic set. In both cases, one unit displacement along the a' axis was equal in length to one unit along the b' or c' set. This is not generally true of the crystallographic set.

ii) goniometer based axes. The x axis is towards 0° on the vertical circle of the goniometer, the z axis towards 90°, and the y axis along the axis of rotation of the circle.

iii) fixed laboratory axes. The Y axis is vertically downwards, the Z axis towards 90° on the magnet rotation circle, and the X axis towards 180°.

iv) rotated magnet axes. These are embedded in the magnet and rotate with it. They are coincident with the fixed laboratory set at zero degrees rotation. The positive rotation direction is taken to be clockwise looking from above the magnet.

The input data for the program are :-

i) the number of faces, NF, on the crystal.

ii) NF sets of numbers. First, the estimated statistical weight of the measurements for one face, followed by the corrected goniometer horizontal and vertical circle readings. If the weight is zero, this means that the particular face was not measured. The data for the next face follow immediately.

iii) for each of the NF faces, the theoretical direction cosines of the face normals in the orthogonal crystallographic axes. These were calculated by hand.

iv) an approximate matrix for the transformation of the orthogonal crystallographic axes to the goniometric set. The matrix is called TRANS, and needs only to be very approximate, since

the program can tolerate errors of up to about 10° in the directions of the crystal axes.

v) The angular distance, THETA, from the direction of the zero on the magnet scale to the direction of the zero on the goniometer vertical circle. If M is the azimuth of the normal to the probe mirror relative to the zero on the magnet circle (measured as in chapter III, page 33), and S is the azimuth of the mirror on the sample holder which is parallel to the probe mirror, relative to the zero on the goniometer vertical circle, then it can easily be shown that

THETA = S - M.

vi) The misorientation of the sample holder in the coil former, as measured in chapter III, page 33. The deviation of the mirror which was parallel to the probe mirror was given first, followed by the deviation of the other mirror. The sign of the deviation is positive if the normal to the mirror had a component in the downward (positive laboratory Y- axis direction). One mirror always had the normal to its front surface nearly parallel to the positive laboratory Z direction. In the case of the other mirror on the sample holder, the sign of the deviation was deduced from the direction of the normal running in the same direction as the positive X axis of the laboratory set.

The program first calculates the direction cosines of the normals to the measured faces, referred to the goniometer axes. It then

transforms the theoretical direction cosines, using TRANS, so the face normals of the 'theoretical crystal' are approximately coincident with the measured face normals. The objective is to minimise the sum of the squares of the angles between the normals to the theoretical crystal faces and the normals to the corresponding measured crystal faces. These angles are called error angles. A real procedure ANGLE2 calculates the square of the error angle for each face, and another real procedure ERRSUM adds up the products of ANGLE2 and the statistical weights. ERRSUM is a measure of the closeness of fit of the transformed 'theoretical crystal' to the measured crystal. The value of ERRSUM is assigned to a variable SUMO at the start of the minimisation. The program sets up three rotation matrices XROT, YROT, ZROT, which, in effect, rotate the theoretical crystal through a small angle, initially 4×10^{-4} radians (1.5' of arc), about the X, Y, Z goniometric axes respectively. The matrix product XROT*TRANS thus transforms the 'theoretical crystal' as described above, then rotates it through 4×10^{-4} radians about the X goniometric axis. This is done, and a new value of ERRSUM is calculated. The difference, GRADX, between SUMO and ERRSUM is nearly proportional to the first derivative of ERRSUM with respect to rotation about the X goniometric axis. Identical rotations about the Y and Z axes give similar quantities GRADY and GRADZ. The quantities THETAX, THETAY, THETAZ are then calculated. They are the magnitudes of small rotations of the crystal made about each of the three goniometric

axes. They are proportional to GRADX, GRADY, GRADZ respectively, and the step length, given by

$$(\text{THETAX}^2 + \text{THETAY}^2 + \text{THETAZ}^2)^{\frac{1}{2}}$$

is kept at 8×10^{-3} radians (about $\frac{1}{2}$ degree).

The product XROT*YROT*ZROT*TRANS is therefore a better transformation matrix. A variable called SUM1 is set equal to the new value of ERRSUM. If it is less than SUMO, then the step was successful, so SUMO is set equal to SUM1 and the program starts another cycle of optimisation. Otherwise, the step length was too great, so it is reduced to .6 times its previous value, SUMO is set equal to SUM1, and the program returns to the start. It continues in this way until the stepsize is less than 4×10^{-4} radians, then exits to the next section.

Since the rotation matrices use the approximations

$$\sin \theta = \theta, \cos \theta = 1,$$

the new transformation matrix TRANS is no longer unitary after several cycles of optimisation. The rows of TRANS are made orthonormal, then the stepsize is set to 2×10^{-3} radians and ERRSUM is minimised as before. The matrix TRANS is printed out, followed by the error angles and statistical weights for each face. Finally, the last three numbers on the data cards are used to obtain the matrix for the transformation from orthogonal crystallographic axes to fixed laboratory axes. If any face had a very large error angle, its statistical weight was reduced, and the program was re-run.

This method of function minimisation using derivatives is rather inefficient, but in practice only 10-15 seconds of computer time were needed for the complete optimisation.

7. SPECTRUM.

The theory of this program, which predicts the rotation pattern for each deuteron in a single crystal, is given in chapter III, page 9.

The input data consist, in part, of :-

i) L, a control integer which determines the course of the calculations.

L = 1 for an axially symmetrical electric field gradient tensor.

L = 2 for a water molecule, or ND_2 group which is flipping about its two-fold axis.

L = 3 for a water molecule, or ND_2 group which is not flipping.

L = 4 for a deuterium atom whose electric field gradient tensor in orthogonal crystallographic coordinates is known.

The data following depend on L. All coordinates are given in the orthogonal crystallographic system, and all matrices are given row by row.

For L = 1, the coordinates of two points which define the Z axis of the efg tensor.

L = 2 or 3, the cordinates of the atoms D_1, O, D_2 (or D_1, N, D_2) followed by half the D-O-D (or D-N-D) bond angle in degrees.

For L = 4, no atomic coordinates are needed. In all cases give the diagonalised efg tensor, then for L = 4 only, give the eigenvectors

of the efg tensor. The last datum is the unitary matrix for the transformation of the orthogonal crystallographic axes to the fixed laboratory set, calculated in ORIENT.

Source of data.

The atomic positions come from X-ray or neutron diffraction structure determinations. Deuteron positions are guessed if not available, and the principal components of the electric field gradient tensor are estimated from the values for similar compounds.

In all cases except the one for which L = 4, the program calculates the directions of the principal components of the efg tensor from the given atomic coordinates, then it transforms the tensor into the orthogonal crystallographic system. It uses the theory given in chapter II, page 9 to calculate half the line splitting for each deuteron, at 10° intervals of magnet rotation angle from 0° to 180°. Up to nine line pairs can be handled. The positions of all the points are gathered together, and plotted on the same set of axes, on the lineprinter. All points on the first line are plotted as digit 1, on the second line as digit 2, and so on up to 9. This provides a very quick picture of the predicted rotation pattern, and is sufficiently accurate for most purposes. The exact figures are given in tables for each deuteron, together with various diagnostic results. Figure 3 shows a predicted rotation pattern.

The final experimental results were checked by running them through SPECTRUM with L = 4, then the predicted rotation patterns were compared with the experimental ones.

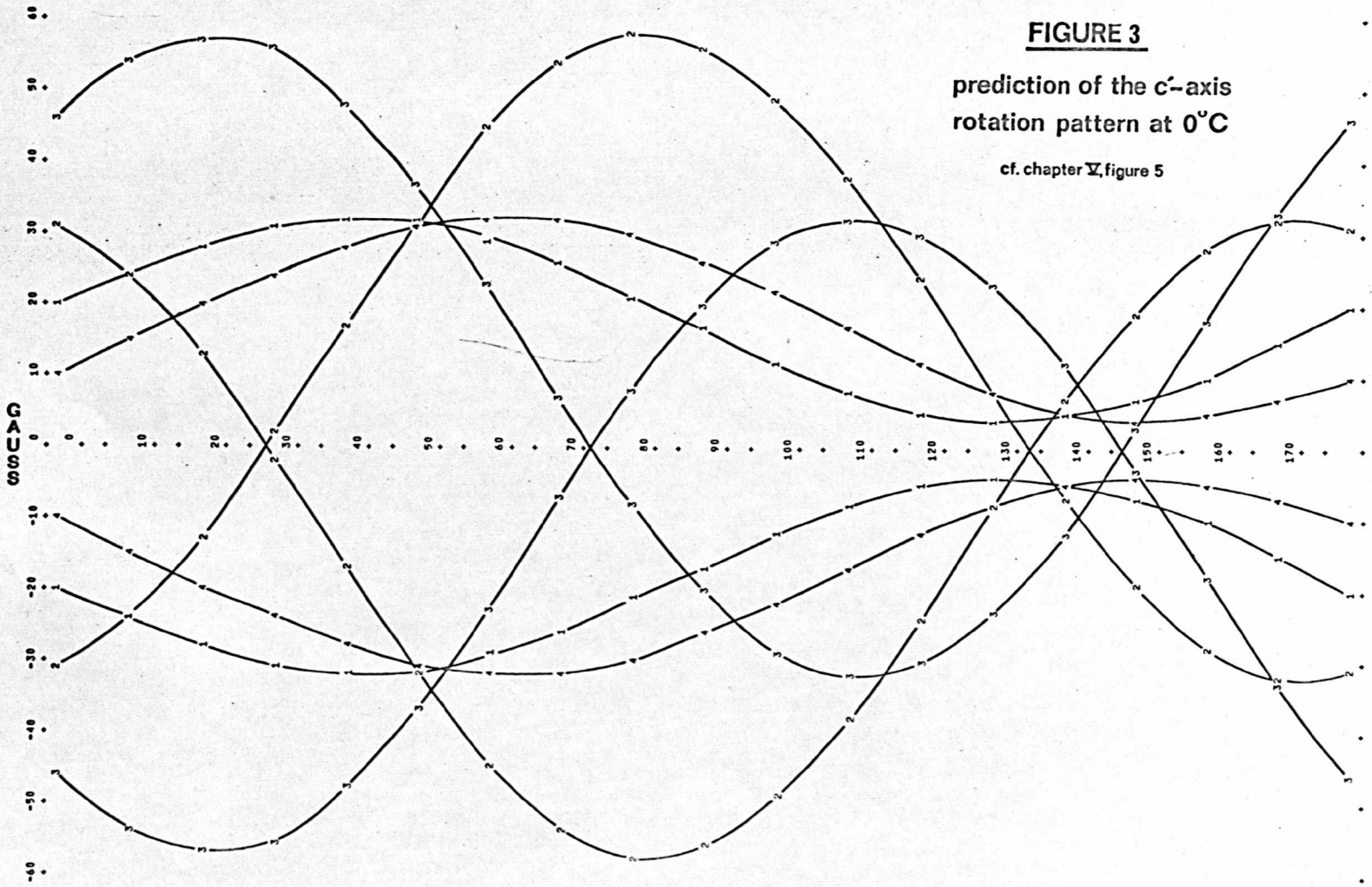

FIGURE 3

prediction of the c′-axis rotation pattern at 0°C

cf. chapter V, figure 5

8. TENSOR.

This program uses the experimental results from three rotation patterns to give the eigenvalues and eigenvectors of the efg tensor for each crystallographically different deuteron in the crystal. The treatment described in Volkoff (5/4) cannot be used, since the crystals were not aligned so that the magnet rotation axis was parallel to a crystallographic axis. The calculation is very nearly the reverse of that in the prediction program, SPECTRUM.

The program first reads in the transformation matrices, calculated in ORIENT, for each of the three rotation patterns. It then evaluates the 6- vectors MA, MB, MC (see chapter II, $_{p.11}$) for the 3 rotation patterns, and loads the nine vectors into a 9 x 6 array, AA. It can easily be shown (cf. chapter II, page$_{13}$) that :-

AA*PHI = CONST

where PHI is a 6 x 1 array related to the efg tensor in the orthogonal crystallographic coordinate system, and CONST is a 9 x 1 array containing the experimentally determined constants A, B, C, for the three rotation patterns. The three sets of constants are in the same order as the transformation matrices which were first read in.

We thus have nine simultaneous equations in the six unknowns. They are solved as in chapter II, page$_{12}$, then the elements of PHI are loaded into the 3 x 3 array ϕ. The library procedure SYMMETRIC QR 2 (6/4) is used to calculate the eigenvalues and eigenvectors of ϕ, which are then printed out. The eigenvalues are

in kHz.

To check the eigenvalues and eigenvectors, they were fed into SPECTRUM, setting L = 4, and the three rotation patterns obtained for each temperature were compared with the experimental results.

CHAPTER V.

CUPRIC ACETATE MONOHYDRATE DIMER.

RESULTS AND DISCUSSION.

V 1. Introduction.

Cupric acetate monohydrate dimer was chosen for study by deuterium magnetic resonance, since there was some doubt about the magnitude of the quadrupole coupling constant for a deuteron in a methyl group (1/5, 2/5, 3/5). Deuterated cupric acetate was easily made, and its structure has been determined by X-ray diffraction methods. It may have been possible to obtain some information about the interaction of the deuterons with the copper atom magnetic system, which would be expected to decrease the spin lattice relaxation time of the deuterons, thus giving a higher signal to noise ratio than that which would be obtained with a similar diamagnetic compound. Cupric acetate was also interesting, as it is the prototype of a series of copper (II) compounds of low magnetic moment (4/5).

V 2. The crystal structure of cupric acetate.

a) External morphology.

The form of the crystal has been described by Brooke, Schabus, Groth, and Hull (5/5, 6/5, 7/5, 8/5). The Miller indices given in Barker (9/5) were in an unspecified

coordinate system, and were of little use in assigning the indices of certain faces.

A drawing of a typical crystal, with the Miller indices of each face and the direction cosines of the face normals in the orthogonal crystallographic set of axes (see chapter IV, p.47), is given in Figure 4.

The crystal is monoclinic with a = 13.90 b = 8.52 c = 13.15Å, and β = 117°.0' (13/5).

Indexing the faces.

The crystallographic b axis was easily found, since it was perpendicular to a mirror plane. It was confirmed by taking a 15° oscillation photograph on a Unicam X-ray diffraction camera. The layer spacing was 8.56 ± .1 Å. (cf. 8.52 Å given above).

The other crystallographic axes were found by combining the results of optical goniometry and back-reflection X-ray diffraction photographs. The former results were difficult to interpret, since even very small crystals were badly formed. The measurements were put into the program ORIENT (chapter IV, p.47), which showed errors of up to 3.5°. The crystal was set on the X-ray camera goniometer head with the b-axis perpendicular to the rotation axis. 15° oscillation photographs of the crystal, first with the X-ray beam perpendicular to face 1, then perpendicular to face 2, showed

FIGURE 1.

The crystal structure of cupric acetate monohydrate

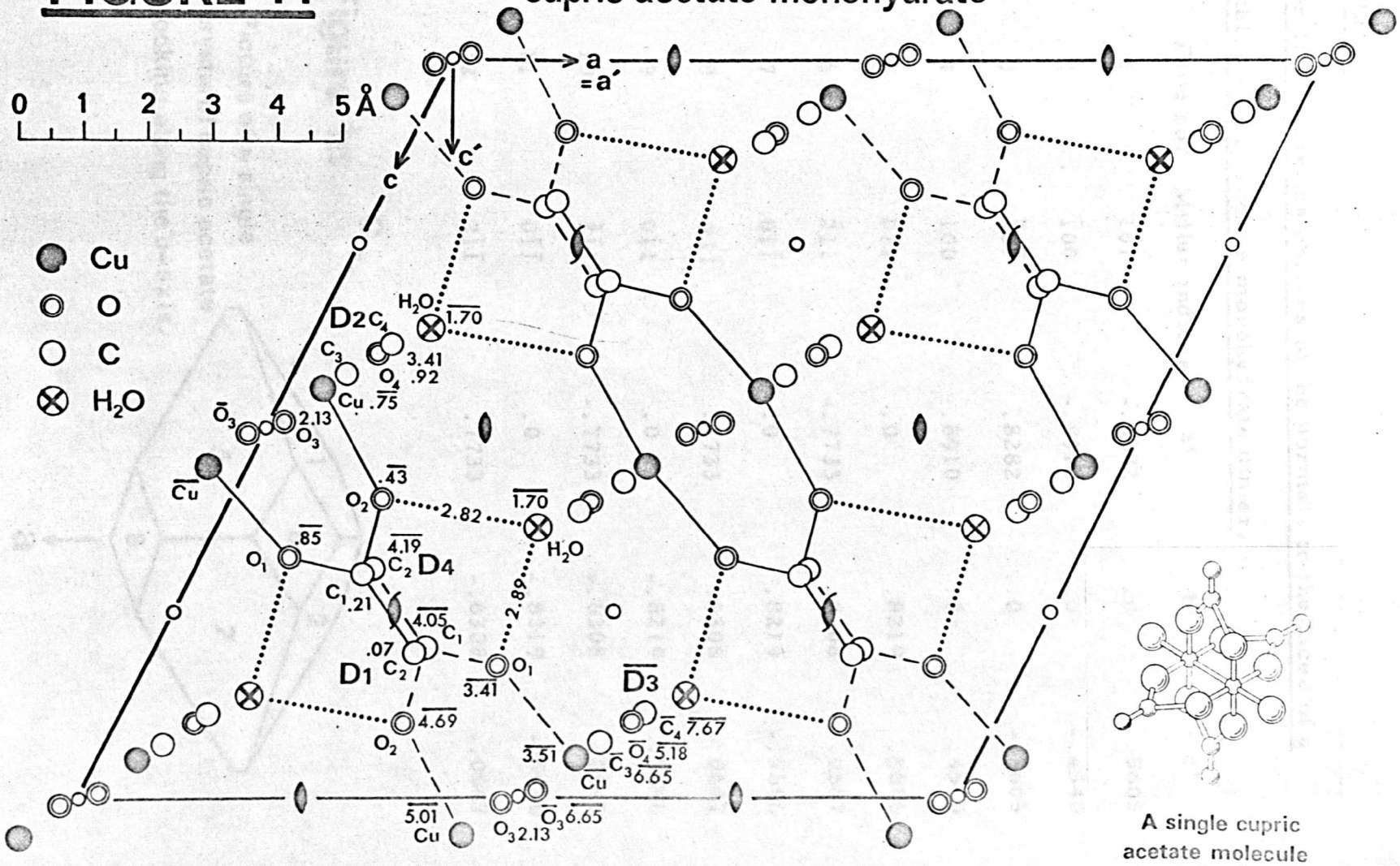

A single cupric acetate molecule

TABLE 1a

Theoretical direction cosines of the normals to the faces of a crystal of cupric acetate monohydrate dimer.

Face no.	Miller indices	a'	b'	c'
1	$\bar{1}0\bar{1}$	-.8282	.0	.5605
2	$\bar{1}00$	-.8910	.0	-.4540
3	$\bar{1}0\bar{1}$	.8282	.0	-.5605
4	100	.8910	.0	.4540
5	011	.0	.8219	.5696
6	$\bar{2}11$	-.7733	.6308	.0647
7	$01\bar{1}$	.0	.8219	-.5696
8	$21\bar{1}$	.7733	.6308	-.0647
9	$0\bar{1}1$	.0	-.8219	.5696
10	$\bar{2}\bar{1}1$	-.7733	-.6308	.0647
11	$0\bar{1}\bar{1}$	.0	-.8219	-.5696
12	$2\bar{1}\bar{1}$	.7733	-.6308	-.0647

Figure 1a

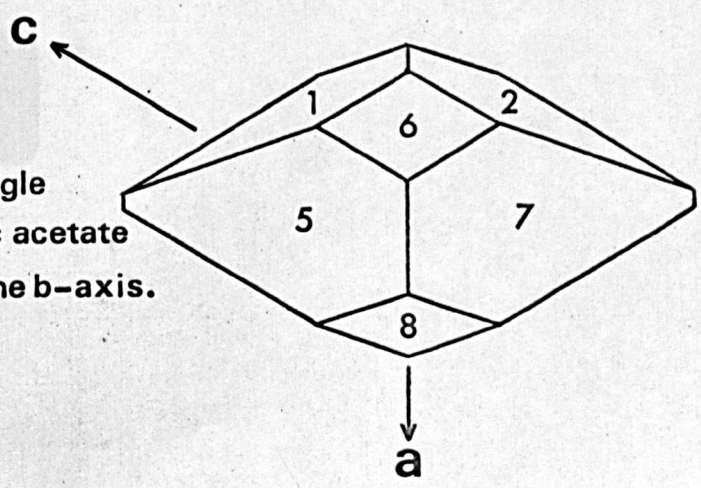

Picture of a single crystal of cupric acetate looking along the b-axis.

layer spacings of 14.3 ± .2 and 13.4 ± .2Å. The first figure was greater than any of the unit cell axial lengths, so the oscillation axis could not have been coincident with any of the crystallographic axes. It was easily shown (10/5) that the repeat distance between ($\bar{1}$0 1) planes of cupric acetate was 14.15Å. Face 1 was therefore ($\bar{1}$01). The layer spacing deduced from the other photograph was, within experimental error, equal to the repeat distance along the a-axis, so the face was ($\bar{1}$00) or (100).

The Miller indices of the remaining faces were found using the optical goniometric data and the Weiss zone law (11/5). The faces {211} were especially difficult to assign, as their normals were several degrees away from the expected places.

The table of direction cosines of the face normals was calculated by hand, using elementary coordinate geometry.

b) Crystal structure and the deuterium magnetic resonance spectrum.

The structure of cupric acetate has been determined by van Niekerk and Schoening (13/5), using the X-ray diffraction method. The unit cell, of dimensions a = 13.90, b = 8.56, c = 13.15 Å, β = 117° 0', contains four $Cu_2(CH_3COO)_4 2H_2O$ molecules. The space group is C2/c (Number 15 in the International Tables, ref. 14/5). A projection of the structure on the a c plane, and a drawing of a single molecule are shown in Figure 1. The numbering of the atoms in the drawing and

TABLE 1.

Orthogonal coordinates of atoms in cupric acetate monohydrate dimer.

i) Molecule at (0, 0, $\frac{1}{2}$).

Atom	a'	b'	c'
Cu	-2.075	-.750	5.273
O_1	-2.638	.852	7.932
O_2	-1.138	-.426	7.007
O_3	-2.701	2.130	5.765
O_4	-1.179	.920	4.687
H_2O	- .356	-1.704	4.300
C_1	-1.492	.213	8.167
C_2	- .703	.068	9.456
C_3	-1.673	2.130	5.003
C_4	- .978	3.408	4.511

ii) Molecule at ($\frac{1}{2}$, $-\frac{1}{2}$, 1).

Atom	a'	b'	c'
Cu	.070	-5.010	12.303
O_1	.633	-3.408	9.643
O_2	- .867	-4.686	10.569
O_3	.696	-2.130	11.811
O_4	- .826	-3.340	12.889
H_2O	-1.649	-5.964	13.275
C_1	- .513	-4.047	9.409
C_2	-1.302	-4.192	8.120
C_3	- .332	-2.130	12.572
C_4	-1.027	- .852	13.064

in Table 1 follows that in the paper by van Niekerk and Schoening.

The main feature in the structure is the close proximity of two copper atoms, which are joined by four acetate groups. There is one water molecule attached to each copper atom, and each copper acetate dimer unit is linked to four other units by eight hydrogen bonds through these water molecules.

In predicting the deuterium magnetic resonance spectrum we assume that the methyl groups are rotating at a rate fast compared with the quadrupolar coupling constants, since many studies have shown that the barrier to rotation is only about 1.2 kcal/mole. (15/5). Each magnetically non-equivalent methyl group will thus give one line pair in the DMR spectrum.

There are four $Cu_2(CD_3COO)_4\ 2D_2O$ molecules per unit cell. The cell is centro-symmetric, with two magnetically different molecules, related to two equivalent molecules by a centre of symmetry at ($\frac{1}{2}$, 0, $\frac{1}{2}$). We will consider the molecules whose centres of symmetry are at ($\frac{1}{4}$, 0, $\frac{1}{2}$) and ($\frac{1}{4}$, $\frac{1}{2}$, $\frac{1}{2}$), which are related by a two-fold screw axis passing through the point ($\frac{1}{4}$, 0, $\frac{3}{4}$). Each of these molecules contains four methyl groups, but since they are centro-symmetric, there are only two non-equivalent methyl groups per molecule. We thus predict that the methyl groups will give four line-pairs in the DMR spectrum

of the crystal. Similar arguments show that the water molecules will give rise to four line pairs if they are static, and two line pairs if they are flipping at a rate high compared with their quadrupolar coupling constants.

The four magnetically different methyl groups will be referred to as D1, D2, D3, D4. The coordinates of the methyl carbon atoms in the orthogonal crystallographic system are :-

	a'	b'	c'
D1	-.70	.07	9.46
D2	-.98	3.41	4.51
D3	-1.03	-.85	13.064
D4	-1.30	-4.19	8.12

The orthogonal crystallographic coordinates of the other atoms in the unit cell are given in table 1. They were obtained by transforming the coordinates in terms of the unit cell edges (Table 2 of 13/5) with the relationship :-

$$\begin{vmatrix} a' \\ b' \\ c' \end{vmatrix} = \begin{vmatrix} 13.90 & 0 & 13.15 \cos\left(\frac{\pi}{2} - \beta\right) \\ 0 & 8.52 & 0 \\ 0 & 0 & 13.15 \sin \beta \end{vmatrix} \begin{vmatrix} a \\ b \\ c \end{vmatrix}$$

where $\beta = 117^{\circ}\ 0'$, the angle between the a and c crystallographic axes,

a', b', c' are the orthogonal crystallographic coordinates,

a, b, c are the crystallographic atomic coordinates.

The precision given is higher than the experimental accuracy warrants, but the figures in Table 1 were used to avoid large rounding errors in the later stages. The coordinates were used later in the prediction and interpretation of the results.

V. 3. Experimental technique.

The method used to grow single crystals of deuterated cupric acetate have been described in Chapter III, page 26. Three crystals were grown, each with a maximum dimension of 14 - 15 mm. This was done so that a separate crystal could be used for each rotation axis, since a crystal which had been used, say, for the b-axis rotation pattern would not give a good filling factor ~~after it had been used~~ for the c-axis rotation pattern.

The crystals, especially those for the a and b-axis rotation patterns, were too large to fit in the sample coil. It was found that they could most easily be cut to size by grinding them on an electrically driven silicon carbide grindstone. This cut the crystal quickly and gave a very smooth and flat surface, without the danger of chipping it. The exposed surface was immediately painted with a solution of polystyrene in benzene to prevent deuterium exchange with atmospheric moisture. As well as adjusting the size of the crystal, a small flat was ground perpendicular to the appropriate rotation axis. This face and the sample holder were carefully cleaned with carbon tetrachloride, then the crystal was stuck to the sample holder with 'Araldite'. After

FIGURE 10. Two spectra of cupric acetate.

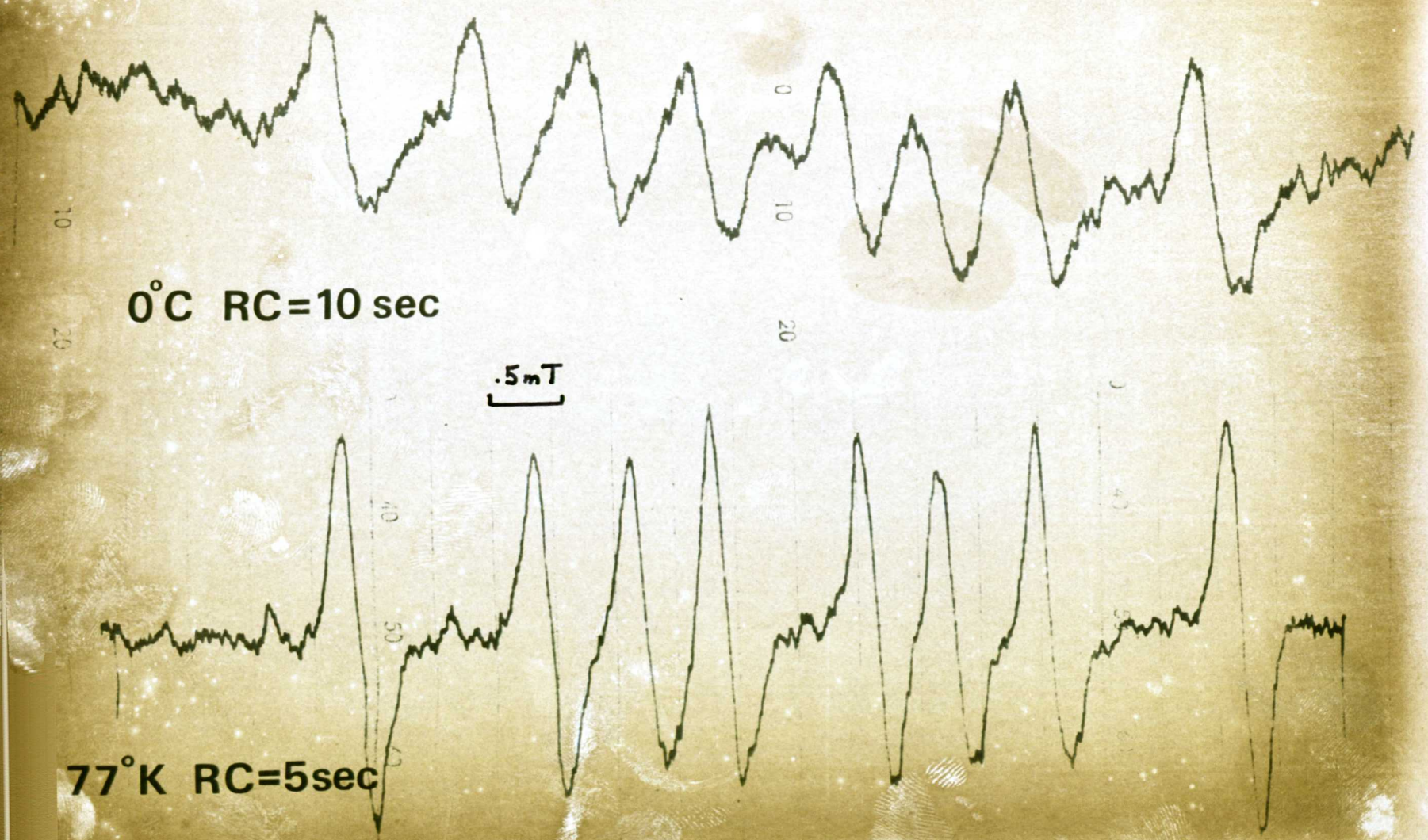

a few failures it was found that only 'Araldite' would give a good bond to the crystal, and that the minimum amount of the adhesive should be used. The probe unit was subject to cycling between room temperature and 77°K, because it did not contain enough liquid nitrogen to last overnight, and the crystal always cracked off at some stage. This is the reason why none of the rotation patterns at 273°K and 77°K were recorded with the crystal in the same orientation.

Experimental conditions.

The spectra were run as described in Chapter III, page 38. The conditions were as follows :-

Sweep rate	4 or 5 gauss per minute
Time constant	5 seconds for liquid nitrogen temperature, 10 seconds for 0° C runs
RF level	15 μA detector current, equivalent to about 110mV at the sample coil.

Figure 10 shows two typical spectra. The first was recorded with the crystal at 77°K, the second at 0° C. It can be seen that the low temperature spectrum shows a much greater signal to noise ratio and narrower lines than the spectrum recorded at 0° C.

V. 4. Experimental Results.

The results for each rotation pattern are given in the following order :-

i) the rotation pattern, as drawn by the program LEAST,

ii) the matrix for the transformation from orthogonal crystallographic

axes to fixed laboratory axes (Chapter IV, page47), calculated in the program ORIENT,

iii) a table of the coefficients a, b, c for each line in the rotation pattern, with the standard deviation of each at the 95% confidence limit (14/5, table 5). The numbers in the second column are those assigned to the lines for the program LEAST,

iv) a table of the line separations for each deuteron, with approximate standard deviations of each coefficient, again at the 95% confidence limit.

The units of the line separations are gauss, and the equations of the lines are of the form

$$y = a + b \sin 2\theta + c \cos 2\theta,$$

where y is the separation,

θ is the magnet rotation angle.

TABLE 2. Results for a' axis rotation pattern at 0° C.

Transformation matrix		a'	b'	c'
	X	.0987	-.9312	-.3513
	Y	-.9871	-.0466	-.1539
	Z	.1269	.3619	-.9235

Equations of lines

Methyl gp.	line no.	a		b		c	
D1	3	-1.50	.23	17.78	.31	18.39	.33
	6	5.76	.19	-18.97	.27	-18.16	.27
D2	4	7.83	.21	-35.96	.31	- 3.27	.33
	5	-4.62	.21	36.63	.29	2.78	.31
D3	1	-6.10	.25	- 4.54	.33	37.85	.40
	8	8.95	.23	3.83	.31	-37.11	.41
D4	2	-1.22	.23	12.34	.31	21.90	.37
	7	5.56	.23	-12.11	.42	-23.20	.44

Separations.

Methyl gp.	a		b		c	
D1	7.26	.15	-36.75	.20	-36.55	.21
D2	-12.45	.15	72.59	.21	6.05	.22
D3	-15.05	.17	- 8.37	.23	74.96	.28
D4	6.78	.16	-24.45	.25	-45.10	.29

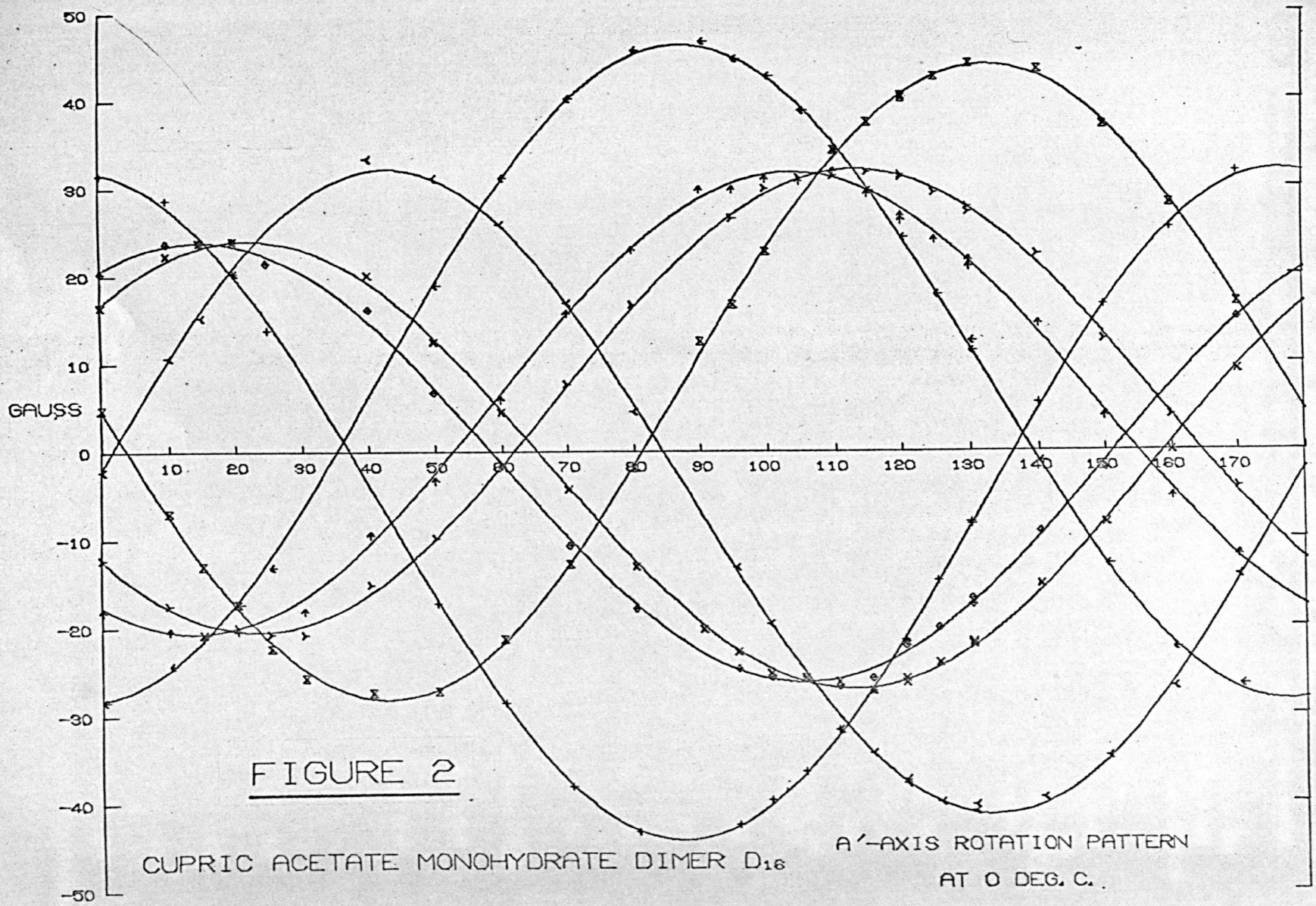

FIGURE 2

CUPRIC ACETATE MONOHYDRATE DIMER D_{16}

A′-AXIS ROTATION PATTERN

AT 0 DEG. C.

TABLE 3. Results for a' axis rotation pattern at 0°C (repeat).

Transformation matrix

	a'	b'	c'
X	.0408	.7558	.6536
Y	-.9992	.0375	.0191
Z	-.0101	-.6538	.7567

Equations of lines.

Methyl gp.	line	a		b		c	
D1	4	5.74	.27	-26.57	.35	- 1.56	.40
	5	-1.84	.27	24.37	.35	2.99	.37
D2	1	7.36	.27	-29.49	.37	21.29	.40
	8	-4.44	.18	28.54	.25	-21.61	.25
D3	2	-6.17	.29	20.71	.40	32.20	.40
	7	9.11	.29	-21.89	.40	-30.49	.43
D4	3	-1.42	.25	22.82	.33	9.07	.37
	6	5.28	.21	-24.71	.31	- 9.67	.33

Separations

Methyl gp.	a		b		c	
D1	7.58	.19	-50.94	.25	-4.55	.27
D2	-11.80	.16	58.03	.22	-42.90	.23
D3	-15.28	.20	42.60	.28	62.69	.29
D4	7.70	.16	-47.53	.23	-18.74	.25

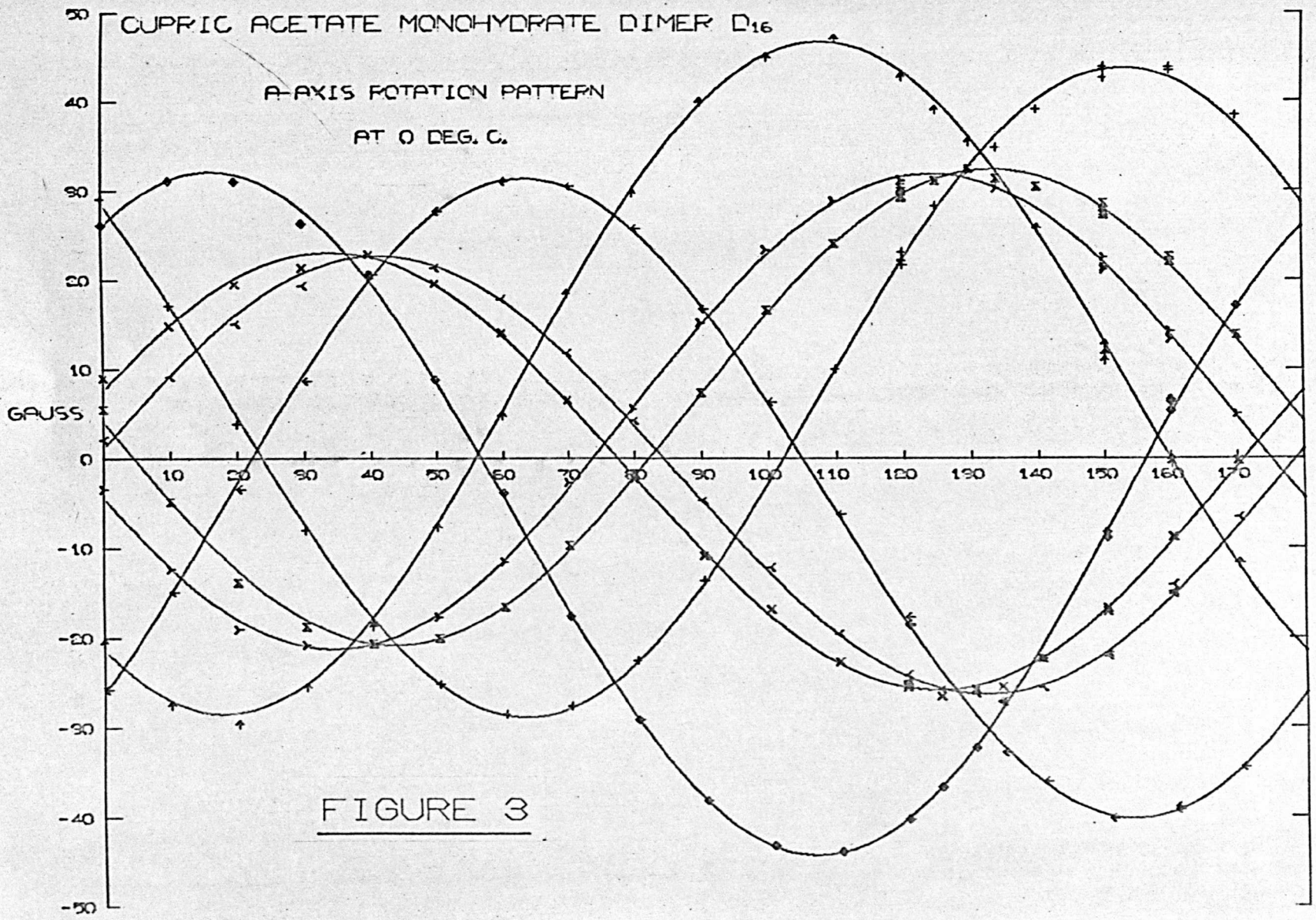
CUPRIC ACETATE MONOHYDRATE DIMER D_{16}
A-AXIS ROTATION PATTERN
AT 0 DEG. C.
GAUSS
50
40
30
20
10
0
-10
-20
-30
-40
-50
10
20
30
40
50
60
70
80
90
100
110
120
130
140
150
160
170

FIGURE 3

TABLE 4. Results for b' axis rotation pattern at 0°C.

Transformation Matrix

	a'	b'	c'
X	.9396	.0128	.3421
Y	.0305	-.9985	-.0465
Z	.3409	.0541	-.9385

Equations of lines

Methyl gp.	line	a	b	c
D1, D4	1	-12.97 .20	41.61 .31	21.84 .31
	2	15.82 .27	-42.18 .35	-21.36 .39
D2	4	17.06 .31	-13.44 .41	- 7.25 .43
	5	-13.33 .27	11.25 .35	4.92 .35
D3	3	19.53 .27	-10.65 .37	- 4.64 .37
	6	-15.95 .27	8.84 .37	2.84 .39

Separations

Methyl gp.	a	b	c
D1, D4	-28.79 .17	83.79 .23	43.20 .25
D2	30.39 .20	-24.69 .27	-12.17 .27
D3	35.48 .19	-19.49 .26	- 7.48 .27

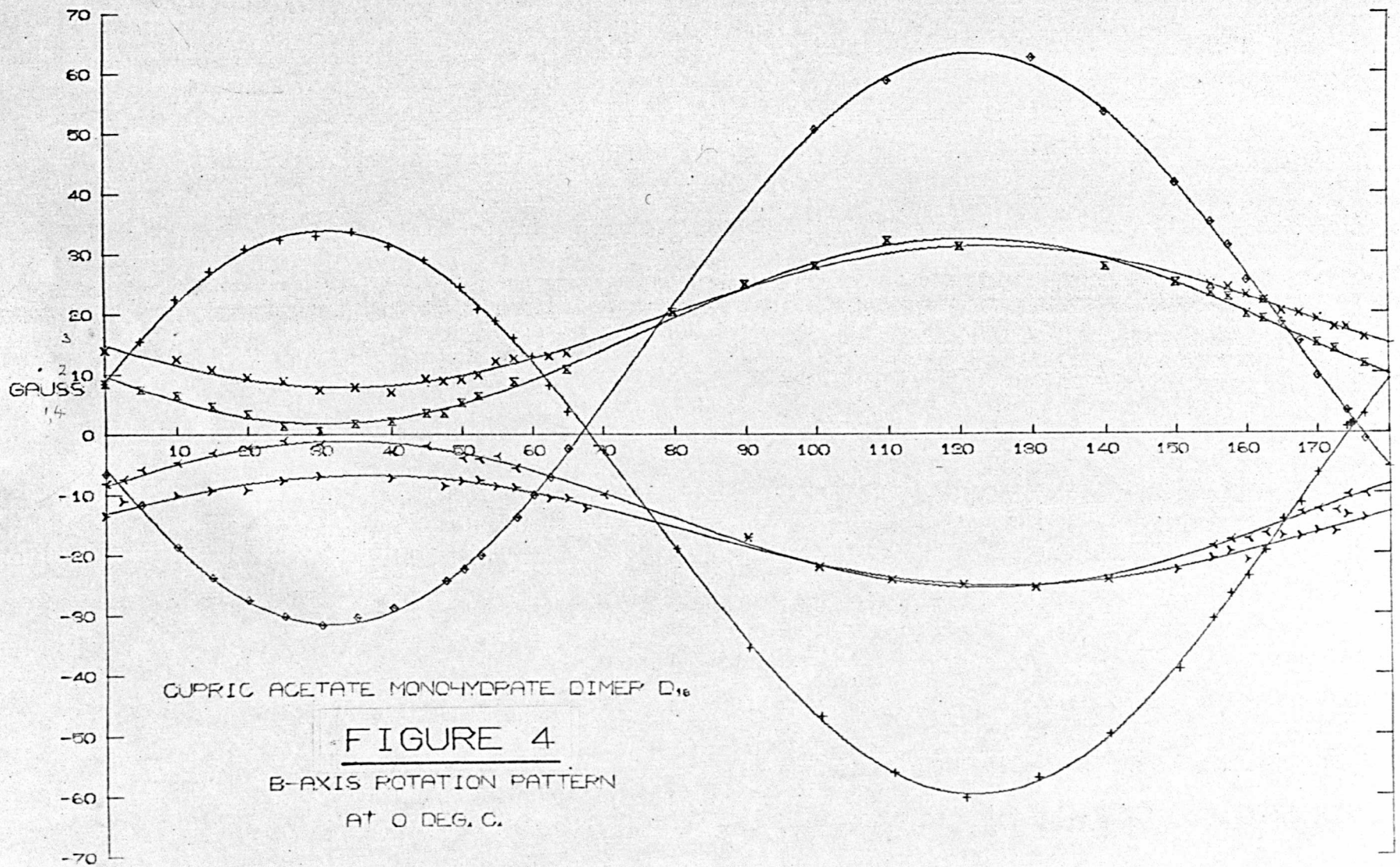

CUPRIC ACETATE MONOHYDRATE DIMER D_{16}

FIGURE 4

B-AXIS ROTATION PATTERN

AT 0 DEG. C.

TABLE 5. Results for c-axis rotation pattern at 0°C.

Transformation matrix

	a'	b'	c'
X	.6175	.7867	.0019
Y	.0115	-.0067	-.9999
Z	-.7865	.6174	-.0132

Equations of lines

Methyl gp.	line	a		b		c	
D1	3	21.60	.22	11.08	.31	4.63	.33
	6	-16.17	.18	-11.63	.27	-5.10	.27
D2	2	- 9.58	.22	-17.07	.31	44.23	.37
	7	14.43	.22	15.27	.31	-43.06	.31
D3	1	12.69	.25	25.12	.33	36.83	.39
	8	- 8.21	.29	-26.70	.41	-37.75	.43
D4	4	21.15	.20	8.75	.31	-10.18	.31
	5	-15.97	.20	- 8.96	.29	10.70	.31

Separations

Methyl gp.	a		b		c	
D1	37.77	.14	22.71	.20	9.73	.21
D2	-24.01	.16	-32.34	.22	87.31	.24
D3	-20.90	.19	-51.82	.26	-74.58	.29
D4	37.12	.14	17.71	.21	-20.88	.22

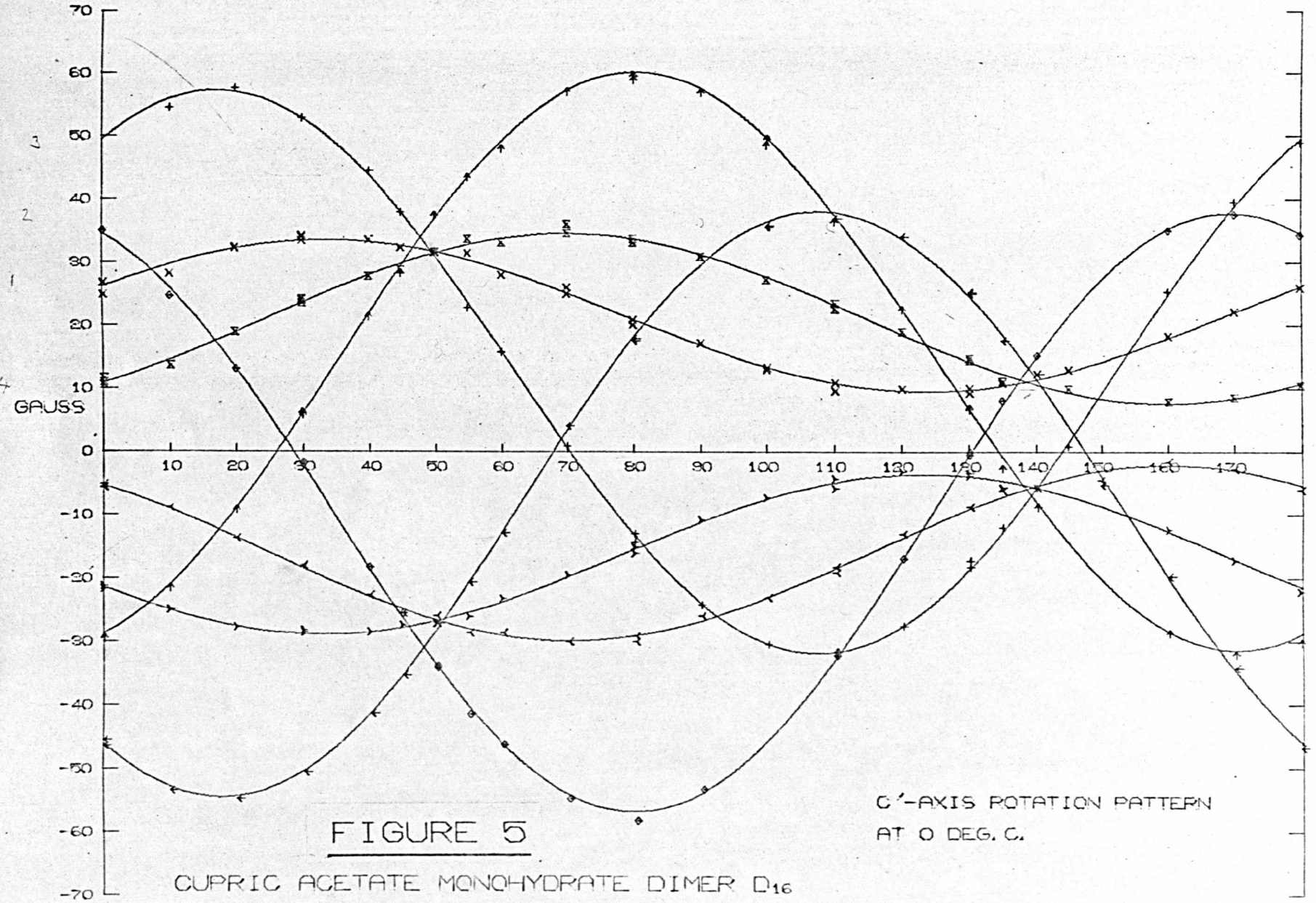

FIGURE 5

CUPRIC ACETATE MONOHYDRATE DIMER D_{16}

TABLE 6. Results for a' axis rotation pattern at 77°K.

Transformation matrix

	a'	b'	c'
X	-.1534	-.2019	.9673
Y	-.9854	-.0428	-.1652
Z	.0747	-.9785	-.1924

Equations of lines

Methyl gp.	line	a		b		c	
D1	3	7.49	.15	12.48	.23	21.70	.19
	6	-3.47	.25	-12.32	.38	-21.89	.33
D2	4	8.51	.31	35.33	.46	11.04	.42
	5	-4.53	.29	-35.30	.44	-11.50	.40
D3	1	10.27	.25	-14.79	.40	35.07	.33
	8	-6.35	.21	14.85	.31	-35.17	.27
D4	2	7.27	.15	6.48	.21	23.74	.19
	7	-3.20	.25	- 6.38	.38	-23.84	.33

Separations

Methyl gp.	a		b		c	
D1	10.96	.14	24.80	.22	43.59	.18
D2	-13.04	.21	-70.63	.32	-22.54	.29
D3	-16.62	.16	29.64	.25	-70.24	.21
D4	10.47	.15	12.86	.21	47.58	.18

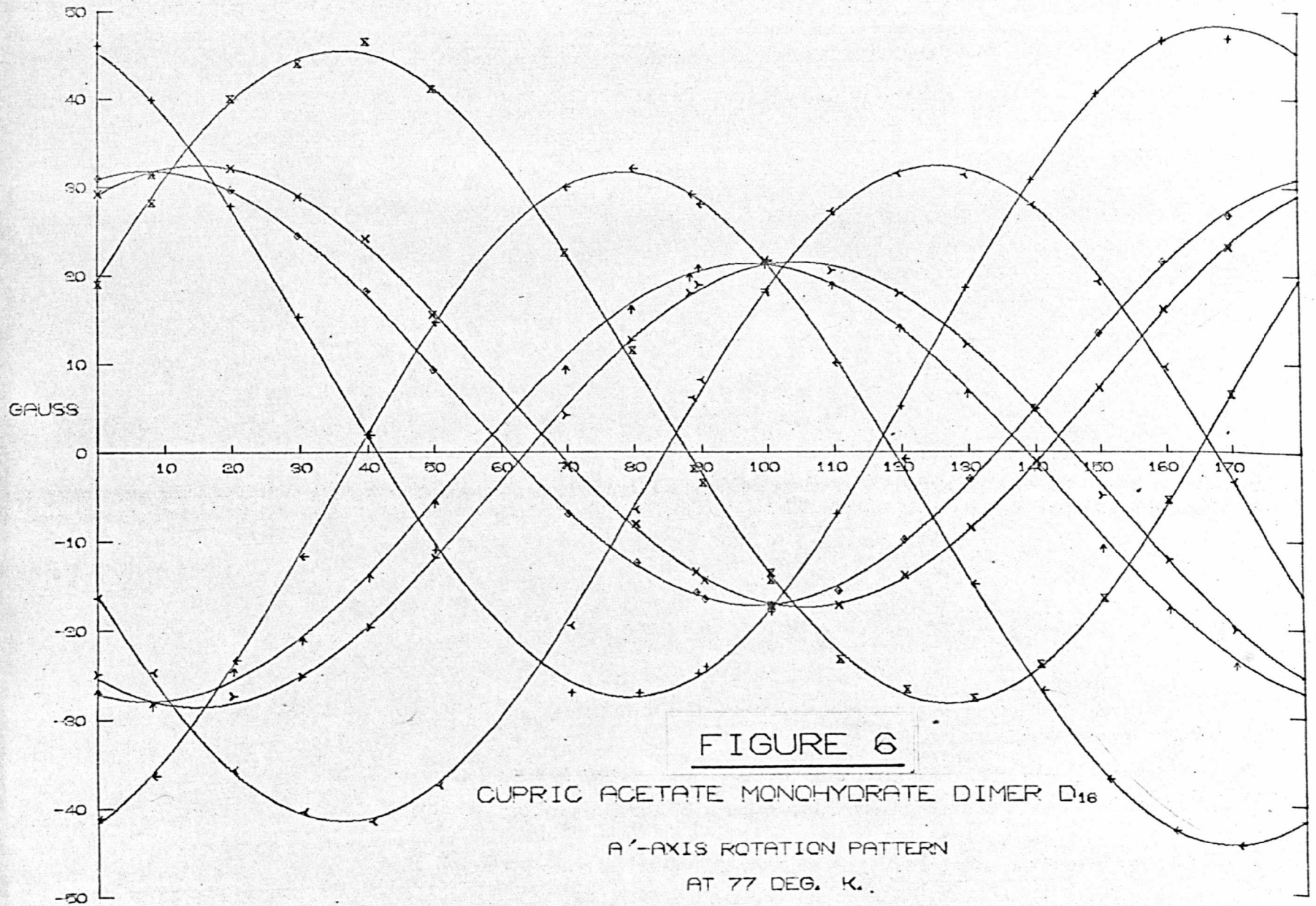

FIGURE 6

CUPRIC ACETATE MONOHYDRATE DIMER D_{16}

A′-AXIS ROTATION PATTERN

AT 77 DEG. K.

TABLE 7. Results for b' axis rotation pattern at 77° K.

Transformation matrix

	a'	b'	c'
X	.9333	-.0027	.3592
Y	.0174	-.9984	-.0529
Z	.3586	.0556	-.9318

Equations of lines

Methyl gp.	line	a		b		c	
D1, D4	1	-13.06	.39	39.47	.59	26.81	.55
	6	17.72	.53	-40.21	.78	-26.06	.70
D2	3	17.41	.23	-12.22	.35	- 7.81	.33
	4	-12.66	.25	11.19	.39	8.60	.35
D3	2	20.09	.19	-10.43	.27	- 4.72	.25
	5	-15.37	.17	9.59	.25	5.23	.23

Separations

Methyl gp.						
D1, D4	-30.78	.33	79.68	.49	52.87	.45
D2	30.07	.17	-23.41	.26	-16.41	.24
D3	35.46	.13	-21.02	.18	- 9.95	.17

In addition, weak absorption lines due to the water molecules were observed over a limited range of magnet rotation angle. Due to the small range and poor signal to noise ratio, and the small number of

points on each line, the standard deviations of the values of a, b, c are very high. In the cases below where the standard deviation of a coefficient is not given, it is at least 25 gauss.

Line	range (degrees)	a		b		c	
7	60 - 94	-14.4	16.3	-62.3	7.9	88.4	16.0
8	60 - 90	- 4.6	18.5	78.2	9.8	-106.0	17.3
9	84 - 94	-45.0		-78.9	14.8	104.2	
10	138 - 16	34.9	10.3	74.1	6.3	-134.2	11.4
11	136 - 16	25.8	7.4	77.4	4.8	-120.9	8.1
12	134 - 8	-14.4	21.0	-84.6	18.3	111.2	13.6
13	138 - 8	36.5	17.0	-88.5	11.6	134.2	16.3
16	142 - 156	84.1		116.7		121.6	

It can be seen that there is a slight asymmetry in the range of appearance of the two lines from one deuteron. This is probably not significant, since the signal to noise ratio near the ends of the range was too low to get an exact idea of the point where a line disappeared.

Only one point was observed on the lines 14, 15, 17. Line 16 is probably fictitious. No corresponding line was found at high field, and plausible efg tensors did not give such a line when used as data for the prediction program.

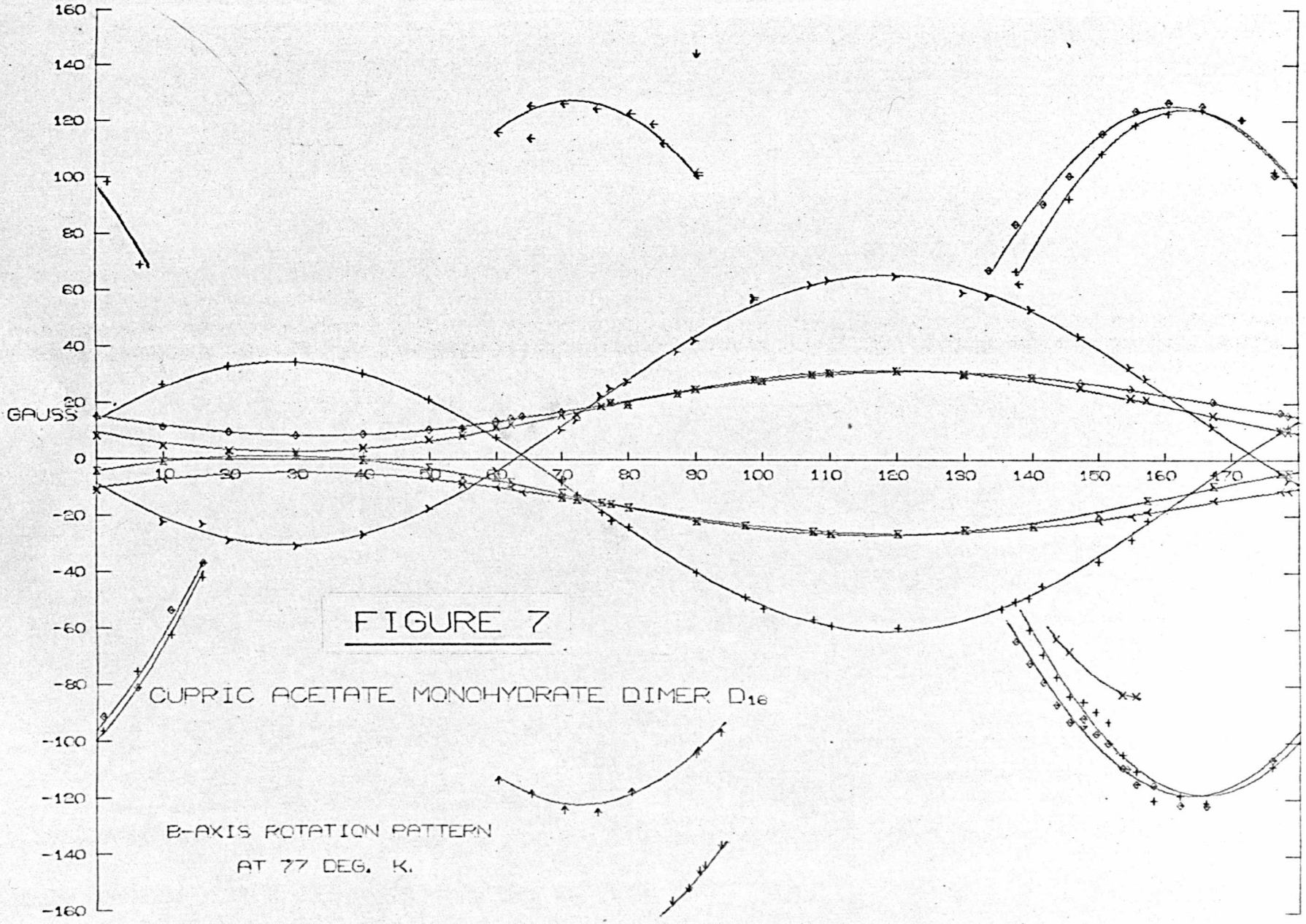

FIGURE 7

CUPRIC ACETATE MONOHYDRATE DIMER D_{16}

B-AXIS ROTATION PATTERN

AT 77 DEG. K.

TABLE 8. Results for c' axis rotation pattern at 77° K.

Transformation matrix

	a'	b'	c'
X	.7738	.6333	.0238
Y	.0583	.0338	-.9979
Z	-.6309	.7733	-.0631

Equations of lines

Methyl gp.	line	a		b		c	
D1	2	17.11	.27	13.08	.38	9.65	.40
	7	-12.97	.34	-13.40	.46	-9.54	.48
D2	3	- 9.00	.27	-31.33	.38	33.88	.40
	6	13.52	.19	31.16	.25	-33.87	.27
D3	1	11.84	.19	12.18	.27	42.65	.25
	8	- 7.41	.30	-12.75	.38	-42.51	.42
D4	4	16.73	.32	16.54	.44	- 6.24	.46
	5	12.59	.27	-16.52	.38	6.25	.40

Separations

Methyl gp.	a		b		c	
D1	31.08	.22	26.48	.30	19.19	.31
D2	-22.52	.16	-62.49	.23	67.75	.24
D3	-19.25	.18	-24.93	.24	-85.16	.23
D4	29.32	.21	33.06	.29	-12.49	.30

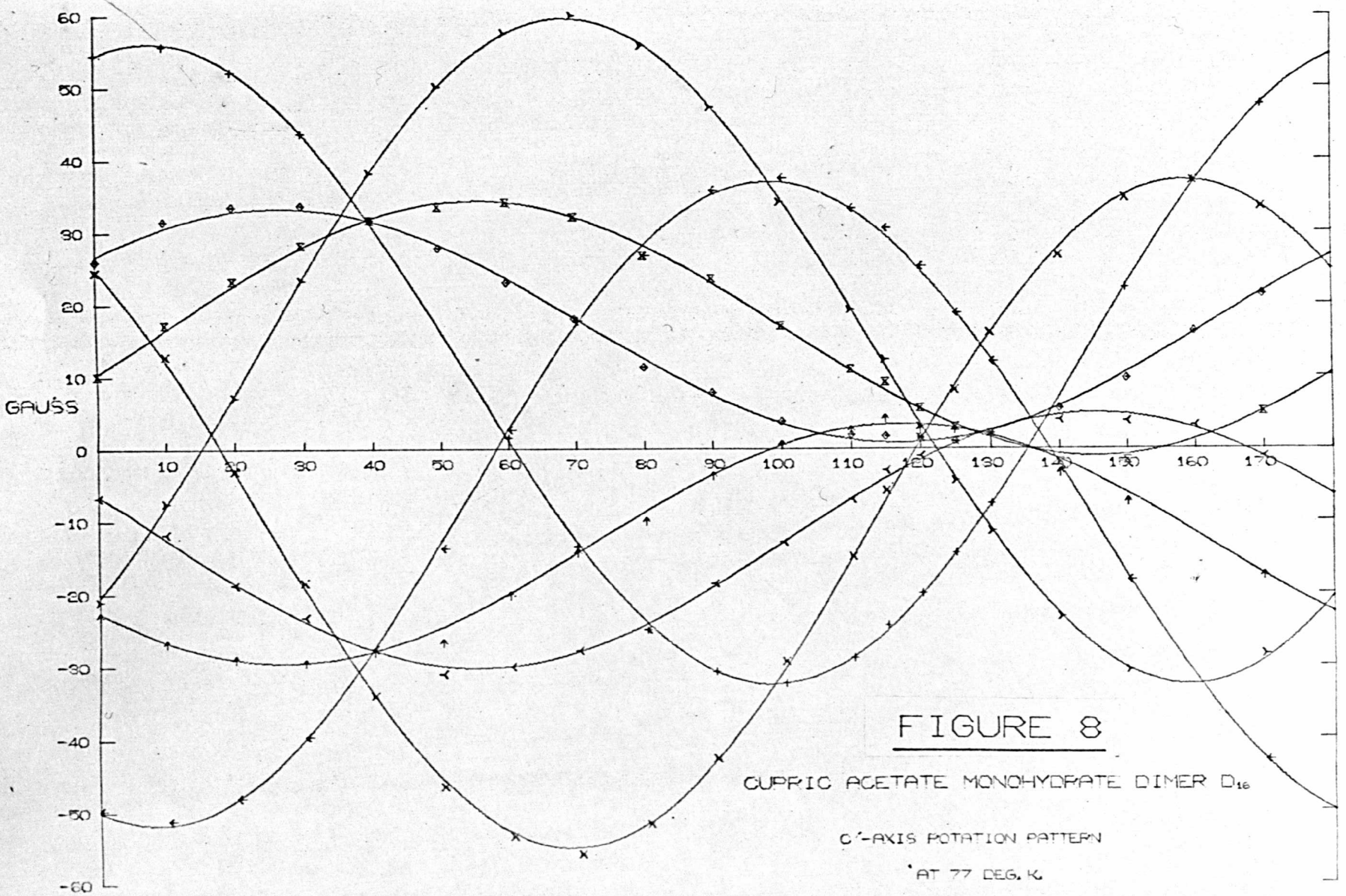

FIGURE 8

CUPRIC ACETATE MONOHYDRATE DIMER D_{16}

C'-AXIS ROTATION PATTERN

AT 77 DEG. K

Note to Tables 9 and 10.

The constant term for all the deuterons is 1.4 - 2.7 gauss. It is slightly in error due to the incorrect value adopted for γ_H/γ_D (3/4) used in the data reduction. The value was later determined experimentally by running the DMR spectrum of a sample of 99.5% heavy water (Norsk Hydro) in the same way as for a single crystal. In order to check that there was no shift due to the ferric chloride in the field measuring probe sample, the high resolution spectrum of .05M ferric chloride in water was compared with that of pure water. (The spectra were kindly recorded by R.J. Lynch on a Perkin-Elmer spectrometer.) It was found that the relative difference was less than .2 ppm, although the peak from the doped sample was about 5 ppm wide. The measured value for γ_H/γ_D was 6.51431 $\pm$ 4 ppm, which may be compared with 6.514399 $\pm$ .5 ppm determined by Wimett (22/5) in HD. However, the experimental value will be used, since it was measured in the conditions which were actually used. It will include the appropriate susceptibility and shielding corrections. In this case .5 $\pm$ .1 gauss should be subtracted from all the values of a in tables 9 and 10. Wimett's value would lead to a correction of .9 gauss in the same direction.

TABLE 9.

Centre of gravity shifts for the rotation patterns run at 0°C.

The units of a, b, c are gauss.

a) a-axis rotation pattern

Deuteron	a	b	c
D1	2.13	-.59	.11
D2	1.6	.33	-.24
D3	1.42	-.35	.37
D4	2.17	.11	.65

b) a-axis rotation pattern, repeat.

Deuteron	a	b	c
D1	1.95	-1.1	.71
D2	1.46	- .43	-.16
D3	1.47	- .59	.85
D4	1.93	- .94	-.30

c) b-axis rotation pattern.

Deuteron	a	b	c
D1, D4	1.43	-.28	.24
D2	1.86	-1.09	-1.16
D3	1.59	-.90	-.90

d) c'-axis rotation pattern

Deuteron	a	b	c
D1	2.71	-.27	-.23
D2	2.42	-.9	.58
D3	2.24	-.79	.46
D4	2.59	-.1	.26

TABLE 10.

Centre of gravity shifts for the rotation patterns run at 77° K.

a, b, c are given in gauss.

a) a-axis rotation pattern.

Deuteron	a	b	c
D1	2.01	.08	-.10
D2	1.99	.01	-.23
D3	1.96	.03	-.05
D4	2.03	.05	-.05

b) b-axis rotation pattern.

D1, D4	2.33	-.37	.37
D2	2.37	-.52	.40
D3	2.73	.42	.26

c) c-axis rotation pattern.

D1	2.07	-.16	.05
D2	2.26	-.08	.0
D3	2.21	-.28	.07
D4	1.61	.01	.0

TABLE 11.

Electric field gradient tensors for the methyl groups in cupric acetate at 77°K.

D1.

ϕ_{zz} = -56.09, ϕ_{yy} = 30.50, ϕ_{xx} = 25.59kHz Exp. trace = -.29

Eigenvectors.				C-C vector	Cu-Cu vector
a'	-.5939	-.7058	-.3863	-.5950	-.6913
b'	-.1070	.5451	-.8315	-.0950	.5698
c'	-.7974	.4525	.3993	-.7981	.4444

η =.088.

D2.

ϕ_{zz} = -55.92, ϕ_{yy} = 31.79, ϕ_{xx} = 24.13kHz Exp. trace = -.26

Eigenvectors.				C-C vector	Cu-Cu vector
a'	-.4756	-.8404	.2598	-.5029	-.6913
b'	-.8333	.5251	.1731	-.8294	-.5698
c'	.2819	.1341	.9500	.2434	.4444

η =.137.

D3.

ϕ_{zz} = -55.48, ϕ_{yy} = 31.55, ϕ_{xx} = 24.23kHz Exp. Trace = .29

Eigenvectors.				C-C vector	Cu-Cu vector
a'	.4997	.8639	.0632	.5029	.6913
b'	-.8211	.4956	.2832	-.8294	.5698
c'	-.2760	.0896	-.9570	-.2434	-.4444

η =.132.

D4.

ϕ_{zz} = -54.84, ϕ_{yy} =31.50, ϕ_{xx} = 23.34 kHz Exp. trace = -.14

Eigenvectors.				C-C vector	Cu-Cu vector
a'	-.6009	.6417	-.4767	-.5947	.6913
b'	.0695	.6360	.7686	.0950	-.5698
c'	-.7963	-.4287	.4267	-.7983	-.4444

=.149.

TABLE 12.

Electric field gradient tensors for the methyl groups in cupric acetate at 0°C.

D1.

ϕ_{zz}= -55.38, ϕ_{yy}= 31.45, ϕ_{xx}= 23.93kHz. Exp. trace = .83

Eigenvectors.

				C-C vector	Cu-Cu vector
a'	-.5689	-.7505	-.3364	-.5950	-.6913
b'	-.0936	.4654	-.8801	-.0950	.5698
c'	-.8171	.4692	.3350	-.7981	.4444

η =.136

D2.

ϕ_{zz}= -55.15, ϕ_{yy}= 30.63, ϕ_{xx}= 24.52kHz. Exp. trace = -.74

Eigenvectors.

				C-C vector	Cu-Cu vector
a'	-.4586	-.8817	.1109	-.5029	-.6913
b'	-.8523	.4718	.2261	-.8294	.5698
c'	.2517	-.0091	.9678	.2434	-.4444

η =.111

D3.

ϕ_{zz}= -55.70, ϕ_{yy}= 32.14, ϕ_{xx}= 23.56kHz. Exp. trace = .87

Eigenvectors.

				C-C vector	Cu-Cu vector
a'	-.5250	.8036	.2804	-.5029	.6913
b'	.8029	.5769	-.1500	.8294	.5698
c'	.2823	-.1464	.9481	.2434	-.4444

η =.154

D4. ϕ_{zz}= -55.94, ϕ_{yy}= 30.66, ϕ_{zz}=24.30kHz. Exp. trace = 1.14

Eigenvectors.

				C-C vector	Cu-Cu vector
a'	-.5762	.7238	-.3797	-.5950	.6913
b'	.0905	.5182	.8504	.0950	.5698
c'	-.8123	-.4557	.3641	-.7981	-.4444

η =.114.

V. 5. Interpretation of the results for cupric acetate.

a) Centre of gravity shift.

The centre of gravity shifts for the lines originating from each deuteron in all the rotation patterns are given in Tables 9 and 10. They are shown in the form :-

$$s = a + b \sin 2\theta + c \cos 2\theta$$

where s is the centre of gravity shift in gauss,

a, b, c are the coefficients given in Tables 9 and 10,

and θ is the magnet rotation angle in degrees.

Standard deviations are not given, since they are identical with those given in the corresponding tables, (2 - 8), for the line splittings. Typical values lie between .2 and .4 gauss at the 95% confidence level, so the anisotropic shifts for the 0° C rotation patterns are significant.

It was at first thought that the isotropic part of the shift, which is large for both the 77°K and 0°C spectra, was due to the bulk magnetic susceptibility of the crystal. However, the susceptibility changes by a factor of about five between the two temperatures (17/5), while the shift changes very little. The coefficients b and c would also be identical for all the deuterons if the shift were due to some bulk effect.

Second order perturbation theory (18/5) shows that the centre of gravity shift is of the form :-

$$s = a' + b' \sin 4\theta + c' \cos 4\theta$$

i.e., the coefficients b and c are zero. Since, in fact, the terms in 2θ were observed, even the isotropic centre of gravity shift cannot be due to second order effects.

V. 6 The magnetic system in cupric acetate.

It was considered that the centre of gravity shift observed in the $0^{o}C$ spectra was due to the anti-ferromagnetic interaction between the copper atoms in each pair. The system has been described by Figgis and Martin (16/5).

The position and shape of nuclear resonance absorption lines are influenced by the magnetic environment of the absorbing nuclei. The time average of the magnitude of the magnetic field due to the copper atoms will vary from point to point in the unit cell, thus the centre of gravity of the pair of lines originating from one deuteron will be shifted. If the spin exchange rate is comparable with the Larmor frequency of the deuteron, then the resonance line will be broadened as well as shifted. It can be shown (19/5), in the case where the copper atoms are magnetically anisotropic, that the time average of the magnetic moment of a copper atom is :-

$$= \tfrac{1}{4}\beta^{2}g^{2}H_{o}/3kT \qquad (5.1);$$

where β is the Bohr magneton,

H_o is the external magnetic field in gauss,

k is Boltzmann's constant,

T is the absolute temperature,

and g^2 is a tensor, the square of the g-tensor.

Poulis (20/5) has shown that the dipolar field, h, at a deuteron due to a single copper atom is :-

$$h = \langle\mu\rangle\ (3\cos^2\theta - 1)/r^3 \qquad (5.2)$$

where r is the distance from the copper atom to the deuteron and

θ is the angle between the vectors r and H_o. This relationship neglects components of the dipolar field transverse to H_o. Hence the centre of gravity shift of a pair of resonance lines originating from one deuteron, due to one copper atom, is given by :-

$$\Delta H = \frac{\beta^2 H_o}{12kT}\, g_1^2\, \frac{3\cos^2\theta - 1}{r^3} \qquad (5.3)$$

g_1^2 is the magnitude of the component of g^2 in the direction of H_o.

V. 7 Calculation of the centre of gravity shifts.

The expected shift is calculated by summing equation (5.3) over all the copper atoms which produce a significant contribution to the magnetic field at a particular deuteron. Equation (5.3) can therefore be written, after substitution of the values of the constants, as :-

$$\Delta H = 5.324 \sum_{j=1,2} \left(g_{1j}^2 \sum_i \frac{3\cos^2\theta_i - 1}{r_i^3} \right) \text{gauss} \qquad (5.4)$$

T in (5.3) is taken to be 273°K.

The summation over j = 1,2 is taken because there are two magnetically different copper atom pairs in the crystal, typified by those centred on the points $(0, 0, \frac{1}{2})$ and $(\frac{1}{2}, -\frac{1}{2}, 1)$. The index i cycles over all the

copper atoms in the crystal. If we extend this summation over all copper atoms within a distance LIMIT of the deuteron, it is easy to show that the contribution from atoms near the surface of the sphere is roughly proportional to 1/LIMIT. It is also necessary to average the quantity $\frac{3\cos^2\theta_i - 1}{r_i^3}$ over one revolution of the methyl group. For these two reasons a computer program was written to deal with the large amount of calculation.

The program first generates the positions of the molecule inversion centres which are within LIMIT of the methyl group being studied. It then sets up the g-tensors in orthogonal crystallographic coordinates for the two different copper atoms. These g-tensors transform in the same way as the e f g tensor, so the program at this stage is identical with SPECTRUM. The magnitudes of the principal components are taken from Bleaney and Bowers (21/5), they are $g_x = g_y = 2.08$, $g_z = 2.42$. A comparison of Bleaney and Bowers' results with those of van Nekerk and Schoening (13/5) shows that the g_z eigenvector is parallel with the Cu - Cu vector. The program has thus calculated the coefficients a_j, b_j, c_j, in the relationship :-

$$\Delta H = \sum_{j=1,2} \left\{ (a_j + b_j \sin 2\Theta + c_j \cos 2\Theta) \times \sum_i \frac{3\cos^2\theta_i - 1}{r_i^3} \right\} \qquad (5.5)$$

where Θ is the magnet rotation angle

FIGURE 9.

Centre of gravity shifts for the a′-axis rotation pattern at 0°C

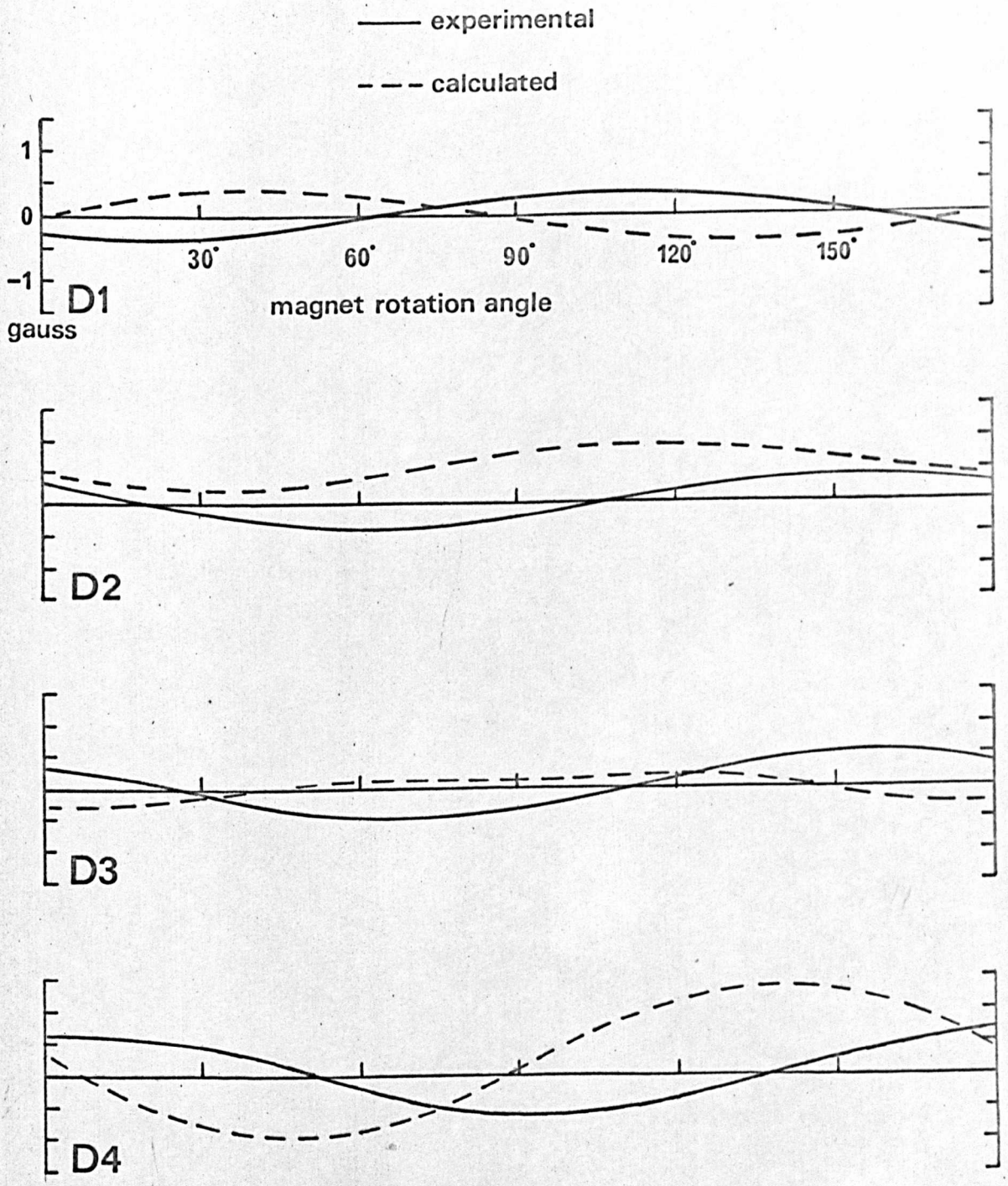

j = 1 for copper atoms with an integral b-coordinate, and j = 2 for copper atoms with a half-integral b-coordinate. It remains to calculate the values in the second summation. For copper atoms close to the methyl group, this factor is taken to be its average value over one rotation of the methyl group, while for atoms which are more than 10 Å distant from the methyl carbon atom, the deuteron is taken to be in its mean position. This was done in order to save computation time, since otherwise the factor had to be calculated 624 times the number of copper atoms considered. The program outputs a graph of the results using the procedure GRAPHICAL from the prediction program.

Some typical results of the calculation are shown in Figure 9. It can be seen that there is little agreement between the experimental results and the calculation. The model proposed is therefore incorrect. One part which is wrong is that the magnetic system was taken to follow the Curie law, while in fact it does not do so. This will only affect the magnitude of the shift, and not its phase.

V 8. The electric field gradient tensor.

The figures in Tables 2-8 were used as data in the program TENSOR. At first it was found that the program gave very poor results if the transformation matrices from ORIENT were used directly in TENSOR. On reversing the directions of the b' and c' axes in the a' axis rotation pattern satisfactory tensors were obtained

from the $0^{o}C$ runs. Similarly, in the $77^{o}K$ runs, the axes perpendicular to the rotation axis were reversed for the a' and c' axis rotation patterns. The eight possible permutations were tried in order to find the correct combination. It was always easy to see which was the right set, since this gave small traces for the calculated efg tensors. Previously the program SPECTRUM had given a very poor prediction for the a' axis $0^{o}C$ rotation pattern, but this was thought to be because at this stage only an approximate efg tensor was used. The rotation pattern was repeated to check that the discrepancy was not due to the crystal falling off the holder. The repeated pattern is shown in Figure 8. SPECTRUM and TENSOR use the same theory, so on using the right transformation matrix the prediction was much better. We can see that reversing two of the axes corresponds to turning the crystal through 180° about the remaining axis, and that the new transformation matrix fits the crystal just as well as the old one derived in ORIENT.

The results from TENSOR are shown in tables 11 and 12. The direction cosines of the C-C and Cu-Cu vectors (calculated from van Niekerk and Schoening, reference 13/5) are shown for comparison with the eigenvectors corresponding to q_{zz} and q_{yy} respectively. It can be seen that the asymmetry parameter, η , is non-zero. Since the explanation of this has some effect on q_{zz}, the value of η will be discussed first.

i) The asymmetry parameter.

Since the methyl group rotates very rapidly compared with the quadrupolar splitting frequency, the apparent efg tensor for it can be obtained by averaging the efg tensor for the static deuteron over a complete rotation of the methyl group about the C-C vector. By using an extension of the theory given by Das and Hahn (32/5), the apparent efg tensor, ϕ', is :-

$$\phi'_{11} = \phi'_{22} = \tfrac{1}{2}(\phi_{xx}\cos^2\alpha + \phi_{yy} + \phi_{zz}\sin^2\alpha)$$

$$\phi'_{33} = \phi_{xx}\sin^2\alpha + \phi_{zz}\cos^2\alpha$$

$$\phi'_{12} = \phi'_{13} = \phi'_{23} = 0, \qquad (5.6)$$

where ϕ is the diagonalised efg tensor for the non-rotating deuterium atom, α is the angle between the direction of the largest principle component of ϕ and the rotation axis,

η is the asymmetry parameter for the static deuteron, it does not change as the methyl group rotates.

Since $\phi_{xx} = -\tfrac{1}{2}(1-\eta)\phi_{zz}$,

$$\phi'_{33} = \tfrac{1}{4}[(3-\eta)\cos 2\alpha + 1 + \eta]\phi_{zz}. \qquad (5.7)$$

We would thus expect the apparent efg tensor to be axially symmetric, even if the original tensor were not so. As an example, if $\cos\alpha = -\tfrac{1}{3}$ (tetrahedral methyl group) and $\eta = 0$, then $\phi_{33} = -\tfrac{1}{3}\phi_{zz}$. ϕ'_{33} is very sensitive to η - for $\eta = .1$, $\phi'_{33} = -\tfrac{13}{45}\phi_{zz}$. It is therefore very unwise to estimate ϕ_{zz} from values of ϕ'_{33} by assuming that $\eta = 0$. This point will be discussed later.

A first explanation of the asymmetry was that the electric charge

distribution on the CO_2- group had two-fold rotational symmetry about the C-C band axis, so the averaged efg at the deuterium atom might be non-axially symmetric. This is the direct electric field effect. A program was written to do the calculation, and it was found that although the asymmetry was high in certain positions of the deuteron, the averaged efg tensor was no different from that derived without the direct electric field effect.

ii) The indirect electric field effect.

Electric field gradient calculations by Bishop (27/5), Harrison (28/5), and Henderson and Ebbing (29/5) showed that the greatest contribution to the efg at the deuterium atom comes from the bonding region. At first it would appear from the form of the operator for q_{zz} that the major part would come from electron density close to the nucleus. A simple model was proposed to explain the non-zero value of η for the methyl groups. The electric field due to charges on the atoms near the deuteron polarises the electrons in the C-D bond and the induced dipole produces an electric field gradient at the deuteron. The effect must be averaged over one revolution of the methyl group.

A program, INDUCE, was written to make the appropriate calculation. The molecule based coordinates (z axis along the methyl carbon to carboxyl carbon atom vector, x axis parallel to the Cu-Cu vector, origin at the methyl carbon atom) of all charged atoms are read in together with their respective charges, and the resultant electric field at a point 1.09X RT Å from the origin, along the C-D vector is

calculated. RT can take any value between 0 and 1. The induced dipole $\underline{\mu}$ is given by :-

$$\underline{\mu} = \alpha \underline{V}. \tag{5.8}$$

where α is the polarisability tensor and

$\underline{V}$ is the electric field at the point considered. It should be noted that the polarisability tensor here is obtained by transforming the tensor in coordinates based on the C-D bond to the molecule based system.

It is simplest at this stage to set up orthogonal coordinates based on the induced dipole, with z' along the dipole, x' parallel to the molecular xy plane and origin at the position of the dipole. The position of the deuterium atom is transformed into this system. If its coordinates in the dipole based setare (x, y, z) then it is easy to show that the efg tensor due to the dipole is :-

$$V_{xx} = 3\mu z\,(5x^2/r^2-1)/r^5$$

$$V_{yy} = 3\mu z\,(5y^2/r^2-1)/r^5$$

$$V_{zz} = 3\mu z\,(5z^2/r^2-3)/r^5$$

$$V_{xy} = 15\mu xyz/r^7$$

$$V_{zx} = 3\mu x\,(5z^2/r^2-1)/r^5$$

$$V_{yz} = 3\mu y\,(5z^2/r^2-1)/r^5 \tag{5.9}$$

where $r = (x^2 + y^2 + z^2)^{\frac{1}{2}}$.

These tensor components are transformed into the molecule based system and added to the tensor derived by transforming the efg tensor for the static deuteron into the same system. The above

calculation is repeated for six positions of the deuteron, spaced by 60° and starting from the orientation where the C-D vector lies in the z-x molecular plane. As a check the apparent efg tensor was calculated without the induced terms and gave a result identical with equation 5.7 in part (i) of this section. The input data for the calculation were :-

atomic coordinates, derived from van Niekerk and Schoening (13/5),

atomic charges, taken to be -2 electronic charges on the copper ions and $\frac{1}{2}$ unit on the oxygen atoms,

the efg tensor for the static deuteron,

the parameter RT, which controls the position of the induced dipole along the C-D bond,

the principal components of the polarisability tensor for the C-D band, from Rowell and Stein (30/5). Earlier values for this quantity, for example, those measured by Yoshimo and Bernstein (25/5) and in all the references quoted in Table I of Rowell and Stein's paper are unreliable, since they do not take into account the internal electric field of the molecule. The tensor was taken to be axially symmetric with $b_1 = 1,934$, $b_2 = .024\mathring{A}^3$, although the C-D bond is not axially symmetric in this compound. Rabinovich (31/5) has shown that there is only a 5% isotope effect on the C-H bond polarisability, so the above figures for the C-H bond can safely be used for the C-D bond.

As expected, the induced efg tensor was very sensitive to the value of RT. The data which gave the best fit to the observed tensor were :-

q_{zz} = 168 kHz, η = .05 for the static deuteron and RT = .25.

The calculation gave :-

$$\phi'_{33} = -56.3 \quad \phi'_{22} = 31.8 \quad \phi'_{11} = 24.5 \text{ kHz},$$

which may be compared with the average of the tensors from the liquid nitrogen rotation patterns :-

$$\phi'_{33} = -55.6 \quad \phi'_{22} = 31.3 \quad \phi'_{11} = 24.3 \text{ kHz}.$$

The eigenvectors of the calculated efg tensor in the molecular axis system were :-

	ϕ'_{33}	ϕ'_{22}	ϕ'_{11}
x	.0289	.9996	.0
y	.0	.0	1.0
z	-.9996	.0289	.0

As in the experimental results, the ϕ'_{33} eigenvector is very close to the z axis. It is rather unexpected that the calculated ϕ'_{33} direction deviates from the z axis, in view of the symmetrical distribution of charges in the molecule. The fact that ϕ'_{22} is roughly parallel to the Cu-Cu vector is very significant, since this is also found in the experimental results. This is the main piece of evidence in favour of the model.

iii) Validity of the indirect electric field effect model.

The model described above to explain the non-zero value of η gives quite good agreement between theory and experimental results, in spite of its simplicity. The main assumptions made are :-

a) that we take no account of the effective dielectric constant of the medium between the charges and the C-D bonding electrons.

b) that charges on atoms in molecules other than the one considered have no effect. The calculation could be extended to include these without too much difficulty. This might explain the fact that the deviation of the ϕ'_{22} eigenvector from the Cu-Cu vector is different for D1 and D4 from that for D2 and D3 (see tables 11 and 12).

c) that the induced dipoles on other bonds do not affect the efg at the deuteron being considered.

d) that the charges on all the carbon atoms are zero.

The accuracy of the calculation could probably be improved by taking these points into account. However, only a full scale quantum mechanical calculation could give a reliable answer, since any simpler model relies on the crude idea that the polarisability of a bond can be represented by a single tensor.

iv) <u>The value of ϕ_{zz}.</u>

In section (ii) it was shown that the value of ϕ_{zz} for the static deuteron was about 168 kHz. This is based on the assumptions below, in addition to the ones given above about the validity of the indirect electric field effect model.

a) a correction of + 4.0 kHz has been made to the apparent ϕ'_{33} to

account for the indirect electric field effect.

b) the asymmetry parameter for the static deuteron is .05. This value is an estimate only, but seems to be reasonable when compared with the value of .100 for water (35/5) and .064 $\pm$ .013 for anthracene-d_{10} (36/5). No determination of η for a deuterium atom bonded to an sp^3 hybridised carbon atom has been made. If η were zero, then ϕ_{33} would increase by about 11kHz.

c) the D-C-D angle in cupric acetate is equal to the tetrahedral angle, 109° 28'. By substituting

$$\cos 2\alpha = \tfrac{1}{3}(4 \cos D - 1),$$

where D is the D-C-D angle, in equation (5.7) of section (i), and then differentiating with respect to D, we can show that ϕ_{zz} decreases by 2.5 kHz if D increases by one degree.

The structure of acetic acid-d_3 has been determined by Tabor (47/5) using microwave spectroscopy, but the error in the D-C-D angle is very large, the value being 108° 34' $\pm$ 4°. It is therefore better to use the tetrahedral angle in the absence of a good measurement.

Before we can compare the value of ϕ_{zz} for cupric acetate with other determinations of the quantity in different compounds we must critically examine the assumptions made in each. The known values are listed in Table 13 with the method of measurement and a few parameters for each compound. None of the determinations can be regarded as very

reliable. All of them assume that η is zero, although the value of ϕ_{zz} is very sensitive to η. In the case of the determinations made by studying solutions in liquid crystals (Rowell et al., reference 12/5, Caspary et al., reference 33/5, and Klein et al., reference 34/5) this leads to an error in the expression for the splitting of the spectra lines. In the compounds studied by Caspary et al. (CD_3 Br, CD_3I, CD_3CN), the value of η will not vary very much, so the coupling constants can be compared with each other. However, in measuring the S- parameters for the liquid crystals they used the protonated compounds; then the results were used to interpret the DMR spectra. There could have been an isotope effect on the S- parameters. Klein et al. also measured the deuterium quadrupolar coupling constant in CD_2 Cl_2 via a determination of the correlation time of the molecule using the ^{35}Cl coupling constant in the solid. This increases from 72.4 mHz in the solid to 78.4 $\pm$ 2 MHz in the gas (37/5), so the value which should have been used lies somewhere between the two figures. In view of the substituent effect found by Caspary et al., it was invalid for Klein et al. to compare their value of the coupling constant with that calculated by Pyykko for the CD_4 molecule (38/5).

All the other measurements of the coupling constant in other methyl compounds can be safely disregarded. The value of 100 $\pm$ 50 kHz deduced by Anderson and Ramsey (39/5) could not be expected to give a good value, as they explained in their paper. Saraswati and Vijayaraghavan (2/5) gave a value of 83 kHz and η = .27 for the apparent efg tensor in

TABLE 13. SOME PROPERTIES OF METHYL COMPOUNDS.

	ϕ'_{zz}	ϕ_{33}	E_x	$\delta^{13}C$	$J^{13}C\text{-}H$	r_s	H-C-X	ν_4
Units	kHz	kHz		ppm	Hz	Å	degrees	cm^{-1}
Source	a	a	b	c	c	d	d	e
Compound								
CD_3CN	54.5	165	2.57	124.0	134.0	1.1014	$109^{o}.5$	2985
Cu-acetate	56.0[f]	168[g]						
CD_3Br	63.0	171	2.94	119.3	154	1.0954	$107^{o}.2$	3057
CD_3I	66.9	180	2.68	151.0	151	1.0958	$107^{o}.0$	3060
CH_3COO^-					105[h]			
CH_4		200[i]		130.8	125			

(a) ref.33/5 (b) ref.43/5 (c) ref.49/5 (d) ref.48/5 (e) ref.50/5

(f) apparent efg. (g) assumed that = .05, corrected for indirect electric field effect, present work

(h) ref. 45/5 (i) calculated, ref. 3/5.

polycrystalline acetone-d_6. The DMR spectra of polycrystalline samples are always difficult to interpret, since the signal to noise ratio is so low. Finally, the static deuteron coupling constants of 98 and 107 kHz for liquid CD_3I and CD_3 CN respectively, determined by Zeidler (40/5) from relaxation time studies, are so far from Caspary's results that there is obviously some error.

The results of Caspary are probably the most reliable, in spite of the assumptions which they made. The most important point which comes from their work is that substitution on the carbon atom influences the magnitude of the coupling constant. Weiss and Flygare (41/5) found from the microwave spectra of various acetylenes that the coupling constant was, within the rather large experimental error, independent of the substituent. However, the substituents were not, of course, on the same carbon atom, and it is unsafe to assume that sp^3 bonded compounds behave in the same way as sp compounds.

Table 13 shows some of the physical properties of the methyl halides (except the fluoride), acetonitrile, the acetate ion, cupric acetate and methane. Since the values of the quadrupolar coupling constant determined by Caspary et al. and Klein et al. neglect η, it is rather difficult to make comparisons with the present work. If we accept that they form a consistent set of results, and that cyanide is more electronegative than iodide then the values of the coupling constant for the static deuteron correlate with the electronegativity of the substituent. The electronegativity of the cyanide group was determined

by Dailey and Shoolery (42/5) by an NMR method, and is probably subject to some error due to the diamagnetic anisotropy of the group. The other electronegativities are due to Huggins (43/5). Bersohn has proposed that an electronegative substituent pulls electrons from the deuteron 1s orbital into a carbon bonding orbital. The contribution to the efg from the nuclei is positive, and if we assume that the resultant efg is also positive, then the increased asymmetry of the electron distribution due to an electronegative substituent will decrease the efg at the deuteron. On this basis we can see why the coupling constant for the deuterons in CD_2Cl_2 is much lower than for CD_3Br. However, Harrison's calculations (28/5) seem to show an opposite effect, the coupling constant increases when -OH or NH_2 is substituted for a deuteron in methane. More exact calculations are probably necessary. The D- C- X bond angles are shown in Table 13, where they are available. Although there is a distinct relationship between ϕ_{zz} and this angle, the change in angle with substituent is probably a steric as well as an electronegativity effect, so we can draw no conclusions from this correlation.

Salem (44/5) has shown, at least for diatomic hydrides, that there is a linear relationship between the quadrupolar coupling constant for the deuteron and the force constant. There seems to be a correlation between the CH_3 symmetric stretching (ν_4) frequency and the coupling constant for CH_3Br, CH_3I, CH_3CN, but not for CD_2Cl_2.

Other correlations were attempted which involved the charge on the

carbon atom. The ^{13}C chemical shift is known to be sensitive to charge on the carbon (45/5), and is proportional to the Huggins electronegativity of the substituent. Unfortunately, the ^{13}C chemical shifts of CH_3CN and CH_3I are also subject to diamagnetic anisotropy effects, so it is difficult to make comparisons with other compounds. $J^{13}C$-H is not affected by this anisotropy, but there is still no satisfactory relationship, although Muller and Pritchard (46/5) have pointed out a connection between $J^{13}C$-H and the substituent electronegativity.

It is difficult to compare the results discussed above, firstly because of the neglect of η , and secondly because of the lack of NMR and IR spectroscopic data for cupric acetate. A tentative explanation for the low value of ϕ_{zz} is that the highly charged cupric ions make the groups attached to the methyl group very electronegative.

V.9 Comparison of the results at 0°C and 77°K.

There is a small reduction in the value of ϕ_{zz} in going from 77°K to 0°C. This is in the expected direction, since the increased amplitude of vibration leads to a reduction in ϕ_{zz} - the rotation of the methyl group discussed in the previous section is an extreme example. The change for cupric acetate is significant, and probably arises from very low frequency (100-200 cm^{-1}) lattice modes.

V.10 The accuracy of the results.

The accuracy of the rotation pattern determination is satisfactory, but a comparison of the splittings, calculated from the eigenvectors, eigenvalues and transformation matrices, with the experimental results

shows differences of up to 2 gauss. The values of η are not the same for the pairs D1, D4 and D2, D3. It is believed that the main error arises because of the poor growth of the crystal faces, which resulted in inaccurate transformation matrices. The probe axis was assumed to be parallel to the magnet rotation axis when the outside of the Dewar was parallel with the magnet polepieces. The accuracy of construction was such that this would not give an error of more than a fraction of a degree.

V.11 The water molecules.

Absorptions due to water molecules were only observed over a limited range in the b' axis rotation pattern at 77°K, where the full rotation was explored. In the other 77°K rotation patterns they were only seen rarely, so no complete exploration was made. A prediction was made, and found to agree quite well if it was assumed that q_{zz}=200 kHz and η = .13, with the plane of the water molecule defined by the positions of the three oxygen atoms with which it was involved. The values of q_{zz} and η were similar to those found by Clifford (1/3) for copper sulphate pentadeuterate. A comparison of the b'- axis rotation pattern with the crystal structure showed that signals due to the water molecules only appeared when the magnetic field direction was close to one of the crystallographic axis directions.

A prediction was also made for the 0° spectra - at this temperature the water molecules were taken to be flipping about their two-fold axes. No signal was ever seen; this probably indicated that the deuterons had

such a short spin-lattice relaxation time that their absorptions were too broad to be seen.

V. 12 Suggestions for further work.

It is obvious from the above discussion that more work is required before an unequivocal value of the quadrupolar coupling constant for a deuteron bonded to an sp^3 hybridised carbon atom can be obtained. A suitable compound to start off with would be deuterated cupric propionate monohydrate dimer, where the methylene group is most probably static. This would allow a good determination of ϕ_{zz}, and since there are two different C-D bond directions relative to the Cu-Cu vector, it would be possible to investigate the indirect electric field effect further. The main difficulties in the study of copper propionate would be its cost, the absence of an X-ray structure, and its low solubility, which may lead to troubles in growing a large single crystal. None of them seems to be insuperable.

CHAPTER VI

POTASSIUM SULPHAMATE.

VI. 1. Introduction.

Potassium sulphamate was chosen for study by deuterium magnetic resonance for three main reasons. The structure has been determined by X-ray diffraction (3/6, 4/6) and neutron diffraction (1/6). The proton positions are thus known, so the directions of the bonds to hydrogen atoms can be compared with the directions of the principle components of the efg tensor. The quadrupole coupling constant for the deuterium atoms in urea-d_4 has been determined (5/6), this determination and Emsley and Smith (6/6) gave information on the molecular vibrations. Hence an investigation of DMR spectrum might also yield information on the vibration of the ND_2 group. There have been very few measurements of eqQ/h in compounds containing N-D bonds, they are ND_3, glycine compounds, ND_4^+ compounds. The references may be found in reference 7/6.

VI. 2. The crystal structure of Potassium Sulphamate.

In all of the following chapter, the axial system described by Cox et al. (1/6) will be used. Brown and Cox (3/6) and Jeffrey and Stadler (4/6) used a different set. A table showing the correspondence between the three structure determinations is given

Cox et al.	a = 5.907	b = 8.333	c = 8.302
Brown and Cox	c = 5.90	a = 8.32	b = 8.28
Jeffrey and Stadier	c = 5.907	a = 8.333	b = 8.302

a) External morphology.

The interfacial angles of a small crystal of potassium sulphamate were measured with a 'Techne' optical goniometer. Unlike copper acetate monohydrate, the facial reflections were extremely sharp, so it was possible to achieve a repeatability of 1 - 2' arc. In spite of the small difference between b and c it was easy to assign Miller indices to each face. The a axis is perpendicular to the largest face, and c is along the needle axis. The assignments were checked by taking 15° oscillation X-ray photographs of a small crystal. These gave a = 5.93 ± .03, b = 8.30 ± .02, c = 8.30 ± .04 Å.

b) Crystal Structure.

The structure of potassium sulphamate has been determined in the above mentioned references 1/6, 3/6, 4/6. The space group is Pbcm (No. 57 of the International tables, reference 14/5), with four molecules per unit cell. A projection of the structure on the a b plane is given in Figure 1. The four anions per unit cell are labelled I, II, III, IV; the coordinates of the nitrogen atoms in each are (.2914, .1802, .75), (.2914, .3198, .25), (.7086, .8198, .25) respectively. The proton positions, from Cox, et al., are also shown, but in the projection given it is not possible to distinguish the two protons bound

FIGURE 1.

Projection of the structure of potassium sulphamate on the a b plane

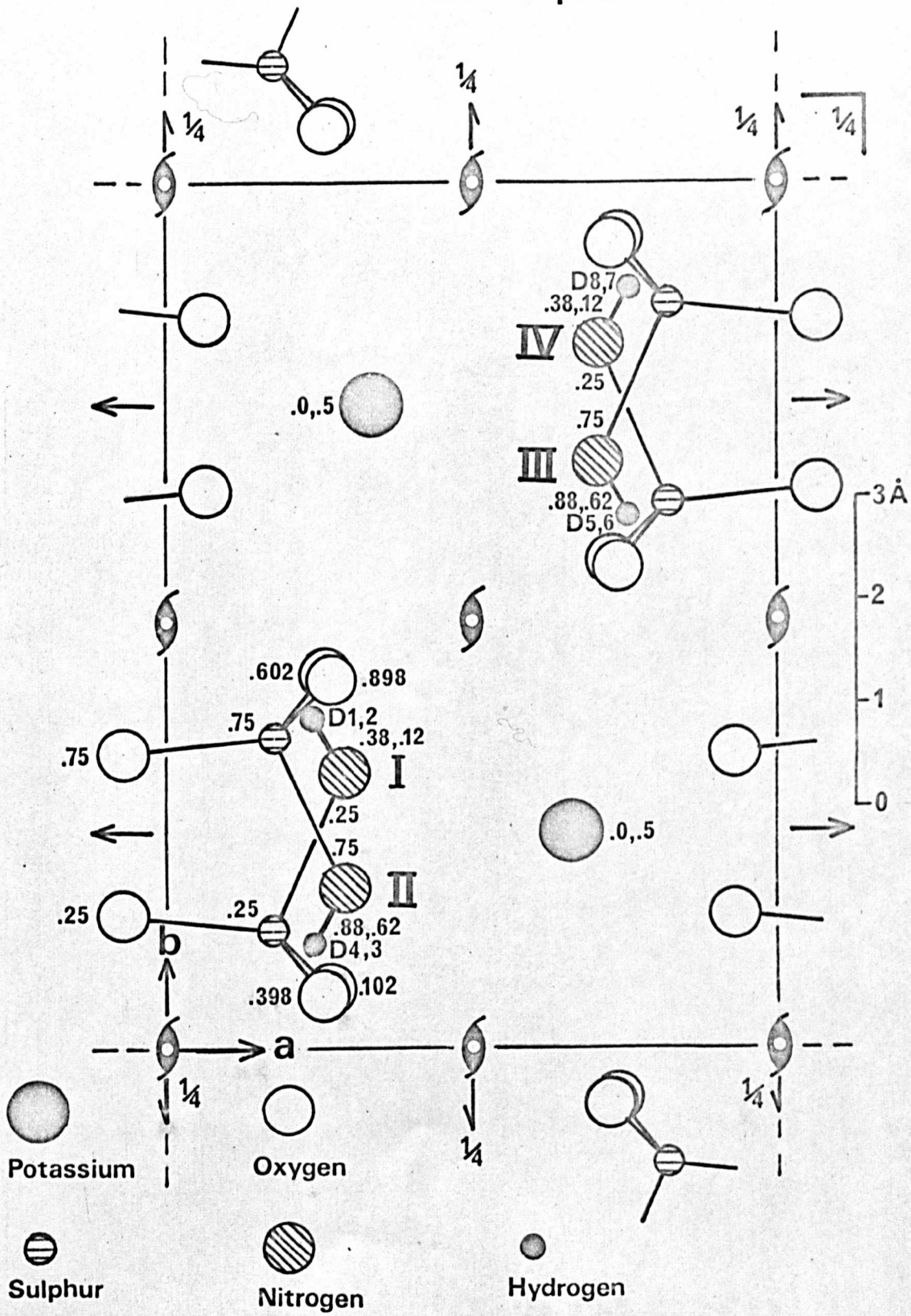

to one nitrogen atom. The two numbers beside each proton in the diagram are the numbers assigned to them in the prediction program SPECTRUM. The first number of the pair is the one belonging to the proton with the higher c' coordinate.

Since the crystal is orthorhombic, the matrix for the transformation from crystallographic coordinates to the orthogonal crystal based set is simple :-

$$\begin{vmatrix} a' \\ b' \\ c' \end{vmatrix} = \begin{vmatrix} 5.907 & 0 & 0 \\ 0 & 8.333 & 0 \\ 0 & 0 & 8.302 \end{vmatrix} \begin{vmatrix} a \\ b \\ c \end{vmatrix}$$

This was used in calculating the coordinates of the nitrogen and hydrogen atoms in Table 1.

c) <u>The expected rotation pattern.</u>

Since the anions I and III, and II and IV are related to each other by an inversion centre at ($\frac{1}{2}$, $\frac{1}{2}$, $\frac{1}{2}$), there are only two magnetically different molecules per unit cell. The anions are not centrosymmetric, so in an arbitrary orientation there will be four line pairs in the DMR spectrum. However, if the crystal rotation axis is coincident with one of the crystallographic axes, the rotation pattern is simplified. For example, in the a'-axis rotation pattern, the relationship between the magnetic field direction and the ND_2 direction will be the same for D_1 and D_8. It can be seen that in the a and b axis rotation patterns there will be two line pairs arising from deuterons 1,3,6,8 and 2,4,5,7. For the

c axis rotation pattern there are also only two line pairs from the sets 1, 2, 5, 6 and 3, 4, 7, 8. The crystals were thus mounted with the crystallographic axis as close as possible to the rotation axis.

VI. 3. Experimental Notes.

Three crystals of potassium sulphamate - d_2 were grown by the method described in Chapter III. Since the crystals were tabular on (100), it was necessary to grow a very large crystal which was thick enough to give a reasonable filling factor for the a-axis rotation pattern.

The experimental conditions were usually :-

RF level	50 mV at the tank coil,
Field sweep rate	4 or 5 gauss per minute,
Modulation depth	up to 2 gauss at 192 Hz,
Time constant	10 seconds, single section.

The c-axis rotation pattern was the first to be run at 0° C. This was easy except for the very weak signals when the magnetic field direction was about 20° from the a axis direction. However, no signals were seen in the other 0° C rotation patterns unless the magnetic field direction was within 5 - 7 degrees of a crystallographic axis direction. These observations will be described in more detail and discussed later.

VI. 4. Experimental results.

The results are presented in Tables 2-5, in the same form as those for cupric acetate (Chapter V. tables 2-9). No tables or graphs are given for unsuccessful a and b rotation patterns run at 0° C.

TABLE 1.

Atomic coordinates in potassium sulphamate (in Å)

Anion	Atom	a'	b'	c'
I	N	1.721	2.665	2.075
	H_1	1.440	3.169	2.901
	H_2	1.440	3.169	1.250
II	N	1.721	1.502	6.227
	H_3	1.440	.997	5.401
	H_4	1.440	.997	7.052
III	N	4.186	5.668	6.227
	H_5	4.467	5.164	7.052
	H_6	4.467	5.164	5.401
IV	N	4.186	6.831	2.075
	H_7	4.467	7.336	1.250
	H_8	4.467	7.336	2.901

The standard deviations on the positions of the nitrogen atoms are about .25 pm (.0025 Å) and are about twice as large for the protons. These figures were calculated from table 4 of reference 1/6.

TABLE 2.

Results for the c-axis rotation pattern at 0° C.

Transformation Matrix.

	a'	b'	c'
X	-.0466	.9989	-.0043
Y	-.0029	-.0044	-.9999
Z	-.9989	-.0466	.0031

Equation of lines.

Deuteron	Line no.	a		b		c	
3,4,7,8	1	62.58	.33	-44.29	.48	48.32	.46
	4	-57.45	.33	44.63	.48	-47.58	.46
1,2,5,6	2	61.80	.71	52.53	1.0	39.94	.90
	3	-57.15	.42	-51.81	.62	-40.01	.56

Line splittings.

Deuteron	a		b		c	
3,4,7,8	-110.03	.23	88.92	.34	-95.90	.33
1,2,5,6	-108.95	.38	-104.34	.55	-79.95	.50

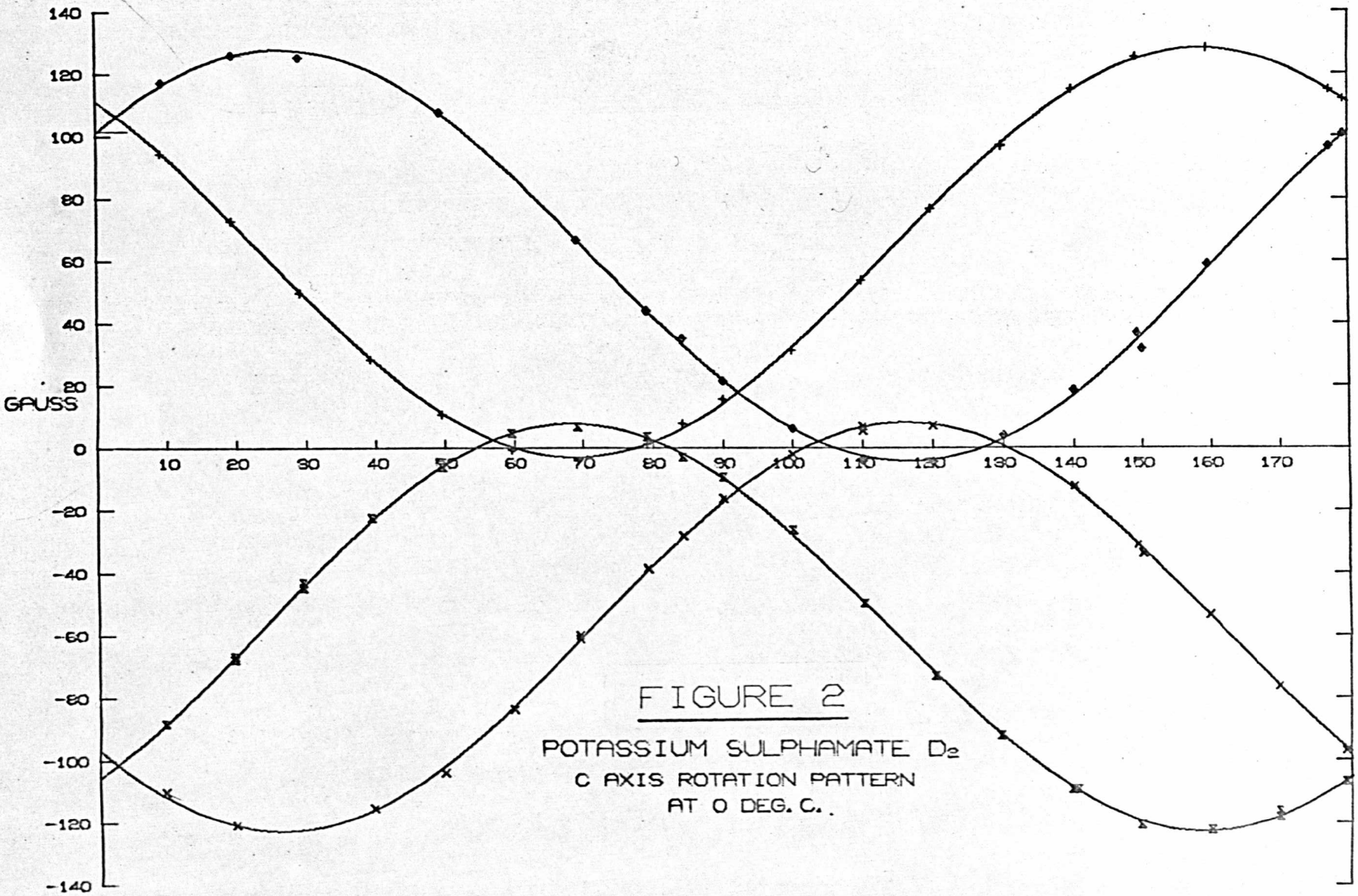

FIGURE 2

POTASSIUM SULPHAMATE D_2
C AXIS ROTATION PATTERN
AT 0 DEG. C.

TABLE 3.

Results for the a'-axis rotation pattern at -78° C.

Transformation matrix.

	a'	b'	c'
X	.0060	-.9973	.0731
Y	-.9996	-.0079	-.0263
Z	.0268	.0729	-.9970

Equations of lines.

Deuteron	Line no.	a		b		c	
1, 6	1	57.03	1.0	126.2	1.4	96.38	1.4
	6	-52.14	1.1	-127.4	1.7	-94.69	1.3
2, 5	2	-47.47	.81	150.2	1.2	-35.64	1.0
	5	51.86	.68	-149.3	.98	35.58	.93
3, 8	3	-44.57	1.1	-122.2	1.7	-87.43	1.3
	8	50.93	.60	122.9	.87	90.02	.77
4, 7	4	-53.07	.73	153.1	.98	-42.37	.93
	7	56.65	.83	-151.8	1.2	41.70	1.1

Line splittings.

Deuteron	a		b		c	
1, 6	109.17	.7	253.6	1.1	191.1	1.0
2, 5	99.33	.53	-299.5	.8	71.20	.68
3, 8	95.50	.57	245.1	.9	177.4	.7
4, 7	109.7	.55	-304.9	.8	84.07	.71

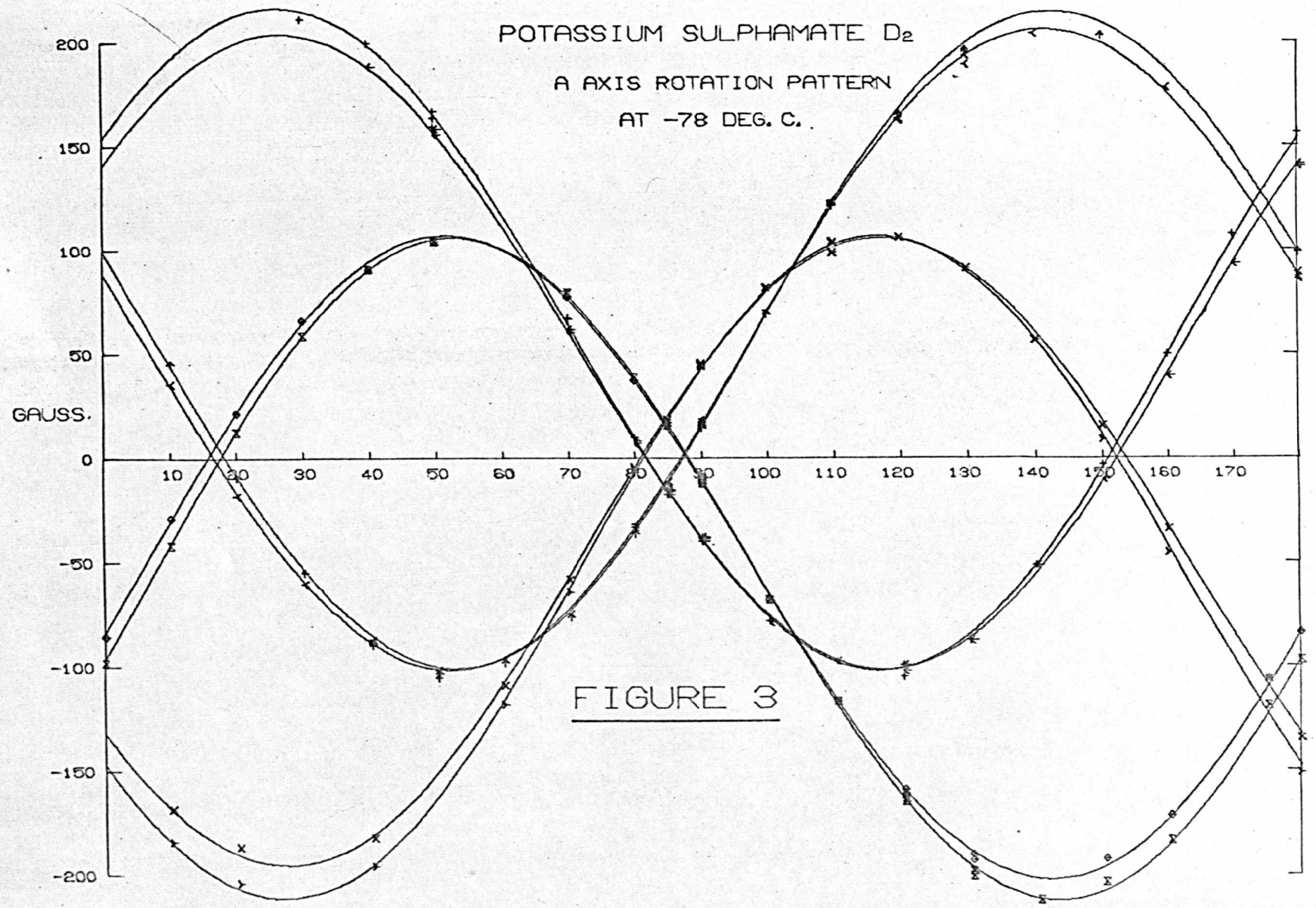
POTASSIUM SULPHAMATE D2
A AXIS ROTATION PATTERN
AT -78 DEG. C.
GAUSS.
200
150
100
50
0
-50
-100
-150
-200
10
20
30
40
50
60
70
80
90
100
110
120
130
140
150
160
170

FIGURE 3

TABLE 4.

Results for the b axis rotation pattern at -78° C.

Transformation matrix.

	a'	b'	c'
X	-.0859	.0045	.9963
Y	-.0194	-.9998	.0028
Z	.9961	-.0191	.0860

Equations of lines.

Deuteron	Line no.	a		b		c	
1,4,6,7	1	-5.14	.48	61.24	.77	128.9	.60
	4	9.24	.73	60.99	1.0	-128.6	1.0
2,3,5,8	2	-5.80	.98	-109.0	1.5	93.00	1.2
	3	9.20	.33	108.9	.48	90.97	.50

Line separations.

Deuterons	a		b		c	
1,4,6,7	14.38	.42	-122.2	.62	-257.5	.55
2,3,5,8	15.00	.40	217.9	.60	-184.0	.55

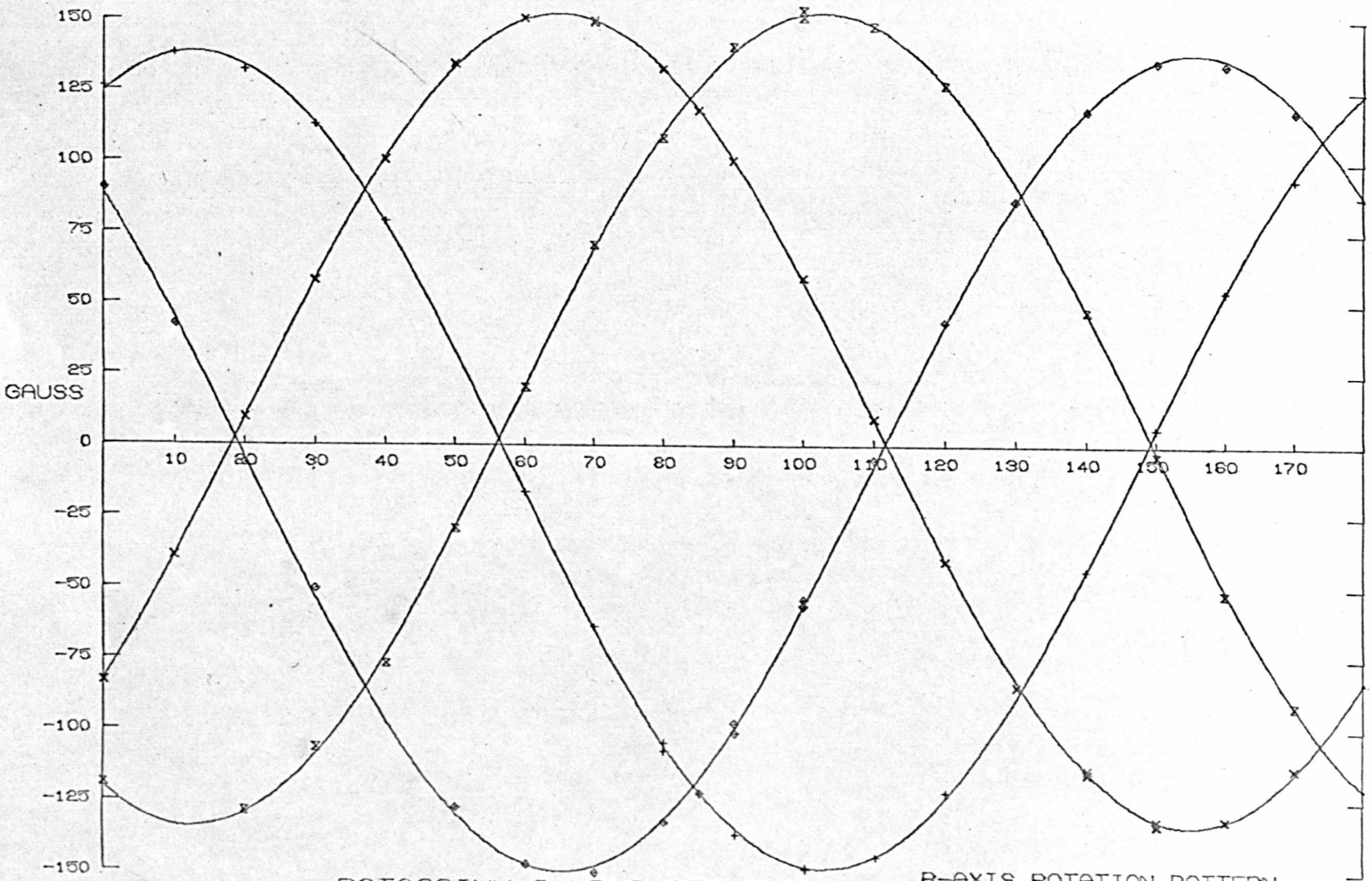

POTASSIUM SULPHAMATE D_2

B-AXIS ROTATION PATTERN
AT -78 DEG. C.

FIGURE 4

TABLE 5.

Results for the c'-axis rotation pattern at -78° k

Transformation matrix.

	a'	b'	c'
X	-.0515	-.9987	-.0031
Y	-.0231	.0043	-.9998
Z	.9984	-.0515	-.0232

Equations of lines.

Deuterons	Line no.	a		b		c	
1, 6	1	60.75	.48	-53.28	.54	37.67	.65
	6	-59.78	.44	54.30	.54	-38.65	.61
2, 5	2	-59.51	.50	54.47	.65	-39.04	.70
	5	61.20	.67	-54.18	.86	38.46	.88
3, 8	3	-59.40	.65	-42.52	.90	-50.12	.86
	8	61.69	.50	42.01	.67	50.64	.65
4, 7	4	-59.56	.61	-42.14	.86	-49.87	.80
	7	61.83	.54	41.56	.73	50.31	.71

Line separations.

Deuterons	a		b		c	
1, 6	-120.5	.3	107.6	.4	-78.32	.44
2, 5	-120.7	.4	108.6	.5	-77.50	.56
3, 8	-121.1	.4	-84.53	.56	-100.8	.5
4, 7	-121.6	.4	-83.70	.56	-100.2	.5

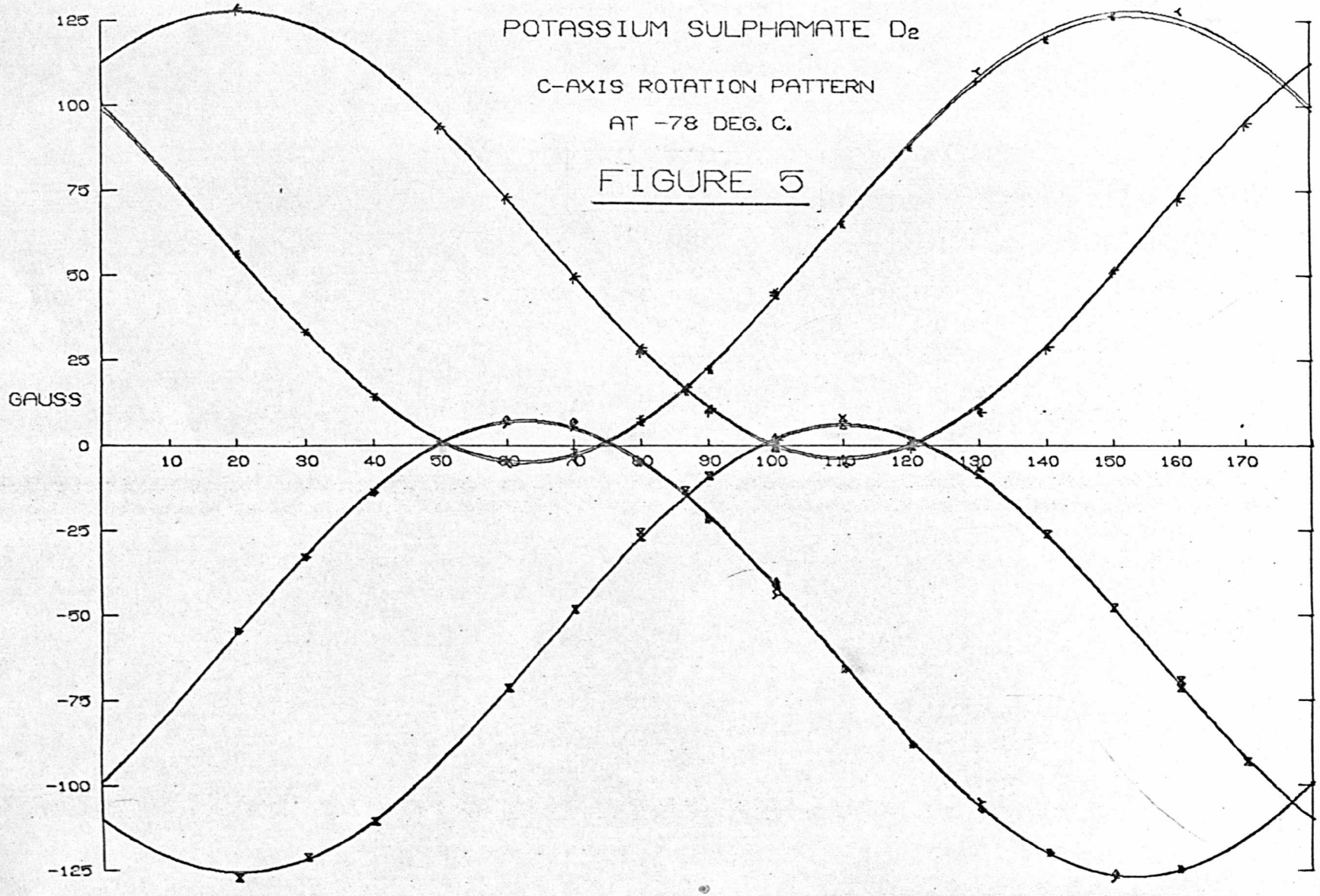
POTASSIUM SULPHAMATE D2
C-AXIS ROTATION PATTERN
AT -78 DEG. C.
GAUSS
125
100
75
50
25
0
-25
-50
-75
-100
-125
10
20
30
40
50
60
70
80
90
100
110
120
130
140
150
160
170

FIGURE 5

TABLE 6.

Electric field gradient tensors for the deuterons in Potassium Sulphamate at -78°C.

D1, D6

ϕ_{zz}= 205.3, ϕ_{yy}= -116.8, ϕ_{xx}= -88.5 Exp. trace = -4.23 kHz

η=.138

Eigenvectors

				N-D vector	O-D direction
a'	-.2685	.9560	-.1178	-.2792	.0475
b'	.4976	.0330	-.8668	.5008	.2123
c'	.8248	.2914	.4846	.8193	.9760

D2, D5

ϕ_{zz}=208.0 ϕ_{yy}=116.4, ϕ_{xx}=91.6 Exp.trace = .46 kHz

η=.138

Eigenvectors

				N-D vector	O-D direction
a'	-.2816	.9585	-.0433	-.2792	.0475
b'	.5217	.1151	-.8453	.5008	.2123
c'	-.8053	-.2607	-.5325	-.8193	-.9760

D3, D8

ϕ_{zz}= 205.4, ϕ_{yy}= -117.1, ϕ_{xx}= -88.3 Exp.trace = -.36 kHz

η= .140

Eigenvectors

				N-D vector	O-D direction
a'	-.2914	.9490	-.1203	-.2792	.0475
b'	-.4959	-.0424	.8673	-.5008	-.2123
c'	-.8180	-.3124	-.4830	-.8193	-.9760

D4, D7

ϕ_{zz}= 208.9, ϕ_{yy}= -121.0, ϕ_{xx}=-87.9 Exp.trace = -.87 kHz

η = .154

Eigenvectors

				N-D vector	O-D direction
a'	-.2735	.9151	-.2963	.2792	.0475
b'	-.5156	.1206	.8483	.5008	-.2123
c'	.8120	.3806	.4388	.8193	.9760

VI 4. continued.

Table 6 shows the results obtained when the data in Tables 3-5 were used for the program TENSOR. The N-D vector direction cosines (calculated from the figures in Table 1a) are also shown for comparison with the ϕ_{zz} eigenvectors.

VI 5. Discussion of the results.

a) The value of ϕ_{zz}

The observed values of ϕ_{zz} fall into two pairs, with magnitudes of 205.4 and 208.5 kHz. There appears to be no physical reason why there should be this difference, since the environments of D1 and D2 are identical, so it must be due to experimental error.

The only other $-ND_2$ compounds which have been studied by DMR are urea (5/6) and ND_3 (Rabideau and Waldstein, reference 8/6). For urea, ϕ_{zz} = 210.7 kHz and η = .143 $\pm$ .01. This similarity with the values for potassium sulphamate is surprising, since in urea the nitrogen coordination is planar (Worsham, reference 8/6), and in the sulphamate it is tetrahedral. It would appear that the value of ϕ_{zz} is controlled by hydrogen bonding to the neighbouring oxygen atom. The N-D and O-D distances in the two compounds are very similar, as the table below shows :-

	Urea	Potassium Sulphamate
O---H	2.07	2.147 Å
N - H	.991	1.007
N - H_1 --- O^1 angle	167.°4	153°.2
N - H_2 --- O angle	151.°7	153°.2

The coupling constants for the two different deuterons in urea are not perceptibly different, so ϕ_{zz} is not very sensitive to the N-H---O angle. The N - H bond length in urea is probably too short, because no correction was made for the large librational motion of the molecule (Emsley and Smith 6/6). It appears that hydrogen bonding has a large influence on the quadrupolar coupling constant of ammonia; it is 291 kHz in gaseous NH_2D (9/6), and 156 kHz in solid ND_3 8/6). The value for NH_2D is more reliable than the 200 $\pm$ 12 kHz for gaseous ND_3, found by Herrmann (10/6), since the spectrometer had about eighty times the resolution of Herrmann's. The difference between the coupling constants of NH_2D and ND_3 should be very small, so that it is valid to use the NH_2D result.

There seems to be little doubt that urea, potassium sulphamate and ammonia are hydrogen bonded. The D-O distances in the first two compounds are less than the van der Waal radic sum of 2.8Å. The X-ray diffraction study by Olovsson and Templeton (11/6) indicates that hydrogen bonding is present in ND_3. However, Vuagnet (12/6), in an IR spectrum study says that there is no hydrogen bonding in

potassium sulphamate. He quotes Brown and Cox's structure determination as evidence for this, but they did not determine the proton positions.

b) The eigenvectors.

The ϕ_{zz} eigenvectors lie very close to the N-D directions calculated from Table 1. The angle between the ϕ_{zz} eigenvectors for D1, D2 is $109.^{\circ}2$, the same as for D3, D4. This may be compared with $110.^{\circ}1 \pm .7$ from the neutron diffraction study. Chiba found that in urea ϕ_{zz} deviates $3.^{\circ}4$ from one N-D vector and $1.^{\circ}2$ from the other N-D vector. This may be connected with the difference in the two N-H---O angles in urea - they are $151.^{\circ}7$ and $167.^{\circ}4$ respectively.

The ϕ_{yy} eigenvectors are inclined at about 20° to the a-b plane. We will call this angle A, and its sign will be positive if the a' and b' components of the ϕ_{yy} eigenvector have the same sign. The sign of A is found to be the same as that of the c' component of the D-O vector. The sign of the b' component of the O-D vector is always opposite to that of the b' component of the ϕ_{xx} eigenvector, and the normal to the N-D-O plane is not far from the ϕ_{yy} direction. For D1 the normal is in the direction (.7056, -.6845, .1836) and ϕ_{yy} has the direction cosines (.9560, .0330, .2914). The orientation of ϕ_{xx} and ϕ_{yy} thus seem to be controlled by the hydrogen bonding, but the direction of ϕ_{zz} is unaffected. This is evidence for hydrogen bonding in potassium sulphamate. In urea the hydrogen bonds are in the plane of urea molecule so ϕ_{yy} is perpendicular to the $-ND_2$ plane. The situation

in urea and potassium sulphamate is thus similar to that in hydrogen bonded water, where ϕ_{zz} is nearly parallel to the O-D bond and ϕ_{yy} is normal to the O-D..O plane.

VI. 6 Variation of line strength with magnet rotation angle.

At 0°C, only the c'-axis rotation pattern was successful, but the lines were very weak when the magnetic field was about 30° from the a' axis direction. In the a and b axis patterns, signals were only seen when the magnetic field direction was close to one of the axes perpendicular to the rotation axes.

Complete rotation patterns were observed at -78°C. Again, the lines in the c'-axis pattern were weak at about 30° from the a' axis. In the a'-axis pattern the signals were weak at about 30° from the c'-axis, and in the b'-axis pattern, no absorption was seen within a few degrees of the c axis.

There seems to be little correlation between the directions of the magnetic field when the signal was weak and the structure, except for the c-axis rotation patterns, where the magnetic field was normal to the $-ND_2$ plane. The disappearance could be due to very rapid dipolar relaxation, which is known to have angular dependance. No sign was ever seen of dipole-dipole splitting of the resonance lines.

CHAPTER VII

APPENDIX

The original intention in the project was to study some single crystals which melted below room temperature, but no signals were ever observed in the compounds chosen. However, a little of the work done for this project is still of interest.

VII. 1 Crystal growth apparatus.

The apparatus, which is similar to that described by Emsley and Smith (1/7), is shown in Figure 2. It was found that, without the copper tube, the part at which the temperature was equal to the melting point of the substance moved downwards as the refrigerant sublimed away, about as fast as the crystal was lowered.

Method of growing crystals.

The sample tube was filled with the liquid and sealed, then the tip of the capillary was touched on a piece of solid carbon dioxide to seed the crystal. The tube was then suspended in the apparatus at the approximately correct height for about half an hour. The height was adjusted until about 3mm of the liquid was frozen, then the drive motor was started to drop the tube at about 1mm/hr. Up to 4cm long single crystals of benzene, nitrobenzene and HOD were grown by this technique. Only aniline failed to grow as a single crystal.

FIGURE 1.

LOW TEMPERATURE X-RAY CAMERA

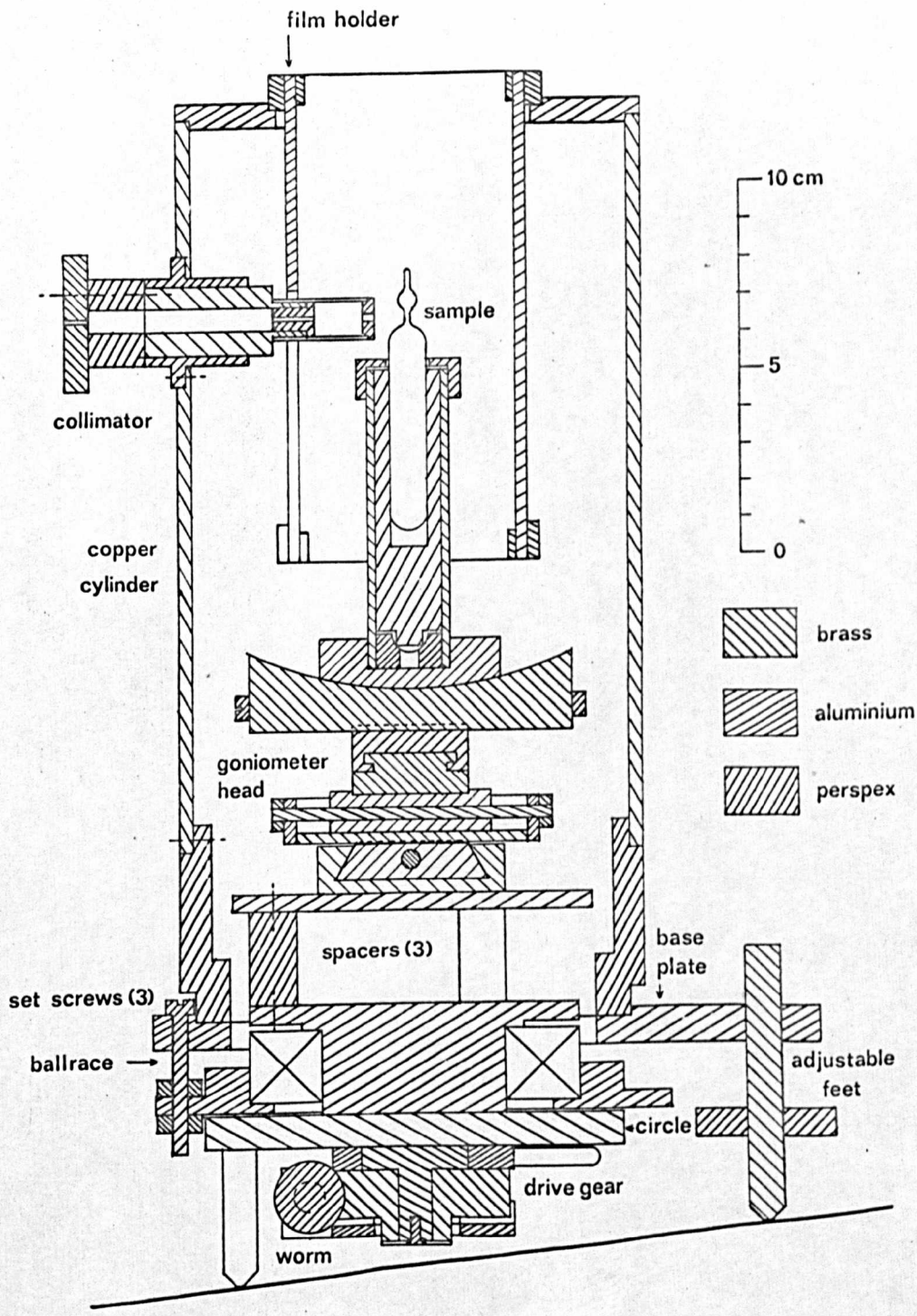

FIGURE 2.

Crystal growing apparatus

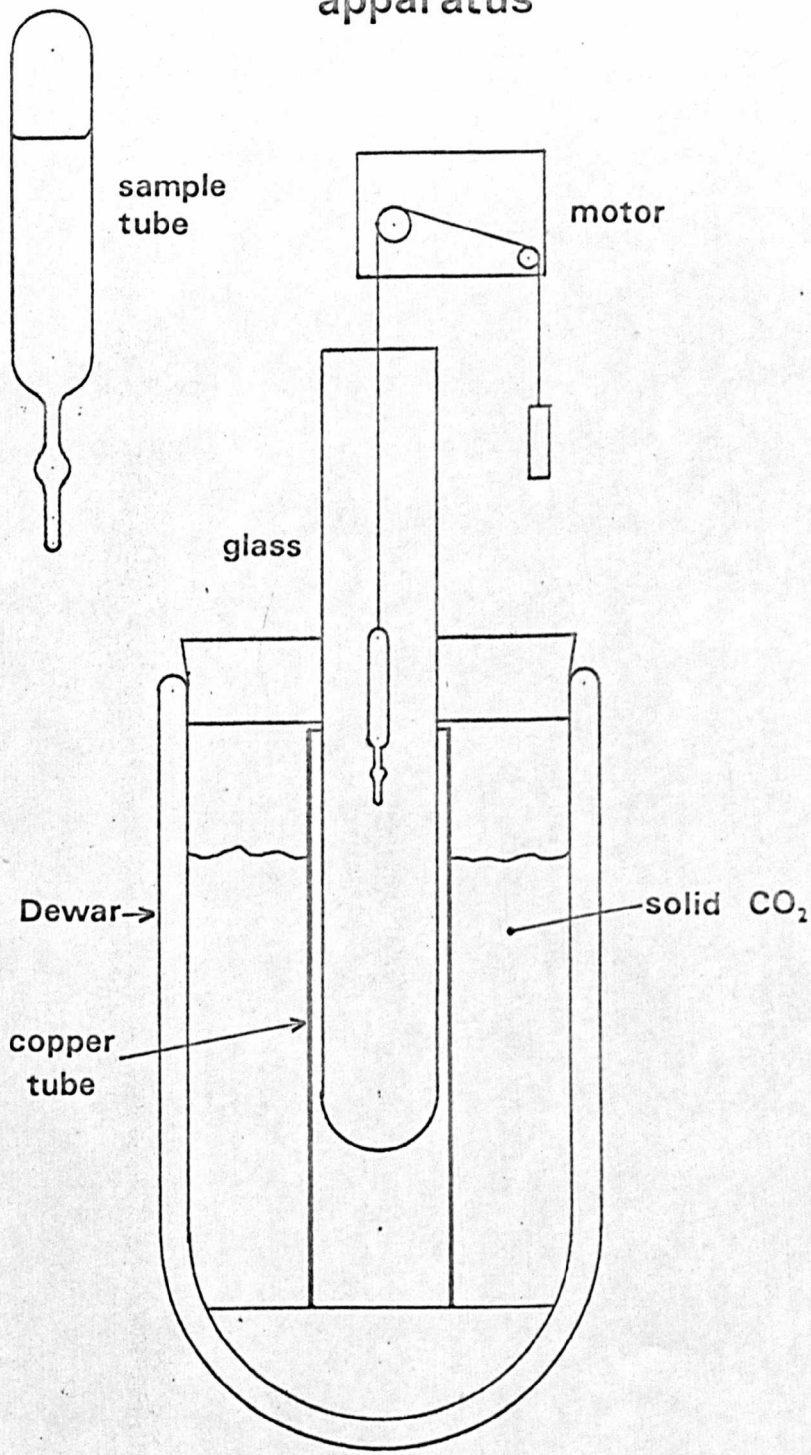

VII. 2 Low temperature X-ray camera.

The camera, without refrigerant or insulation, is shown in Figure 1. The solid carbon dioxide coolant surrounds the 12cm i.d. copper tube and is contained in a foamed polystyrene box.

A Unicam oscillation camera was considered, but this camera was built for the following reasons :-

a) The inconvenient size and shape of the sample makes it impossible to mount on the small goniometer head of a Unicam oscillation camera. The maximum available distance between the top of the goniometer head and the X-ray beam is much less than the length of the capillary on the sample tube.

b) The difficulty of relating the orientation of the sample to the camera.

c) The play in a small goniometer head is large, especially under the weight of the sample.

d) The difficulty of maintaining the sample at a low temperature.

The camera was in fact never used, but the design seems to overcome the above difficulties. Techniques were devised to relate the orientation of the crystal found from X-ray photographs to the probe orientation, and a method worked out to transfer a low melting point crystal to the probe at -60°C was successful.

VII. 3 A method to eliminate breakthrough.

Many marginal oscillator spectrometers suffer from modulation

breakthrough. The usual methods used to eliminate it are either to place an rf choke from the grid of the first oscillator valve to ground to shunt l.f. voltages induced in the signal coil, or to place a coil, coaxial with the signal coil, round the probe unit. This coil is fed with a current at the modulation frequency, of appropriate amplitude and phase so that the resultant magnetic field cancels out the voltages induced in the signal coil. A simpler solution is to use a difference amplifier between the spectrometer audio output and the tuned amplifier (see Chapter III, figure 1). One of its inputs is from the spectrometer, the other is from a voltage source of the correct amplitude and phase to balance out the breakthrough. Since the audio signal is at a relatively high level, no extra noise is produced by the difference amplifier. This system was used successfully by John Clifford (3/1, p.56), to eliminate breakthrough caused by spurious amplitude modulation in a frequency modulated Robinson oscillator.

BIBLIOGRAPHY.

Chapter I.

1. E.A. Uehling and J.L. Bjorkstam, Phys. Rev., 1959, 114, 961.

2. R. Blinc and D. Hadzi, Nature, 1966, 212, 1307.

3. R.M. Sternheimer, Phys. Rev., 1951, 84, 244; 1952, 86, 316; 1954, 95, 736.

4. R. Blinc, 'Magnetic Resonance in Hydrogen-bonded Ferroelectrics', in 'Advances in Magnetic Resonance, Volume 3, Editor, J.S. Waugh, Academic Press, New York, 1968.

5. V.H. Schmidt and E.A. Uehling, Phys. Rev., (1962), 126, 477.

Chapter II.

1. R.V. Pound, Phys. Rev., 1950, 79, 685.

2. C.P. Slichter, 'Principles of magnetic resonance', Harper and Row, New York, 1963, Chapter 6.

3. J.F. Nye, 'Physical Properties of Crystals', Clarendon Press, Oxford, 1964, Chapters II and IX.

4. B.L. Anderson, and T.A. Bancroft, 'Statistical Theory in Research', McGraw Hill, 1952, page 170.

Chapter III.

1. J.O. Clifford, Ph.D. Thesis, Leeds, 1968.

2. F.N.H. Robinson, Rev. Sci. Instr., 1959, 36, 481.

3. R.J. Blume, Rev. Sci. Instr., 1958, 29, 574.

4. G.D. Watkins, Ph.D. Thesis, Harvard University, Cambridge, 1952.

5. S. Ketudat, Ph.D. Thesis, Harvard, 1957.

6. F.N.H. Robinson, J. Sci. Instrum. 1965, 42, 653.

7. J. Texereau, 'How to make a telescope', p.147-153, (Interscience, 1957).

8. L. D. Pettit, private communication.

9. H. B. Weiser, W. O. Milligan, E. L. Cook, J. Am. Chem. Soc., 1942, 64, 503.

10. A. I. Vogel, 'A textbook of quantitative inorganic analysis', p.351, (Longmans 1961).

11. G. Gordon and H. Yamatera, Anal. Chem., 1964, 36, 1866.

12. L. Foucault, Compt. Rend., 1870, 70, 389-392.

13. D. D. Maksutov, J. Opt. Soc. America, 1944, 34, 270.

14. D. H. Howling, Rev. Sci. Instrum., 1965, 36, 660.

Chapter IV.

1. The Computer Journal, Jan. 1963, 5 no. 4, 'Revised Report on the Algorithmic Language ALGOL 60'.

2. NCR Elliott 4100 Manual Vol. 2, Part 2 Sections 2,4,5. Elliott-Automation Ltd., 1967, June.

3. Varian table, Fifth edition, 1965, Varian Associates.

4. As ref. 3, above.

5. G. M. Volkoff, H. E. Petch, and D. W. L. Smellie, Can. J. Phys., 1952, 30, 270.

6. G. M. Volkoff, Can. J. Phys., 1953, 31, 820, CACM algorithm no. 254.

Chapter V.

1. J. C. Rowell, W. D. Phillips, L. R. Melby, and M. Panar, J. Chem. Phys., 1965, 43, 3442.

2. V. Saraswati and R. Vijayaraghavan, Proceedings of the 14th Colloque Ampere, Ljublana, 1966, ed. R. Blinc, North-Holland Pubg. Co., 1967, p.767.

3. T.Caves and M.Karplus, J.Chem.Phys., 1966, 45, 1670.

4. M.Kato, H.B.Jonassen and J.C.Fanning, Chemical Reviews, 1964, 64, 99.

5. H.J.Brooke, Annals of Philosophy (London) 22 (new series 6), 38.

6. J.Schabus, 'Bestimmung der Krystallgestalten in chemischen Laboratorien erzeugter Produkte', Vienna, Holder (1855).

7. P.Groth, 'Chemische Krystallographie', part 3, Liepzig, Engelmann (1910).

8. R.B.Hull, University of Pittsburgh, Bulletin, 35, 142.

9. 'Barker Index of Crystals', ed. M.W.Porter and R.C.Spiller, Heffer, Cambridge, 1956. Volume II, part 2, no. M891A, B.

10. M.J.Buerger, 'X-Ray Crystallography', John Wiley & Sons Inc., 2nd Edition, (1949), p.149.

11. F.C.Phillips 'An Introduction to Crystallography', Longmans, Green & Co., London 1946, p.205 et.seq.

12. J.C.Rowell, W.D.Phillips, L.R.Melby and M.Panar, J.Chem.Phys., 1965, 43, 3442.

13. J.N.van Niekerk and F.R.L.Schoening, Acta Cryst. 6, 227, (1953).

14. International Tables for X-ray Crystallography, VolI.

15. B.Starck, Landolt Bornstein, Band 4, 'Molekelkonstanten aus mikrowellenspectroskopischen Messungen', ed. K.H.Hellwege and A.M.Hellwege, Springer Verlag, Berlin, 1967, Section 2.8, nr.1-17.

16. B.N.Figgis and R.L.Martin, J.Chem.Soc., (1956), 3837.

17. Edwin A.Crow, Frances A.Davis, Margaret W.Maxfield, 'Statistics Manual', Dover Publications, Inc., New York, 1960, Table 3.

18. G.M. Volkoff, Can.J. Phys., 1953, 31, 820.

19. A. Abragam, 'Nuclear Magnetism', O.U.P. 1961, p.197-8.

20. N.J. Poulis, Thesis, Leiden, 1952.

21. B. Bleaney and K.D. Bowers, Proc. Roy. Soc., (London), A214, 451, (1952).

22. T.F. Wimett, Phys. Rev., 1953, 91, 499.

23. T. Chiba, J. Chem. Phys., 1963, 39, 947.

24. G.W. Chantry and R.A. Plane, J. Chem. Phys., 1960, 33, 634.

25. T. Yoshimo and H.J. Bernstein, J. Mol. Spectroscopy, 1958, 2, 241.

26. C.G. Le Fevre and R.J.W. le Fevre, Rev. Pure and Appl. Chem., 1955, 5, no.4, pp 261-318.

27. D.M. Bishop, J. Chem. Phys., 1968, 49, 3718.

28. J.F. Harrison, J. Chem. Phys., 1968, 48, 2379.

29. R.C. Henderson and D.D. Ebbing, J. Chem. Phys., 1967, 47, 69.

30. R.L. Rowell and R.S. Stein, J. Chem. Phys., 1967, 47, 2985.

31. I.B. Rabinovich et al. Zhur. Fiz. Khim., 1958, 32, 1499-1505.

32. T.P. Das and E.L. Hahn, 'Nuclear Quadrupole Resonance Spectroscopy', Academic Press, New York, 1958.

33. W.J. Caspary, F. Millet, M. Reichbach and B.P. Dailey, J. Chem. Phys., to be published.

34. M.P. Klein, D. Gill and G. Kotowyez, Chem. Phys. Letters, 1968, 2, 677.

35. P. Waldstein, S.W. Rabideau and J.A. Jackson, J. Chem. Phys., 1964, 41, 3407.

36. D.M. Ellis, and J.L. Bjorkstam, J. Chem. Phys., 1967, 46, 4460.

37. W.H.Flygare, and W.D.Gwinn, J.Chem.Phys., 1962,36,787.

38. P.Pyykko, Proc.Phys.Soc., 1968, 92, 841.

39. C.H.Anderson and N.F.Ramsey, Phys.Rev., 1966, 149, 14.

40. M.D.Zeidler, Ber.Bunsenges., 1965, 69, 659.

41. V.W.Weiss and W.H.Flygare, J.Chem.Phys., 1966, 45, 3475.

42. B.P.Dailey and J.N.Shoolery, J.Am.Chem.Soc.,1955,77,3977.

43. M.L.Huggins, J.Am.Chem.Soc., 1953, 75, 4123.

44. L. Salem, J.Chem.Phys., 1963, 38, 1227.

45. W.J.Horsley and H.Sternlicht, J.Am.Chem.Soc., 1969, 90, 3738.

46. N.Muller and D.E.Pritchard, J.Chem.Phys., 1959, 31, 1471.

47. W.J.Tabor, J.Chem.Phys., 1957, 27, 974.

48. C.C.Costain, J.Chem.Phys., 1958, 29, 54.

49. H.Spiesecke, and W.G.Schneider, J.Chem.Phys., 1961,35,722.

50. Documentation of Molecular Spectroscopy, Butterworth's Scientific Publications, London, 1967 and 1968.

Chapter VI.

1. G.W.Cox et al., Acta Cryst., 1967, 23, 578.

2. ref. 9/5, crystal number 0552.

3. D.Brown, and A.J.Cox, J.Chem.Soc., 1940, p.1.

4. G.A.Jeffrey and H.P.Stadler, J.Chem.Soc., 1951, 1467.

5. T.Chiba, Bull.Chem.Soc., Japan, 1965, 38, 259.

6. J.A.Emsley, and J.A.S.Smith, Trans.Faraday Soc.,1961,57,1233.

7. P.Pyykko, Annales Universitatis Turkuensis,1967, 103A,9-46.

8. S. W. Rabideau, and P. Waldstein, J. Chem. Phys., 1966, 45, 4600.

9. S. G. Kukolich, J. Chem. Phys., 1968, 49, 5523-5.

10. G. Herrmann, J. Chem. Phys., 1958, 29, 875.

11. I. Olovsson, and D. H. Templeton, Acta Cryst., 1959, 12, 832.

12. A. M. Vuagnet, and E. L. Wagner, J. Chem. Phys., 1957, 26, 77.

Chapter VII.

1. J. W. Emsley and J. A. S. Smith, Trans. Faraday Soc., 1961, 57, 1248.